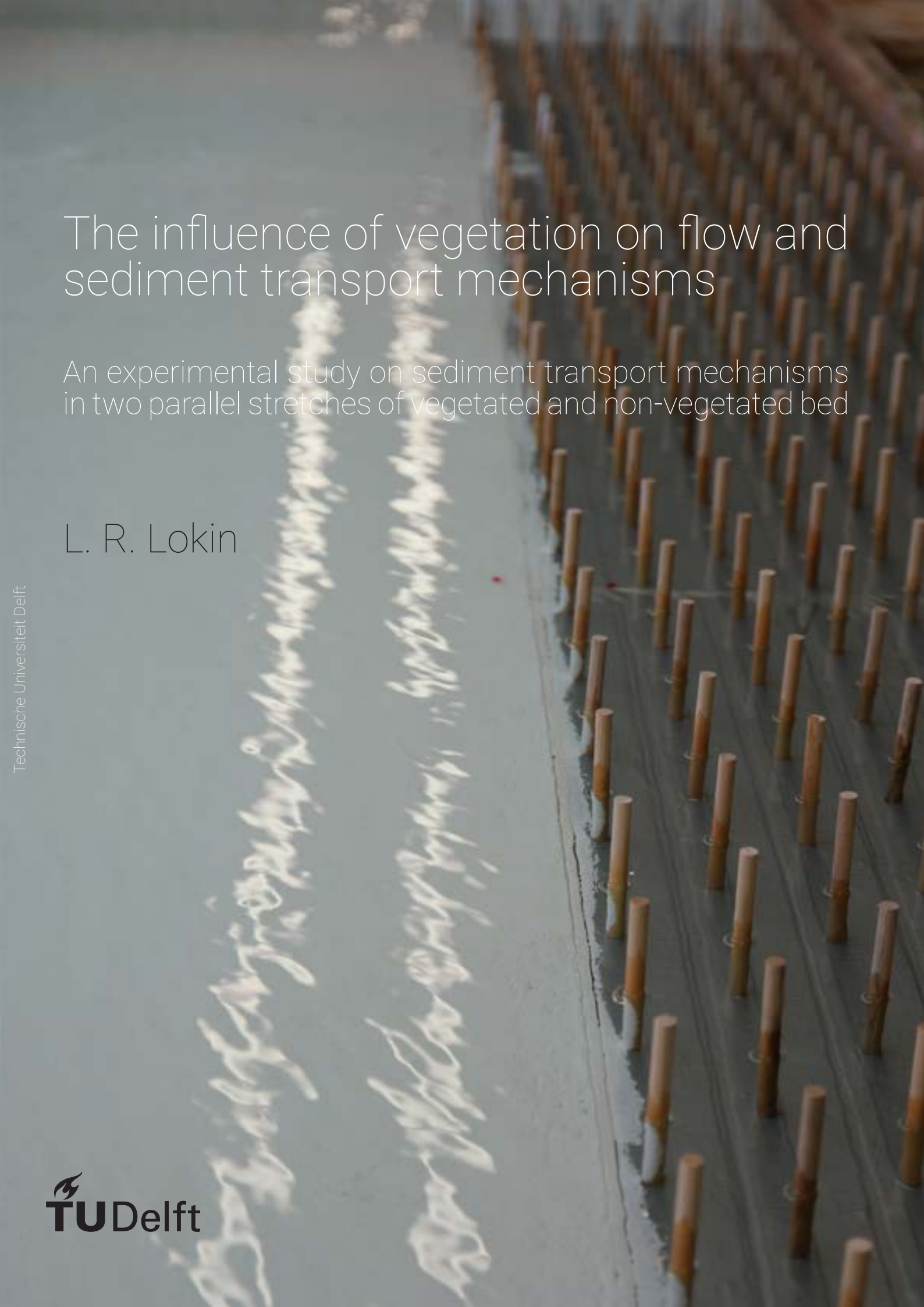


The influence of vegetation on flow and sediment transport mechanisms

An experimental study on sediment transport mechanisms in two parallel stretches of vegetated and non-vegetated bed

L. R. Lokin

Technische Universiteit Delft

TU Delft

The influence of vegetation on flow and sediment transport mechanisms

An experimental study on sediment transport mechanisms in two parallel stretches of vegetated and non-vegetated bed

by

L. R. Lokin

to obtain the degree of Master of Science
at the Delft University of Technology,
to be defended publicly on Thursday October 26, 2017 at 4:00 PM.

Student number:	4141067	
Project duration:	January 2017 – October 31, 2017	
Thesis committee:	Prof. dr. ir. W. S. J. Uijttewaal,	TU Delft, chair
	Dr. ir. E. Mosselman,	TU Delft and Deltares
	Dr. ir. C. J. Sloff,	TU Delft and Deltares
	Dr. W. E. Penning,	Deltares

An electronic version of this thesis is available at `http://repository.tudelft.nl/`.

TU Delft

Preface

Before you lies the result of my research on the interaction between flow and vegetation, which I have undertaken in the past 9 months. This research is the last step in order to obtain my Master's degree in Hydraulic Engineering at Delft University of Technology.

The topic of this research originates from my fascination on rivers, especially the complexity of the organized chaos below an apparently smooth water surface, as well as my interest in a more natural approach towards engineering rivers and coasts. Combining these two resulted in an experimental study in which flow processes and their interaction with vegetation and sediment were the main objectives. I have got the opportunity to do the research at the Environmental Fluid Mechanics Laboratory, which was, in my opinion, the best way to get a better understanding of complex flows.

This thesis would not have been here without my thesis committee, whom I would like to thank for asking the right questions and the discussions during our meetings from which I have got a broader view on the topic of vegetated flows and their dynamics. Prof. Wim Uijttewaal for giving me the opportunity to work in the lab and the discussions on turbulence and flow. Dr. Erik Mosselman and dr. Kees Sloff for helping me to synthesize the right topic and the critical views on my work and dr. Ellis Penning for asking the right questions which pulled me out of the comfortable engineering perspective.

I would also like to thank the technical staff of the laboratory, Sander, Jaap, Hans, Frank and Arno, for helping me with the adjustments on the flume, input on how the setup could be improved and for the many cups of hot chocolate brought to me in the middle of the experiments.

Last but not least I would like to thank my parents, who have supported me in every step throughout the journey that is called University.

L. R. Lokin
The Hague, October 2017

Summary

Vegetation on river banks and bars contribute to the stability of these morphological features. However, the exact processes contributing to this stabilization are still subject to research. This study has looked into the flow phenomena at the streamwise interface between vegetated and non-vegetated bed. Flow velocities in vegetated flows are lower than in non-vegetated flows under otherwise similar conditions, due to increased drag by the plants. Therefore a shear layer develops across the interface. Within this shear layer, Kelvin-Helmholz like vortices develops, which govern the exchange of mass and momentum through the interface. These vortices are present in the water column, but their strength near the bed governs sediment transport mechanisms, which are the basis of morphological activity. Therefore, the objective of this study was: to obtain a better understanding of the coherent flow structures in the interface between vegetated and non-vegetated river bed and the effect of these structures on sediment transport mechanisms.

This has been done with flume experiments in a vegetated compound channel, consisting of three parts: a deep channel, a transverse slope of 1:10 and a vegetated floodplain. The vegetation on the floodplain has been simplified by rigid cylinders. Different measuring techniques have been used to map the flow patterns. First Acoustic Doppler Velocimetry (ADV) was used to obtain mid-depth and near bottom flow profiles and statistics. Second, a Particle Tracking Velocimetry (PTV) technique was used to observe the movement of spherical tracers rolling over the bed. The last technique was injecting colored fluid to visualize the vortices. Multiple water depth and discharge combinations were studied for two different vegetation densities.

The flow profile in the channel part and on the transverse slope is independent of the vegetation density. Also, the depth does not influence the mean velocity profile; equal channel velocities give the same transverse flow profile. The flow velocity inside the vegetation is governed by the vegetation density. A higher density gives a lower velocity; this results in a larger difference between the interface velocity and the constant vegetation velocity resulting in a larger velocity gradient. The Reynolds stress in the transverse direction, $\overline{u'v'}$, however, shows dependence on the vegetation density and the water depth. This value is negative over the whole shear layer and has a peak at the interface between vegetated and non-vegetated bed. This peak increases with vegetation density and becomes wider for larger water depths. Outside of the shear layer, the Reynolds stress goes to zero. Streamwise momentum is transported in the transverse direction from the channel towards the vegetation in the shear layer.

The near-bed flow profile shows the same curve as the mean flow at mid-depth only with a smaller velocity due to the bed friction. The Reynolds stress, however, shows an entirely different profile. The peak at the interface is similar to the one in the middle of the water column. However, the near-bed Reynolds stress wiggles around zero with a second peak in the middle of the slope. At the interface the vortices influence the exchange of momentum, on the transverse slope, towards the channel, the vortices are not the primary mechanism for the exchange of momentum. There still are oscillations of the flow velocity with the same periodicity as the vortices. So the vortices still drive near bottom mass exchange in the transverse direction.

At the location within the vegetation where the Reynolds shear is zero, still, significant movement of the tracers and oscillations of the flow velocity both in streamwise and transverse direction have been measured. Mass is transported into the vegetation by sweeps and out of it by the ejections of the vortices. During the sweep, mass transported into the vegetation is blocked by the wall at the boundary, where the water level increases. During the ejection, the opposite happens, creating gradients in the water level, which strengthens variations in the velocity. This indicates that the exchange of mass between the channel and the floodplain is important and can strengthen the vortices. While the period and size of the vortices increase with increasing vegetation density, the exchange of mass is larger creating a stronger enhancement of the vortices.

The vortices can transport the PTV spheres up-slope. However, only the spheres present within the first 15 cm from the interface could be transported into the vegetation. Inside the vegetation, there is a specific zone from the interface to a specific distance into the vegetation where the exchange of tracers took place. At the inner edge of this zone tracers accumulated between the sweep an ejection. The width of this zone increases with decreasing vegetation density. This indicates the formation of a dune at this location. Within the inner layer, exchange thickness is likely to be transported out of the vegetation while spheres located

further into the vegetation still move in the transverse direction with the passing of a vortex but are not likely to be transported out of the vegetation.

The movement of the tracers combined with the flow statistics gives insight into the flow processes. The results indicate a location within the vegetation where sediments transported from the channel into the vegetation may deposit. This can create a dune distance from the interface which increases with decreasing density. The net deposition depends further on the difference in transport capacity between the channel and vegetation. The spherical tracers were always mobile in the being more affected by the ejection part of the vortices, resulting in a net erosion. However, most sediments are granular which need higher bed shear stress to become mobile. Once settled in the vegetation, where the bed shear stress is lower, they are less likely to be transported out of the vegetation.

Contents

List of Figures ix

List of Tables xiii

1 Introduction 1
- 1.1 Problem statement . . . 2
- 1.2 Objective and research questions . . . 2
- 1.3 Approach . . . 3
- 1.4 Outline . . . 3

2 Literature and theoretical framework 5
- 2.1 Morphology of vegetated flow systems . . . 5
- 2.2 Characterization of vegetation . . . 6
  - 2.2.1 Vegetation density . . . 6
  - 2.2.2 Submergence . . . 6
- 2.3 Flow through emergent vegetation . . . 7
  - 2.3.1 Turbulence . . . 7
  - 2.3.2 Drag . . . 8
  - 2.3.3 Momentum balance . . . 8
- 2.4 Flow at the interface between vegetation and no vegetation . . . 9
  - 2.4.1 Mean transverse flow profiles in equilibrium . . . 10
  - 2.4.2 Reynolds stresses . . . 12
  - 2.4.3 Near-bed conditions . . . 12
- 2.5 Sediment transport in vegetated flows . . . 12
  - 2.5.1 Initiation of motion in vegetated flow . . . 12
  - 2.5.2 Transport in the shear layer . . . 13
- 2.6 Transverse slope effects . . . 13
  - 2.6.1 Flow in a compound channel with a transverse slope . . . 13
  - 2.6.2 Sediment transport on transverse slopes . . . 14
- 2.7 Literature summary and conceptual framework . . . 14

3 Methodology 17
- 3.1 Experimental setup . . . 17
  - 3.1.1 Vegetation . . . 18
  - 3.1.2 Sediment . . . 18
  - 3.1.3 Experimental conditions . . . 20
- 3.2 Measurements . . . 20
  - 3.2.1 Acoustic Doppler Velocimetry (ADV) . . . 21
  - 3.2.2 Particle Tracking Velocimetry (PTV) . . . 21
- 3.3 Data processing and analysis . . . 23
  - 3.3.1 Image pre-processing . . . 23
  - 3.3.2 PTV . . . 23
  - 3.3.3 Velocity time series . . . 23

4 Results 25
- 4.1 General observations . . . 25
- 4.2 Flow . . . 26
  - 4.2.1 Mean streamwise velocity component . . . 30
  - 4.2.2 Transverse velocity component . . . 31

4.3 Reynolds stress . . . 32
4.3.1 Reynols shear stress . . . 32
4.3.2 Normal stresses . . . 34
4.3.3 Contribution of the coherent structures vs. 3D turbulence . . . 34
4.3.4 Turbulent viscosity . . . 36
4.4 Vortex structure . . . 37
4.4.1 Sweeps and Ejections . . . 37
4.4.2 Autocorrelation . . . 39
4.4.3 Energy density spectrum . . . 39
4.4.4 Instantaneous flow field . . . 41
4.5 Transport . . . 41
4.5.1 Qualitative observations PTV movies . . . 43
4.5.2 Particle paths . . . 43
4.5.3 Exchange . . . 44

5 Discussion **49**
5.1 Experimental setup and methods . . . 49
5.1.1 Particle tracking . . . 49
5.1.2 ADV . . . 50
5.1.3 Flow profiles . . . 51
5.2 Flow and turbulence . . . 51
5.2.1 Mean flow . . . 51
5.2.2 Near-bed Reynolds stress . . . 52
5.2.3 Secondary circulation . . . 52
5.3 Momentum and mass exchange . . . 53
5.3.1 Width of the vegetation . . . 54
5.3.2 Periodicity . . . 54
5.4 Transport mechanisms . . . 55
5.4.1 Bed load transport . . . 55
5.4.2 Diffusion . . . 55

6 Conclusion and recommendations **57**
6.1 Conclusions . . . 57
6.2 Recommendations . . . 59
6.2.1 Engineering vegetated flows . . . 59
6.2.2 Further research . . . 60

References **61**

A Experimental setup figures and dimensions **65**

B Supporting result figures **69**

C Velocity time series Q60H14 **73**

List of Figures

2.1 Flow profile in vegetated flow (green line) and in open-channel flow (blue line). In vegetated flow the velocity is constant over the depth except near the bed in the laminar sub layer, where the flow is still influenced by the bed. In open channel flow the only source of friction is the bed, the flow follows a logarithmic profile over depth, $u(y) = \frac{u_*}{\kappa} \ln\left(\frac{y}{y_0}\right)$. 7
2.2 Different configurations of compound channels with a vegetated floodplain and a non-vegetated channel. A) The situation as described in the articles of Buckman et al. (2014); White and Nepf (2007, 2008); Zong and Nepf (2010). B) The compound channel as described by Truong et al. (shed) with a gentle slope between the floodplain and the main channel. C) The compound channel as described by Dupuis et al. (2017) 10
2.3 The different zones and the length scales in the cross-sectional profile of the mean velocity. Adapted from White and Nepf (2008). 11
2.4 Vortex structure over a compound channel with a transverse slope. Adapted from Prooijen et al. (2005). 14
2.5 The processes governing flow in the a partly vegetated channel. 15
2.6 Hypothesized sediment transport directions in partly vegetated compound channel flows. . . . 15

3.1 Cross-section of the flume 18
3.2 Top view of the flume 19
3.3 The geometric setup of the dense vegetation. The measurements are in mm 20
3.4 Locations of the ADV measurements, for a water depth of 16 cm. The z-coordinate of the mid-depth measurements scale with the water depth. 22
3.5 Calibration image with the chessboards located on the slope, each square is 5 by 5 cm in reality. 22

4.1 Vortex structure around the interface visualized with colored water. 25
4.2 Time series for the sparse and dense setup for setting Q60H14 in the middle of water column. Top to bottom: in the channel $y = 0.9\ m$, on the slope $y = 0.45\ m$, at the interface $y = 0\ m$ and inside the vegetation $y = -0.2\ m$. The blue line is the streamwise component and the purple line the transverse component 28
4.3 Time series for the sparse and dense setup for setting Q60H14 near the bottom. Top to bottom: in the channel $y = 0.9\ m$, on the slope $y = 0.45\ m$, at the interface $y = 0\ m$ and inside the vegetation $y = -0.2\ m$. The blue line is the streamwise component and the purple line the transverse component 29
4.4 Mean streamwise velocity profiles in the cross section at mid-depth. Left the profiles for the sparse setup. Right the profiles for the dense setup. The same channel velocity gives similar profiles for the different depths. The black line indicates the location of the interface 30
4.5 U for $Q = 60\ l/s$ and $H = 14\ cm$ in the sparse (left) and dense (right) setup. 30
4.6 Normalized velocity profiles. Left) The velocity normalized by the mean mean channel velocity. Right) The profiles scaled by the inner layer thickness δ_I and velocity normalized by the slip velocity. 31
4.7 Comparison of the mean transverse velocity component, V. Left the profiles for the sparse vegetation. Right the profiles for the dense vegetation. The black line indicates the location of the interface 32
4.8 Reynolds shear stress, $\overline{u'v'}$, in the middle of the water column. Left) the shear stress profiles for set 2, $U_C \approx 0.4 m/s$. Right) the shear stress profiles for set 3, $U_C \approx 0.45 m/s$. The solid lines indicate sparse vegetation and the dashed lines the dense vegetation 33
4.9 Reynolds shear stress, $\overline{u'v'}$, near the bottom. Left) the shear stress profiles for set 2. Right) the shear stress profiles for set 3. The solid lines indicate sparse vegetation and the dashed lines the dense vegetation 33

4.10 $\overline{u'v'}$ for $Q = 60\ l/s$ and $H = 14\ cm$ in the sparse (left) and dense (right) setup. The profile of the Reynolds stress is similar for both setups, however the magnitude at the interface is larger for the dense vegetation. 34
4.11 Comparison between $\overline{u'v'}$, $\overline{u'u'}$ and $\overline{v'v'}$, for set 2 in the middle of the water column. The full lines indicate the sparse vegetation, the dashed lines indicate the dense vegetation. 35
4.12 Contributions to the Reynolds stress $\overline{u'v'}$ for $Q = 60\ l/s$ and $H = 14\ cm$ in the sparse (left) and dense (right) setup. The largest part of the Reynolds stress is determined by the vortices. Outside the shear layer the 3D turbulence is more important. 35
4.13 ν_t in the sparse (left) and dense (right) setup. 36
4.14 Sweep and ejections, visualized with colored fluid in the water. The blue line indicates the mean flow direction. 37
4.15 Sweep and ejections in the middle of the water column for Q60H14. The dark green line in the lower panels give the Reynolds stress 38
4.16 Sweep and ejections at the bottom for Q60H14. The dark green line in the lower panels give the Reynolds stress 38
4.17 Autocorrelation of the time signals at the bottom and at mid depth on $y = 0$ for different water depths with similar channel velocities $\left(U_{c,mid} \approx 0.4\ m/s\right)$ (set2). A) At the bottom with sparse vegetation. B) At mid-depth with sparse vegetation. C) At the bottom with dense vegetation. D) At mid-depth with dense vegetation. For the sparse vegetation, the first time autocorrelation changes sign is around $t_{lag} \approx 3\ s$. The lower panel shows the autocorrelation for the dense vegetation, the first time autocorrelation changes sign is around $t_{lag} \approx 5\ s$. 39
4.18 Energy density spectra derived for set 2. Left) energy density spectrum of the streamwise velocity component. Right) energy density spectrum of the transverse velocity component. The green lines indicate the sparse vegetation and the purple lines the dense vegetation. The different water depths are presented as follows: solid line (-) 12 cm, dashed line(–) 14 cm and dash-dot line (-.) 16 cm. 40
4.19 Energy density spectra derived for set Q = 60 l/s and H = 14 cm at four locations in the cross-section. Left) sparse vegetation. Right) dense vegetation 41
4.20 The instantaneous flow field at for frame 2241 of the Q60H14 dataset. Left) The streamwise component of the flow. Right) The transverse component of the flow. The arrows indicate the velocity vector of the detected tracers 42
4.21 The instantaneous flow field at for frame 2100 of the Q60H14 dataset. Left) The streamwise component of the flow. Right) The transverse component of the flow. The arrows indicate the velocity vector of the detected tracers 42
4.22 Tracked particle paths originating at the interface. Left) Sparse. Right) Dense. The scaling of the images is the same. 44
4.23 Tracked particle paths originating at 10 cm down slope of the interface. Left) Sparse. Right) Dense. The scaling of the images is the same. 44
4.24 The amount of observed crossings, these are the total amount of crossings extracted from the PTV data. A positive crossing is in the positive y-direction, out of the vegetation. A negative crossing is in the negative y-direction, into the vegetation 45
4.25 The velocity angles, α, at the moment the particles cross the y-axis. The different sets correspond to the sets shown in table 4.3 with similar channel velocities 46
4.26 The velocity magnitudes, $U = \sqrt{u^2 + v^2}$, at the moment the particles cross the y-axis. The different sets correspond to the sets shown in table 4.3 with similar channel velocities 46
4.27 $X - t$ plot of the crossings of the interface. Each dot indicates a negative crossing, each square a positive crossing. The color indicates the angle. The black line indicates the propagation of a vortex. Left) Setting Q60H14. Right) Setting Q70H14 47

5.1 Comparison between the mean velocity profiles obtained with the ADV technique and the PTV technique, for dataset Q60H14 with sparse vegetation. Left) the mean streamwise velocity. Right) Mean transverse velocity 51
5.2 Concept of the flow where momentum and mass exchange governing the strength of the vortices 53

6.1 Inner and outer layer within a partly vegetated flow 57

A.1 Photo of the flume setup, viewing direction is downstream. In the front is a working platform from where the flume could be overseen, followed by the tracer dispenser and in the end the frame on which the camera was installed . . . 65
A.2 The *Vectrino* ADV device with a bubblescreen installed upstream of the probe . . . 66
A.3 The screen on which the RAW ADV data is gathered . . . 67
A.4 The construction in which the depht measuring lasers are placed. The laser reflects on a floater measuring the water depth . . . 67
A.5 The tracer dispenser. Tracers are stored in the metal storage. The round brush sweeps the tracers into the water . . . 68

B.1 Mean *U* profiles at mid-depth . . . 70
B.2 Mean *U* profiles at the bottom . . . 70
B.3 Mean *V* profiles at mid-depth . . . 71
B.4 Mean *V* profiles at the bottom . . . 71
B.5 Mean *W* profiles at mid-depth . . . 72
B.6 Mean *W* profiles at the bottom . . . 72

C.1 Q60H14 flow time series, at location y = 1.2 m . . . 74
C.2 Q60H14 flow time series, at location y = 0.9 m . . . 74
C.3 Q60H14 flow time series, at location y = 0.75 m . . . 75
C.4 Q60H14 flow time series, at location y = 0.65 m . . . 75
C.5 Q60H14 flow time series, at location y = 0.55 m . . . 76
C.6 Q60H14 flow time series, at location y = 0.45 m . . . 76
C.7 Q60H14 flow time series, at location y = 0.35 m . . . 77
C.8 Q60H14 flow time series, at location y = 0.25 m . . . 77
C.9 Q60H14 flow time series, at location y = 0.15 m . . . 78
C.10 Q60H14 flow time series, at location y = 0.05 m . . . 78
C.11 Q60H14 flow time series, at location y = 0.0 m . . . 79
C.12 Q60H14 flow time series, at location y = -0.05 m . . . 79
C.13 Q60H14 flow time series, at location y = -0.10 m . . . 80
C.14 Q60H14 flow time series, at location y = -0.2 m . . . 80
C.15 Q60H14 flow time series, at location y = -0.35 m . . . 81

List of Tables

3.1 The vegetation characteristics for the sparse and dense setup 18
3.2 Conditions for each experiment set 21

4.1 The flow properties of the different experimental setups 27
4.2 Thickness of the inner and outer layer as calibrated with equations 4.1 and 4.2 31
4.3 Exchange regions for the different comparable sets. The set numbers relate to the set numbers in table 4.1, the channel velocities for each set are approximately equal. 45

5.1 Momentum thickness and inner and outer layer thicknesses found in the current research compared to results from flat-bed experiments 52

B.1 Values of the momentum thickness in m. 69

1 Introduction

In 2009 only 20% of all rivers and their riparian areas in Europe were in pristine conditions, and almost all of these rivers were located in arctic or boreal regions. Of the remaining 80%, more than three quarters are affected by human activity in such way that the ecology is in bad status (ECRR, 2014). This degradation of the ecology was caused by canalization for waterborne transport, plant removal to increase flow capacity and decrease flood risks and reducing floodplain area in favor of agriculture. However, in the last decades, the (ecological) value of more natural rivers has become more evident (Costanza et al., 1998). This has resulted in an increasing amount of river restoration projects where river ecology and habitat creation are included in the design requirements and where solutions are sought to engineer rivers where nature, flood protection, and economic activities coexist. River restoration projects involve reintroducing large morphologic features such as meanders, enlarging the floodplains and planting riverine and floodplain vegetation. Instream and floodplain vegetation provide shelter and food for animals living in the riparian areas of rivers and creeks, increasing the biodiversity (ECRR, 2014). It also increases the economic value of the area around rivers and streams through ecosystem services such as recreation and culture (Costanza et al., 1998).

The presence of vegetation on floodplains and in-stream influences the morphological behavior of a river (Millar, 2000) as it tends to stabilize river bends (Vargas-Luna, 2016). There are two aspects of vegetation that contribute to this stabilization; stabilizing the subsoil with the roots and altering the hydraulic conditions by increasing the flow resistance. The hydraulic conditions determine sediment transport and the morphologic activity. Within vegetation patches the hydraulic resistance is locally higher than on the surrounding nonvegetated bed, affecting the hydraulic conditions. Therefore flow velocities are lower inside a patch than in the surrounding area, providing areas where sediment may settle. Accretion inside vegetation patches enhances bank stability and even bank growth (Vargas-Luna, 2016). On a larger scale, the presence of vegetation on the floodplains and riverbanks can determine the morphodynamics of a river section, as it stabilizes channels, it can determine whether a river section is braided or meandering (Millar, 2000).

Aquatic vegetation creates its ecosystem so it can survive under the different hydraulic conditions, by keeping a balance between the nutrients and sediments captured within a patch. The individual plants can grow and strengthen the patch. Erosion and uprooting during high flow conditions balance this growth. This creates a stable ecosystem adapted to the local environmental conditions (Gurnell, 2014; Schoelynck et al., 2012).

The design of river restoration projects, which make use of vegetation, requires knowledge in many different disciplines, e.g., ecology, hydrology, and geology. Coupling the knowledge on the interaction between the flow, vegetation, and sediments is needed to predict hydraulics and changes in morphology. In predictive models, many different aspects need to be accounted for: the spatial and temporal interaction between hydrodynamics, morphodynamics, and ecodynamics on different scales. The flow regime governs the vegetation dynamics and the specific plant species which can survive. At the same time vegetation present in the riparian area (banks, floodplains, and levees), influences the morphology and thereby the flow conditions (Camporeale et al., 2013). In reality, a riverbed or floodplain is not uniformly covered with the same vegetation species, but there are patches of different species distributed over the riverbed, exhibiting a certain amount of self-organization (Schoelynck et al., 2012). Flow and sediment transport processes in and around these patches need to be understood to be able to make predictive models for morphodynamics.

In flow and morphology modeling software vegetation can be added to the boundary conditions, by assigning parameters for the vegetation density and drag to a grid cell (Delft3D manual). The morphological changes due to the presence of the vegetation are currently hard to predict. Because the different flow properties inside vegetated flows and non-vegetated flows, sediment transport relations cannot be translated one-on-one from 'normal' open-channel flow to vegetated flow. Relationships for the bed shear stress and shear velocity in open-channel flow are derived from the logarithmic flow profile. In vegetated flow, the profile is not logarithmic but dependent on vegetation properties. Because sediment transport models are derived for fully developed open channel flow with a logarithmic flow profile. In vegetated flow the flow profile depends on specific vegetation properties, for uniform vegetation, this results in a depth constant flow velocity (Nepf, 2012a). Therefore the traditional sediment transport relations (based on Shields) are not valid in vegetated flows. Secondly, because turbulence and large-scale structures are hard to model correctly. Especially large coherent structures at the interface between vegetated and non-vegetated flow cause an exchange of mass and momentum between these flows (Nepf, 2012b).

Much research has been done on the understanding of flow in and around vegetation, both in laboratory experiments as well as with mathematical models. The insights gained from these experiments, field research and theoretical knowledge development can be used to make some predictive models for the effect of vegetation on the morphodynamics, many of these models are reviewed by Vargas-Luna et al. (2014). These models can predict flow profiles for infinite patches of vegetation, where the flow has reached a steady state and the time and spatially averaged flow is constant.

1.1. Problem statement

Different models which can describe sediment transport through infinite vegetation patches with steady, uniform flow have been made (Vargas-Luna et al., 2014). These are the basis of vegetation modules for flow models, such as Delft3D. They mimic the flow capacity but not the exact flow. Modeling of the morphology of vegetated flow is mostly done with correction factors which have proven to give reasonable results but are not based on the physics of the flow. The physics behind hydraulic conditions determine sediment transport and the morphologic activity.

At the interface between vegetation and no vegetation a shear layer develops and mass and momentum is exchanged between the two zones through coherent structures (Nepf, 2012a,b; White and Nepf, 2007, 2008; Zong and Nepf, 2010). The influence of these patterns on sediment transport is still subject to research, both suspended and on the bed, The development of these structures and the depth-averaged values has been studied for flat-bed conditions (White and Nepf, 2007, 2008; Zong and Nepf, 2010). From these studies, the flow patterns in this region can be derived. However, this cannot be generalized for all vegetated flows. Missing links are the near-bed flow conditions and the influence of bed topography.

These coherent structures could be modeled with small grid cells, through large eddy simulation. In models on reach scale, these structures are part of parameters for the turbulent viscosity and diffusion. To what extent these structures could create an exchange of sediments, bed load and suspended load, between vegetated flow and the free flow is yet unknown. However, this is important for the sediment balance in these flows and the morphologic changes. When this is known more theory based models can be constructed.

1.2. Objective and research questions

The objective of this thesis is:

To obtain a better *understanding* of the coherent *flow structures* in the interface between vegetated and non-vegetated river bed and the effect of these structures on *sediment transport mechanisms*.

To reach this objective, four research questions are given below. Combined, these questions will set a next step in understanding vegetated flows and sediment transport in vegetated flows.

1. What are the factors influencing the shear layer in vegetated flow?

2. How can an experiment be designed to make relevant observations on sediment transport in and around vegetation?

3. What is the influence of the vegetation density on sediment transport mechanisms in the transition zone?

4. Is it possible to explain bank growth patterns from vegetation density?

1.3. Approach

This research consists of two main parts: a literature study and an experimental study. These two parts are inter-related and are both answering different aspects of the research questions. The literature study focuses on the current knowledge of flow through and around vegetation. Next to the flow study, other aspects of vegetated flows are treated to make a full analysis of the critical features and aspects that influence or are influenced by the flow, such as the morphology. The main parameters and processes that influence the coherent structures at the interface and may influence sediment transport in this area are derived from the literature study and are input for the design of the experiment. The literature study is used in to place the results of the experimental study in a larger context.

The experimental part of this study is carried out at the Environmental Fluid Mechanics Laboratory at Deft University of Technology in a 20 m long and 3 m wide shallow water flume. In the flume, the flow can be studied under predefined constant conditions. A compound channel is constructed with a main channel and a floodplain. Between the channel and the floodplain, a transverse slope is present. On the floodplain, model vegetation can be placed in different vegetation densities. The main goal of the experiments is to answer the third research question as well as to verify whether results from literature are valid for the experimental setup. Also the experiments aim to gain further insight into the flow structures at the interface. This is done with two different techniques: Acoustic Doppler Velocimetry and Particle Tracking Velocimetry. Acoustic Doppler Velocimetry is used to map the flow properties in a cross-section, and the Particle Tracking Velocimetry is used to map the near-bed conditions and possible sediment paths. The exact details on the experimental setup and methods can be found in chapter 3 Methodology.

The last research question is answered through relating the experimental results to literature and proposing further steps which need to be taken to test some insights gained from the experiments in a more complex setting. This can be done based on a conceptual model of the physical processes backed by the results of the experiments and literature study.

While many aspects govern the flow in and around vegetation, the experiments done in this research are limited to emergent vegetation, where the vegetation is represented by wooden cylinders. The flow properties are measured in the fully developed zone. This to decrease the number of variables and distinguish between different processes. Within the literature study, the influence of plant morphology and submergence are given to place the interpretation of the results into larger perspective.

1.4. Outline

Chapter 2 gives the literature study and some background information starting with an overview of the morphology of vegetated rivers and specific aspects that influence the morphology on a large scale. The literature gradually zooms into the fluid mechanics at the scale of an individual patch of vegetation and how this is conceptualized in experimental studies. This chapter also covers sediment transport mechanism important for flow through vegetation and over complex bed topography.

The experimental setup and methods used for the measurements during the experiments and the result analysis are explained in chapter 3. Additional figures and pictures of the flume are given in appendix A.

In chapter 4 the results of the experiments are given. Figures and tables support the observations from the experiments. This chapter is supported by appendix B and C, which gives extra information and supporting figures which may be read for further clarification of the observations.

The results and the experiment itself are discussed in chapter 5. This chapter also reflects on the experimental setup and the measuring techniques used. Further steps which may be taken into resolving a model for sediment transport of vegetated flow and direct implications for modeling practice are elaborated. The last part relates to vegetation in real natural circumstances.

The last chapter gives the conclusions of this research by answering the research questions. Also, the main recommendations for implementation and further research are summarized.

2

Literature and theoretical framework

This literature study reviews the current state of science on the topic of the influence of vegetation on hydrodynamics and morphodynamics and their interrelations. This has four main focus points: 1) the morphology of vegetated river flows, 2) the impact of conceptualization of vegetation, 3) the characterization of flow and sediment transport in and around emergent vegetation and 4) the influence of morphological features on sediment transport, mainly focusing on transverse slopes of (vegetated) river banks and bars.

2.1. Morphology of vegetated flow systems

Plants are ecosystem engineers: vegetation provides a situation such that the plant species in the vegetation has an optimal habitat to survive. This includes altering the morphology. However, the primary control for the morphology is the flow regime (Gurnell, 2014) as it governs the locations where vegetation can survive and erosion and deposition of sediment. The locations on the floodplain where new vegetation can be planted in natural systems are governed by the stream energy. In low-energy systems, pioneer plants can be introduced into the main stream, while in high-energy systems the pioneer plants can only survive at places on the floodplain further away from the main stream where they influence the flow during flood events only (Gurnell et al., 2016). The different processes that influence the morphology in vegetated flows consist of different inter-connected feedback loops between the flow, sediment properties, vegetation and the morphology itself (Curran and Hession, 2013).

The influence of planting or removing vegetation on floodplains has been studied in many fields and experimental studies. Concluding that in most situations floodplain or bank vegetation increase bank stability and creates deeper and narrower channels (Camporeale et al., 2013). Three principal processes are identified that contribute to the enhanced bank stability: 1) lower near-bank velocities which result in less erosion, 2) the strengthening of soil by roots and 3) enhanced deposition of wash load inside patches (Millar, 2000). For moderate rivers, this results in more stable channels. Under similar flow regime and sediment grading, a vegetated river may be meandering while after extensive removal of riparian forest the same reach shows a braided regime (Millar, 2000). While new vegetation is planted upon bars in a braided system, the channels at first tend to become smaller and deeper while the bars become more stable. On longer time scales the system may become meandering (Tal et al., 2004). The transition between a meandering system and a braided system is given by a relation for the transition slope proposed by Millar (2000): $S^* = 0.002 d_{50}^{0.61} \varphi'^{1.75} Q^{-0.25}$ where d_{50} is the median grain size, φ' the bank sediment fiction angle which increases with increasing vegetation density and Q is the bankfull discharge. According to this formula the slope at which a river becomes braided increases with increasing vegetation density. This empirical formula is based on field data and only valid for perennial rivers. Ephemeral rivers tend to show different behavior when vegetation is introduced on banks. This happens mainly because of properties of species that can survive in climates governing ephemeral rivers (Coulthard, 2005).

Rominger et al. (2010) have shown that vegetation on the inner bend of a meandering river reduces the effect of the secondary circulation. The presence of vegetation on the inner bend focuses the flow into the main channel during flood events, and the vegetative drag is too high for the secondary circulation to develop inside the vegetated area. This enhances deposition within the patch due to lower flow velocities while the edge of the vegetation erodes, resulting in a steeper but more stable inner bend. The flow at the interface of

the vegetation patch and the main stream alters in this case. To what extent this flow pattern enhances or dampens the effect of the erosion and deposition pattern is not researched in this case.

Observations on the channel and floodplain morphology after the planting or removing vegetation show that vegetation has a stabilizing effect on the banks. This results in more stable bars in braided rivers or even the transformation of a braided system into a meandering system (Curran and Hession, 2013). The patterns of erosion and deposition are governed by the flow patterns in and around vegetation patches. To predict these patterns the flow processes during over-bank flow need to be better-understood (Camporeale et al., 2013). Lower transport capacities, due to lower velocities when the banks are inundated, result in enhanced sediment entrapment within vegetation. This governs the stabilization of bars and banks. It is important to keep in mind that the studies cited in this section are focused on alluvial sand and gravel bed rivers. Rivers formed in a clay bed show different behavior, as clay is a cohesive sediment, and are not within the scope of this research.

2.2. Characterization of vegetation

As there are many different plant species and various environmental conditions within streams and their riparian areas, there are also many different aspects of the plants that influence the flow. For simplicity, most laboratory experiments use rigid cylinders as idealized plants (e.g., White and Nepf (2007); Zong and Nepf (2010) and others). The influence of cylinders on flow is quite well studied. Cylinders have a uniform geometry over height. Therefore the relevant parameters for flow, such as drag, are also uniform over the depth for each model plant. Also, computational flow models often use only idealized uniform parameters for vegetation patches. In reality, plants have branches, leaves and are often not cylindrical. This implies that the parameters are not uniform but vary spatially and over depth. Therefore the flow velocity is variable over depth depending on the mean geometry of the plants. More complex plant geometries increase the complexity of the flow and mixing processes.

Because of the different hydraulic regimes, the plant species that occur in-stream are different from those on the floodplains. In-stream vegetation often has flexible stems to be able to adapt to different flow velocities. During extreme flow conditions, the bending of the plants lowers the drag and prevents uprooting. On the floodplains, which are only inundated during high discharges, more woody (rigid) vegetation is present. Also, branches, foliage, and stem geometry influence the flow as these characteristics depend on the specific plant species and vary per individual plant. Therefore this aspect is hard to capture in a general model.

2.2.1. Vegetation density

Different parameters can indicate the plant density of a vegetation patch. The projected plant area per unit volume, $a\,[L^{-1}]$, the volume fraction of the plants, ϕ, or the total volume of canopy per square area, λ which has the dimension L. The parameter a is often used in combination with the drag coefficient to indicate the friction coefficient of a patch. The plant morphology can influence these parameters. Depending on the specific features the vegetation density can vary over depth as well as the drag coefficient. In this research the volume fraction of the plants is referred to as the vegetation density, higher volume fractions mean denser vegetation. Floodplain vegetation varies for different kinds of vegetation, where mangroves are one of the densest types with $\phi = O(0.1)$ with a maximum up to $\phi = 0.45$ (Nepf, 2012a) and pioneer vegetation has densities in of order 0.001. Floodplain forests such as willows and herbaceous vegetation have densities of order 0.01 (Vargas-Luna et al., 2016). These two differ in stem diameter amount of stems per square meter.

2.2.2. Submergence

The submergence of the plants, the part of the water column that is occupied by the vegetation, h_v/H, is important for the vertical flow profile and for the flow capacity of a vegetated channel (Buckman, 2013). Within the vegetation, the maximum velocity is determined by the vegetation induced friction. When the vegetation is submerged the flow profile above the vegetation is logarithmic, similar to the logarithmic profile of open-channel flow, but transposed by the vegetation velocity(Nepf, 2012a). Deeply submerged vegetation, up to 10% of the total water depth, can be treated as bed roughness while for submergence of 30% and higher the vegetation should be accounted for in the flow profile (Baptist et al., 2007; Nepf, 2012a). At the top of submerged vegetation, a shear layer exists which induces vortices in the vertical plane. Fully emergent vegetation does not have this additional shear layer at the top of the vegetation is higher than the water surface. The vegetation induced friction determines the entire vertical flow profile in this case. The next section elaborates further on the flow through emergent vegetation. On floodplains, the submergence of the vegetation

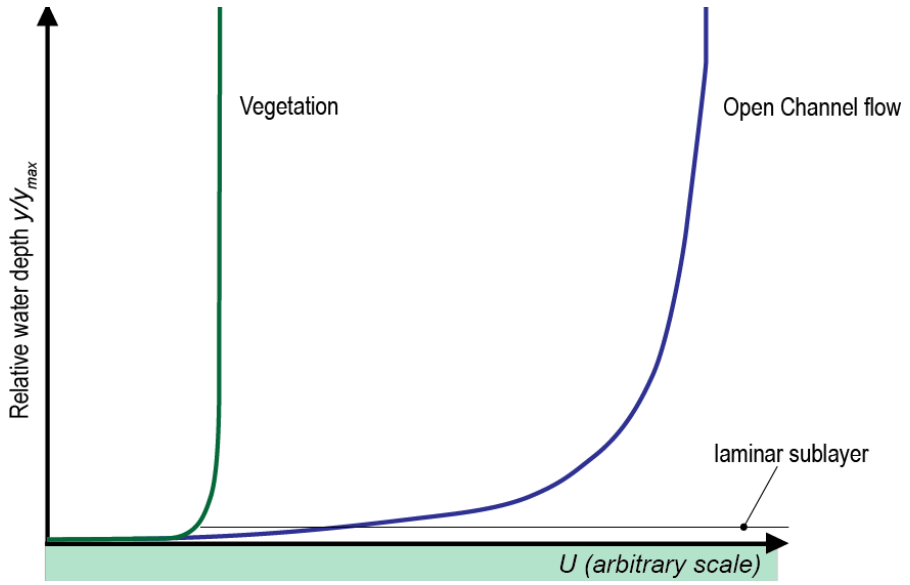


Figure 2.1: Flow profile in vegetated flow (green line) and in open-channel flow (blue line). In vegetated flow the velocity is constant over the depth except near the bed in the laminar sub layer, where the flow is still influenced by the bed. In open channel flow the only source of friction is the bed, the flow follows a logarithmic profile over depth, $u(y) = \frac{u_*}{\kappa} \ln\left(\frac{y}{y_0}\right)$.

depends on the water level and the plant height.

The main focus of this study will be on rigid emergent vegetation, but the heterogeneity of vegetation needs to be kept in mind in the analysis and interpretation of experimental results. Hydraulic processes and especially the sediment dynamics are highly influenced by the different plant and patch morphologies, and therefore caution needs to be taken when results are extrapolated to other circumstances.

2.3. Flow through emergent vegetation

Flow through vegetation is highly affected by the drag from the stems and leaf of the inundated parts of the plants. This section describes the flow through an infinite patch of emergent vegetation, where there are no influences of walls or channel flow at the edges of the vegetation.

2.3.1. Turbulence

In turbulent flows energy from the mean flow is dissipated through turbulent eddies into heat. The size of the largest eddies is the turbulence length scale (ℓ) which depends on the smallest length scale in the flow. In open channel flow, the turbulence length scale depends on the smallest length scale of the geometry, which is the water depth in most environmental flows. Within vegetated flows, the smallest length scale depends on the vegetation density, specifically on the spacing between the plants, S_n, and the plant diameter, d. Eddies larger than the smallest of these length scales are dissipated by the vegetation (Nepf, 2012a).

In open channel flow, the size of the eddies increases with increasing distance from the bed, resulting in the law of the wall and dictating the logarithmic flow profile, where the flow velocity is determined by the bed friction. Within vegetated flows, the influence of friction from the vegetation is much larger than the influence of bed, except for a thin layer near the bed where the bed friction is still dominant. Assuming rigid vegetation with a uniform shape over depth this results in a depth constant flow profile as shown in figure 2.1 (López and García, 1998; Nepf, 2012a; **?**).

In vegetated flows with particle Reynolds numbers, $Re_p = \langle\overline{u}\rangle d/\nu > \approx 200$, the flow is turbulent (Nepf, 2012a). For turbulent flows in the area of depth constant flow velocity, the turbulence in vegetated flows is generated by the vegetative drag; the rate of turbulence production is equal to the rate of energy extraction from the flow. The generation of turbulent kinetic energy is balanced by the viscous dissipation on the Kolmogorov scale. Therefore the turbulence intensity can be derived from the vegetation drag given in equation 2.1 Nepf (2012a,b).

$$\frac{\sqrt{\langle \overline{k} \rangle}}{\langle \overline{u} \rangle} \sim (C_D a \ell)^{1/3} \tag{2.1}$$

From equation 2.1 it can be concluded that the turbulence intensity increases with increasing vegetation density, while the flow velocity is constant. However, the flow velocity is related to the vegetative friction with a quadratic law. This results in much lower flow velocities within denser vegetation under similar driving forces, gravity from bed and surface gradients. Therefore the turbulence within the dense vegetation is lower than in sparse vegetation. The turbulence intensity affects incipient motion near the bed and settling of sediments, which is further analyzed in section 2.5.

2.3.2. Drag

Flow in vegetated areas has to move around each plant or stem. The deflection of the flow upstream and vortex shedding downstream of a plant creates additional drag. For individual plants a drag coefficient, C_D can be determined on the basis of the plant geometry. In a vegetation patch, however, the wake of the individual plants interfere. The amount of interference depends on the distance between individual plants and the stem diameter, and therefore on the vegetation density. This complicates the determination of the drag coefficient.

Tanino and Nepf (2008) have found that the value of the drag coefficient depends on the particle Reynolds number of individual stems and two coefficients, α_0 and $alpha_1$, which depend on the vegetation density as given in equation 2.2. α_0 scales linearly with the vegetation densities between $\phi = 0.091$ and 0.15, varying between 25 and 84 respectively. Above $\phi = 0.15$ the value for the drag remains constant. The value of α_1 can be determined by the empirical relation of equation 2.3. These values are determined for rigid cylinders in a staggered grid and therefore cannot be used for other plant morphologies. However, Koch and Ladd (1997) have shown that the vegetative drag is independent of the arrangement of the plants.

$$C_D = 2\left(\frac{\alpha_0}{Re_p} + \alpha_1\right) \tag{2.2}$$

$$\alpha_1 = (0.46 \pm 0.11) + (3.8 \pm 0.5)\phi \tag{2.3}$$

The influence of the plant geometry and the flexibility on the drag coefficient is significant and differs for each plant species. Flexible vegetation adapts to the flow velocity such that the flow force acting on the plant is balanced by the restoring force as result of the bending (Nepf, 2012b). The shape influences the drag coefficient of each plant. Aquatic species tend to have more aerodynamic shapes, decreasing the drag coefficient and therefore the drag force to prevent uprooting. The flexible plants with aerodynamic shapes adapt easily to the flow velocity and direction, making the determination of the drag coefficient more dependent on the flow characteristics.

For modeling purposes, the value of the drag coefficient is often chosen as unity (Armanini et al., 2005; Vargas-Luna et al., 2016). Multiplied by the projected plant area per unit volume, a, this creates a friction coefficient for vegetated flows which depends on vegetation density. This friction coefficient is used in the momentum balance. Using measurements in a uniform steady flow. The drag force and coefficient can be derived with the momentum balance described in the sections below.

2.3.3. Momentum balance

The mean flow velocity in vegetated flow can be derived with the momentum balance from the Navier-Stokes equations. Within vegetation, the flow velocity is highly variable per location. Therefore both temporal and spatial averaging is needed to derive the mean flow velocity. To describe the flow the coordinate system is defined as x horizontal in the flow direction, y horizontal perpendicular to the mean flow direction and z perpendicular to the bed positive upward. The velocity components $\overrightarrow{u} = (u, v, w)$ correspond to the directions (x, y, z).

Equation 2.4 gives the time and space-averaged streamwise x-momentum balance for flow through vegetation. First, the time average is taken, which is indicated with an overbar. Deviations from the temporal mean are indicated with a single prime. The time average must be taken over an interval long enough to capture the time scale of the velocity fluctuations in between the stems, thus an interval larger than the period of the vortex shedding.

After the time averaging the equations are also averaged in space, following the same principle as for time averaging. The spatial mean is indicated with the angular brackets and deviations with double primes.

The spatial mean must be taken over small increments in the vertical direction to obtain a velocity profile over the depth, but the averaging volume needs to cover multiple stems in the horizontal plane to obtain a good representation. (Nepf, 2012a,b). Assuming a uniform vegetation density, there are no gradients in the horizontal plane.

$$\frac{D\langle\overline{u}\rangle}{Dt} = -\frac{1}{\rho}\frac{\partial\langle\overline{p}\rangle}{\partial x} - \frac{\partial}{\partial z}\langle\overline{u'w'}\rangle - \frac{\partial}{\partial z}\langle\overline{u}''\overline{w}''\rangle + \nu\frac{\partial^2\langle\overline{u}\rangle}{\partial z^2} - D_x \tag{2.4}$$

$\frac{1}{\rho}\frac{\partial\langle\overline{p}\rangle}{\partial x}$ is the pressure gradient, $\frac{\partial}{\partial z}\langle\overline{u'w'}\rangle$ represents the time averaged turbulent diffusion, $\frac{\partial}{\partial z}\langle\overline{u}''\overline{w}''\rangle$ the space averaged turbulent diffusion, $\nu\frac{\partial^2\langle\overline{u}\rangle}{\partial z^2}$ the viscous diffusion and is a bulk term for all other driving and resisting forces. Of the diffusion terms the space-averaged turbulent diffusion is the most significant one for flow through vegetation in the turbulent regime, $Re_p > \approx 200$.

The bulk term, D_x, represents the effect of the bed and vegetation drag. As given in section 2.3.1, the contribution to of the vegetation to the friction is much larger than the bed friction. Therefore the bed friction is neglected. For rigid elements, the drag is relative to the square of the velocity through the quadratic drag law in equation 2.5.

$$D_x = \frac{1}{2}\frac{C_D a}{1-\phi}\langle\overline{u}\rangle|\langle\overline{u}\rangle| \tag{2.5}$$

The length scale over which the mean flow and turbulent fluctuations adjust to the drag, or the efficiency of the vegetation to dissipate momentum from the mean flow, is called the vegetation drag length scale (Belcher et al., 2003), and is defined by:

$$L_c = \frac{2(1-\phi)}{C_D a} \tag{2.6}$$

The bed friction, or bed drag, is not accounted for in this momentum balance. This component determines the boundary layer at the bed. Compared to the drag created by the presence of vegetation this value is relatively small. For determining the flow near the bed, this value will be important as both the bed and vegetative drag are present at that point, and the bed drag cannot be neglected. However, the bed drag is neglected for the analysis of the influence of different vegetation characteristics on the flow, as the flow higher up in the water column is mainly determined by the presence of vegetation.

The momentum equation (equation 2.4) can be simplified assuming that the contribution of the drag in the dissipation of momentum is significantly larger than the contributions of the viscous and turbulent diffusion. Equation 2.7 gives the simplified momentum equation for uniform steady flow: $\frac{D\langle\overline{u}\rangle}{Dt} = 0$. Through the relation of pressure in a water column, $p = \rho g H$, the pressure gradient can be rewritten into a water level gradient (H is the elevation of the water level above the reverence level $z = 0$).

$$g\frac{dH}{dx} = -D_x = -\frac{1}{2}\frac{C_D a}{1-\phi}\langle\overline{u}\rangle|\langle\overline{u}\rangle| \tag{2.7}$$

This equation not valid in the boundary layer where the viscous stresses dominate, and the vegetative drag is larger than the drag from the bed roughness. The driving forces on the left-hand side of equation 2.7 are not dependent on the z coordinate, but only on pressure difference in the streamwise direction and the bed slope. Then on the right-hand side of the equation, the energy is dissipated by the drag. As the velocity is averaged over a thin horizontal plate and a can vary over depth spatially, the time-averaged velocity is inversely related to the density; higher density implies lower velocities. In flow through emergent vegetation, the driving forces are almost entirely balanced by the vegetative drag.

In fully developed flow and with vegetation that has a uniform density over depth this gives a constant flow velocity over depth. Only near the bed, where the bed shear is still relevant, a logarithmic flow profile is present. Figure 2.1 gives a flow profile for emergent vegetation with rigid cylinders compared to a flow profile in open-channel flow.

2.4. Flow at the interface between vegetation and no vegetation

Up to this point, a vegetation patch of infinite width and length has been analyzed. The theory and formulas shown are only valid in the middle of a patch where the flow is not influenced by any boundary conditions. However, at the edges of a vegetation patch, where the bed becomes bare, specific flow phenomena occur

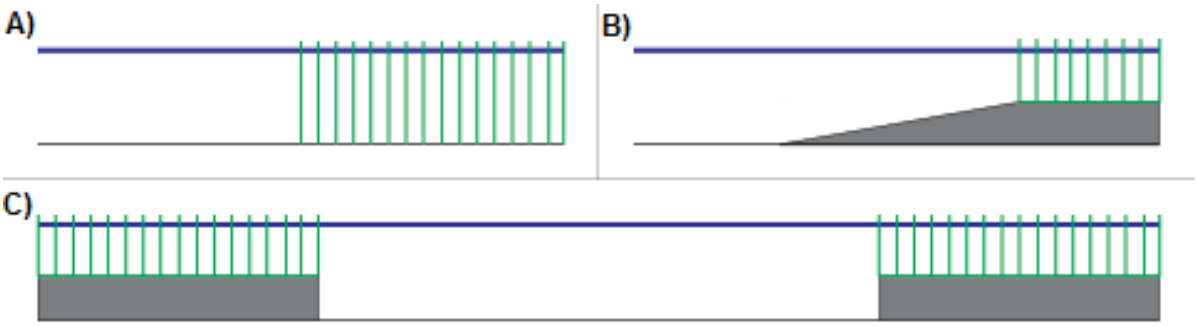


Figure 2.2: Different configurations of compound channels with a vegetated floodplain and a non-vegetated channel. A) The situation as described in the articles of Buckman et al. (2014); White and Nepf (2007, 2008); Zong and Nepf (2010). B) The compound channel as described by Truong et al. (shed) with a gentle slope between the floodplain and the main channel. C) The compound channel as described by Dupuis et al. (2017)

which lead to the exchange of mass and momentum between the non-vegetated flow and the vegetated patch. Such flow is indicated as compound channel flow, where different areas can be identified in the cross-section. Most research on vegetated compound channels focus on horizontal bed conditions (Buckman, 2013; White and Nepf, 2007, 2008; Zong and Nepf, 2010). However situations the vegetated bed is elevated relative to the main channel have also been studied, either with a transverse slope or an elevation step between the channel and floodplain (Dupuis et al., 2017; Truong et al., shed). The introduction of bed topography complicates flow structures, as secondary circulations become more important, especially with sharp corners in the geometry (Dupuis et al., 2017). The different bed geometries are shown in figure 2.2.

These studies have observed the development of strong, coherent vortices at the interface between the floodplain and the channel, driven by a streamwise velocity gradient in the cross section dU/dy. This gradient is caused by the higher drag on the floodplain due to the presence of vegetation. The vegetation drag also limits the penetration of the vortices into the vegetation, whereas they can freely develop in the channel, this creates asymmetrical vortices (White and Nepf, 2007). In the studies with a horizontal bed, the effects of secondary flow structures due to sharp edges in bed elevation are not present. Therefore, these studies give a good insight into the flow structures resulting from the presence of the vegetation only.

In the channel, the friction is much lower than within the vegetation. This results in a difference in flow velocity between the vegetated and non-vegetated part of the channel. A shear layer develops across the interface between the two channel parts. Mean flow profile in the cross-sectional direction has an S-shape. Within this shear layer mass and momentum is exchanged (White and Nepf, 2007, 2008), through Kelvin-Helmholz like vortices (White and Nepf, 2007). Streamwise momentum is transported in the cross-sectional direction towards the vegetation.

At the upstream end of the vegetation, the flow has to adjust to the presence of the vegetation. The development of the shear layer can be divided into two regions. The upstream region where the flow diverges towards the channel due to the lower flow capacity in the vegetation. In the divergence region, the flow velocity in the vegetation decreases. In the second, downstream region the vortices develop until an equilibrium is reached. On a horizontal bed and a vegetation density of $\phi = 0.02$, Zong and Nepf (2010) have found that a divergence region of 3 m is followed by the development of the vortices over a second 3 m. These distances increase with a decreasing vegetation density.

2.4.1. Mean transverse flow profiles in equilibrium

When the flow in a vegetated compound channel is fully developed, a steady and uniform flow in the streamwise direction, the mean velocity profile in the transect can be described in two parts, one governed by the vegetation, the inner region, and the other by the channel flow, the outer region.

White and Nepf (2007, 2008) have found that when the flow velocity in the outer region is normalized by the channel velocity the cross-sectional flow profile is independent of the vegetation density. The flow velocity in the outer region is related to the water depth and the bottom friction and shows a boundary layer profile in the cross-section which is logarithmic. This region can be described with equation 2.8.

$$U_O(y) = U_m + (U_C - U_m)\left[\frac{y - y_m}{\delta_O} - \frac{1}{4}\left(\frac{y - y_m}{\delta_O}\right)^2\right] \tag{2.8}$$

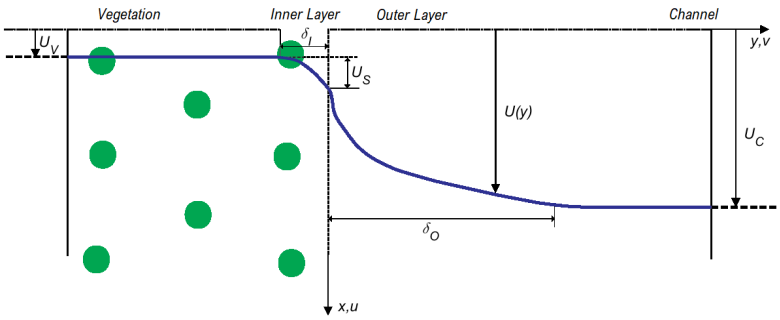


Figure 2.3: The different zones and the length scales in the cross-sectional profile of the mean velocity. Adapted from White and Nepf (2008).

Within the inner region, the profile scales according to a non-linear tangent function, as can be found in free shear layers. This part of the profile scales with the inner layer thickness where the velocity scales with the slip velocity (U_S), the velocity at the point where the hyperbolic tangent has its inflection point. This point is for natural vegetation densities at the interface (White and Nepf, 2007), although at low vegetation densities, $\phi < 0.01$, they have found that this location lies at twice the stem diameter of the cylinders away from the interface, towards the channel.

$$u(y) = U_V + U_S\left(1 + \tanh\left(\frac{y - y_0}{\delta_I}\right)\right) \tag{2.9}$$

The resulting profile consists therefore of three different regimes, the channel and vegetative regimes with constant mean velocity and in between the shear zone which is divided over the inner and outer region. Therefore four different zones, as given in figure 2.3, can be identified with their different governing length scales (White and Nepf, 2007, 2008):

1. the vegetation zone where the velocity, U_V, is uniform and described by the theory for vegetative flow which is a balance between the vegetative drag and the driving surface slope.
2. the inner layer of the shear zone, with governing length scale δ_I, where the velocity profile is determined by the vegetation. The main parameter governing the width of the inner layer is the vegetation density
3. the outer layer of the shear zone, δ_O, where the profile is governed by the channel. The width of the outer layer is governed by the channel velocity.
4. the channel which has a uniform velocity, U_C. In this zone, the mean velocity can be calculated with the theory of open-channel flow where the resulting velocity is a balance between the bed friction and the surface slope.

In a steady and streamwise uniform situation, the velocity in zones 1 and 4 can be determined using the balance between the driving and resisting forces. These are gravitation and drag respectively. Therefore the spatially averaged velocity in zone 1 can be calculated with equation 2.7, rewritten to:

$$U_V = \sqrt{\frac{2gS}{C_D a}} \tag{2.10}$$

In zone 4 the governing balance is between the bed drag and the gravitational force giving:

$$U_C = \sqrt{\frac{2gS}{c_f}} \tag{2.11}$$

In these equations, S is the combined effect of the bed and surface slope and c_f is the friction factor for the bed. The bed friction can be neglected in the vegetated zone as it is much smaller than the vegetative drag. The velocity at the interface (y_0) is called the slip velocity which has been found to be 5 to 10 % of the channel velocity for flat-bed situations (Buckman et al., 2014).

The inner and outer layer are both parts of the shear layer, and the velocity profile in this zone is more complicated. The thickness is determined by the vegetation density while the thickness and characteristics of the outer layer are determined by the channel velocity and the water depth. This implies that although the shear, and in addition to that also the coherent structures, originates in the vegetation, the characteristics of this shear layer are determined by the channel characteristics. White and Nepf (2008) have derived relations for the inner layer (equation 2.12) and the outer layer. Because the thickness of the outer layer is also dependent on the water depth, the relation derived for a flat-bed cannot be directly used for different bed topographies.

$$\delta_I \approx \max\left(0.5(C_D a)^{-1},\, 1.8d\right) \tag{2.12}$$

With equations 2.8 to 2.12 a rough estimation for the cross-sectional flow profile can be made. A more elaborated way to calculate the slip velocity and the full flow profile is given in White and Nepf (2008). There relations derived by White and Nepf (2008) are based on a data set with vegetation densities between $\phi = 0.02$ and $\phi = 0.10$ and a flat bed.

2.4.2. Reynolds stresses

The shear creates coherent motion in Kelvin-Helmholz like vortices around the interface. Due to the presence of the vegetation, these vortices are asymmetrical. The width of the vortices is larger in the channel than in the vegetation. This asymmetrical shape is due to the larger friction in the vegetation.

The lateral Reynolds stress is defined by $\overline{u'v'}$, and indicates the amount of streamwise momentum transported in the transverse direction. The observed Reynolds stress is negative and has a minimum at the interface of vegetated bed to non-vegetated bed, in all the different bed topography studies (Dupuis et al., 2017; Truong et al., shed; White and Nepf, 2007, 2008; Zong and Nepf, 2010). This indicates a net flux of momentum towards from the channel towards the vegetation.

The vortices cause fluctuations around the mean streamwise and transverse velocity components. These variations result are the result of vortices and are called sweeps and ejections. The sweeps (negative u' and positive v') and ejections (positive u' and negative v') are responsible for the exchange of mass and momentum between the floodplain and the channel. The exchange is strongest near the interface. The point of maximum shear and the minimum Reynolds stress coincide at the interface, indicating maximum energy production at this location.

2.4.3. Near-bed conditions

No relevant studies of near-bed conditions within the shear layer have been found. However, it can be expected that the vortex structures are weaker near the bed, as the difference between the flow velocity near the bed in the vegetation and the channel is smaller. Phase differences can be expected, because of the dissipation of flow energy by the bed friction.

Near the bottom, the vortices appear to spiral inwards whereas the vortex spirals outward on the water surface (White and Nepf, 2007). Because of mass balance, this has to introduce secondary circulation in the cross-section with upward fluxes in the center of the vortex and downward flux at the edges. The center of the vortices is located at the length scale of the outer layer into the channel (White and Nepf, 2007).

2.5. Sediment transport in vegetated flows

2.5.1. Initiation of motion in vegetated flow

In open channel flow initiation of motion is calculated with the Shields parameter. The derivation of the Shields parameter is done for fully developed open channel flow, having a logarithmic flow profile, without bed topography. In this approach, a critical bottom shear stress gives initiation of motion. As vegetated flow does not have this profile, a different approach needs to be used to predict initiation of motion. Yang et al. (2016) have proposed a method which uses the turbulent kinetic energy near the bed which can be translated to a shear stress. This resulted in the following relation for the critical velocity in the channel:

$$\frac{U_{crit}}{U_o} = \frac{1}{\sqrt{1 + C\phi^{2/3}}} \tag{2.13}$$

where U_o is the critical velocity for incipient motion for open-channel flow and C a constant depending on the ratio between the vegetative drag and the bed drag. As noted at similar flow velocities the shear stress increases with increasing density.

The increased level of turbulent kinetic energy and the larger velocities in sparse vegetation lead to a loss of fine sediments inside these patches (Curran and Hession, 2013). The low velocities inside dense vegetation result in the capture of fine sediments. The additional decrease of flow velocity inside dense vegetation has a stronger effect than the increase of turbulence, while in sparse vegetation the opposite holds.

2.5.2. Transport in the shear layer

Ejections can transport suspended particles up to twice the outer layer width into the channel. This indicates that the vortex motions are responsible for significant fluxes and can transport mass and momentum over these length scales (White and Nepf, 2007). At the upstream end of a long vegetation patch, the transport of sediments into the vegetation is governed by advection (Zong and Nepf, 2010). The sediments settle within the vegetation, where the settling location relative to the upstream end depends on the grain size (Sharpe and James, 2006).

In the transverse shear layer, fine sediments can be transported through the shear layer. The distance particles can travel into the vegetation depends on the sediment size, flow depth, and the vegetation density (Sharpe and James, 2006). The fine sediments considered are part of the suspended load and settle within the vegetation. The ability of the vortices to transport bedload into the vegetation has not been researched yet.

2.6. Transverse slope effects

In rivers, the bed levels of the channel and floodplain differ. The floodplain elevation is higher than the channel. Therefore an arbitrary slope between these levels is present, which is transverse to the main flow direction. The slope angle of the transverse slope depends on the sediment properties, the location in the river and hydraulic and ecological conditions. The influence of a transverse slope on the flow properties and sediment transport mechanisms is treated in this section. This is split into two parts; the influence of a compound channel on the hydraulics and the effect of a transverse slope on sediment transport. Both sections aim to obtain a better insight into the effects of morphology on the hydraulics and sediment transport. As floodplains are often vegetated, and both effects of vegetation and the elevation are of influence, they need to be understood separately to assign phenomena to the most probable cause.

2.6.1. Flow in a compound channel with a transverse slope

The flow in a compound channel, with a channel, transverse slope, and floodplain, is mainly governed by the difference in bed level between the main channel and the floodplain and therefore the water depth at these locations. The difference in water depth and bed friction results in a difference in flow velocities in the channel and floodplain, with a shear layer in between. The flow in the shear layer is governed by coherent structures, similarly to the flow in a partly vegetated channel, which causes exchange of mass and momentum between the main channel and the floodplain. (Prooijen et al., 2005).

The peak of the Reynolds stress is collocated with the point transition in the bed from the floodplain to the transverse slope (Shiono and Knight, 1991). In contrast with the peak shear stress in the interface of a vegetated compound, channel flows this peak is not as sharp and is more symmetrical. The maximum Reynolds shear increases with an increasing difference in flow velocity between the floodplain and the channel, thus with decreasing water depth (Shiono and Knight, 1991). As the flow velocity increases with the water depth the difference between the flow velocities and the momentum within the flow decreases with the increasing water depth, decreasing the velocity gradient in the transverse shear layer.

At the upstream end of a vortex the transverse component of the flow is directed from the channel towards the floodplain. As the water depth decreases the flow accelerates in this direction due to convergence, the maximum transverse velocity component towards the floodplain is expected to grow at a growth rate inversely proportional to the decrease in water depth ($1/H(y)$). At the downstream end of a vortex the opposite happens, due to flow divergence (Prooijen et al., 2005). This effect is illustrated in figure 2.4. This acceleration due to the flow convection results in increasing bed shear stresses towards the floodplain at the upstream end of the vortex.

On transverse slopes, the secondary circulations are of not important for the exchange of momentum (Prooijen et al., 2005), however when the bed level between the floodplain and channel changes abruptly, a step, secondary flow at the corners becomes significantly strong and influences momentum exchange (Uijttewaal, 2014).

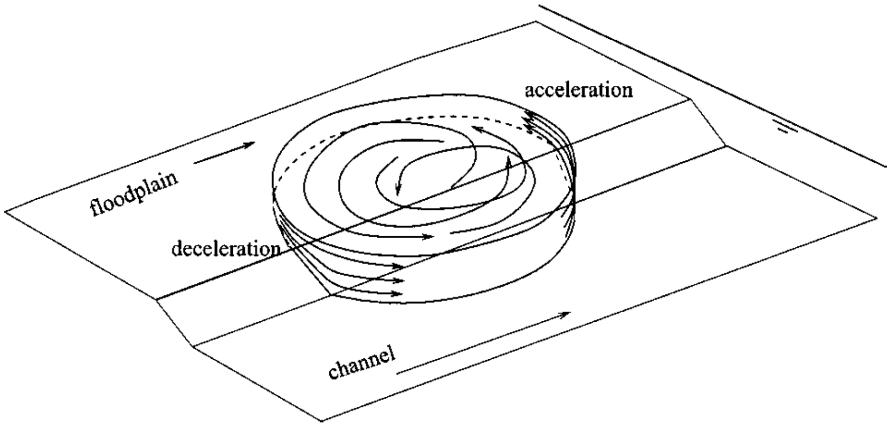


Figure 2.4: Vortex structure over a compound channel with a transverse slope. Adapted from Prooijen et al. (2005).

2.6.2. Sediment transport on transverse slopes

Sediment located on a transverse slope is influenced by the transverse gravity component in the downslope direction. This force is a decomposition of the bed-normal force and scales with the slope angle. For the prediction of sediment transport on a transverse slope different relations have been proposed, either based on a shear stress approach (Ikeda and Kanazawa, 1996; Sekine and Parker, 1992; Talmon et al., 1995) or on a force-based approach using equations of motion (Jammers, 2017; Nabi et al., 2013). All these transport models include the slope angle α for the transport direction.

The total downslope transport not only scales with the slope angle but also with a transverse bed slope coefficient. This coefficient is inversely related to the root of the critical shear stress. Downslope transport is related to the slope and a transverse bed coefficient, the Shields parameter and to the ratio of d_{50}/H (Talmon and Wieseman, 2006).

Sekine and Parker (1992) developed a relation for transverse sediment transport on a transverse slope under unidirectional flow conditions based on saltating particles. The developed model was based on a thought experiment, where they argued that when a saltating particle bounces on the slope, it is reflected by elastic reflection, resulting in a dimensionless transverse sediment transport which is proportional to $1/\tan\alpha$. This relation was tested for grain sizes between 0.4 and 1.3 mm and slope angles between 0 and 30 degrees and performed quite well.

The researchers cited give relations for the direction and magnitude of sediment transport on a transverse slope. It should be noted that the relations using the shear stress are based on unidirectional flow. These relations do not take variable flow or variations in the transverse direction into account.

A model based on the equations of motion can use the instantaneous flow field and therefore the influence of turbulence and larger scale variations on the transport can be calculated, as initiation of motion is based on the instantaneous forces acting on a particle (Nabi et al., 2013). The model proposed by (Nabi et al., 2013) uses a forces model for initiation of motion, while in consecutive steps empirical relations are used to calculate the bulk transport.

When the effect of the transverse slope is added to the equations, a the bed-normal force has to be separated in a vertical and bed transverse component. The transverse component scales with $\tan\alpha$. In numerical experiments with the forces model flow with transverse component upslope was able to transport particles in the upslope direction (Jammers, 2017).

2.7. Literature summary and conceptual framework

From the combined knowledge of this literature study a framework of the relevant processes and parameters for sediment transport in and around vegetated flow has been constructed and is shown in figure 2.5. This figure shows the concept of flow in a compound channel with a vegetated floodplain and an arbitrary slope angle α, which represents the half cross-section of a river branch with its floodplain or bank.

In this setup two mechanisms cause differences between the flow velocity on the floodplain and the channel which creates a shear layer between the floodplain and the channel:

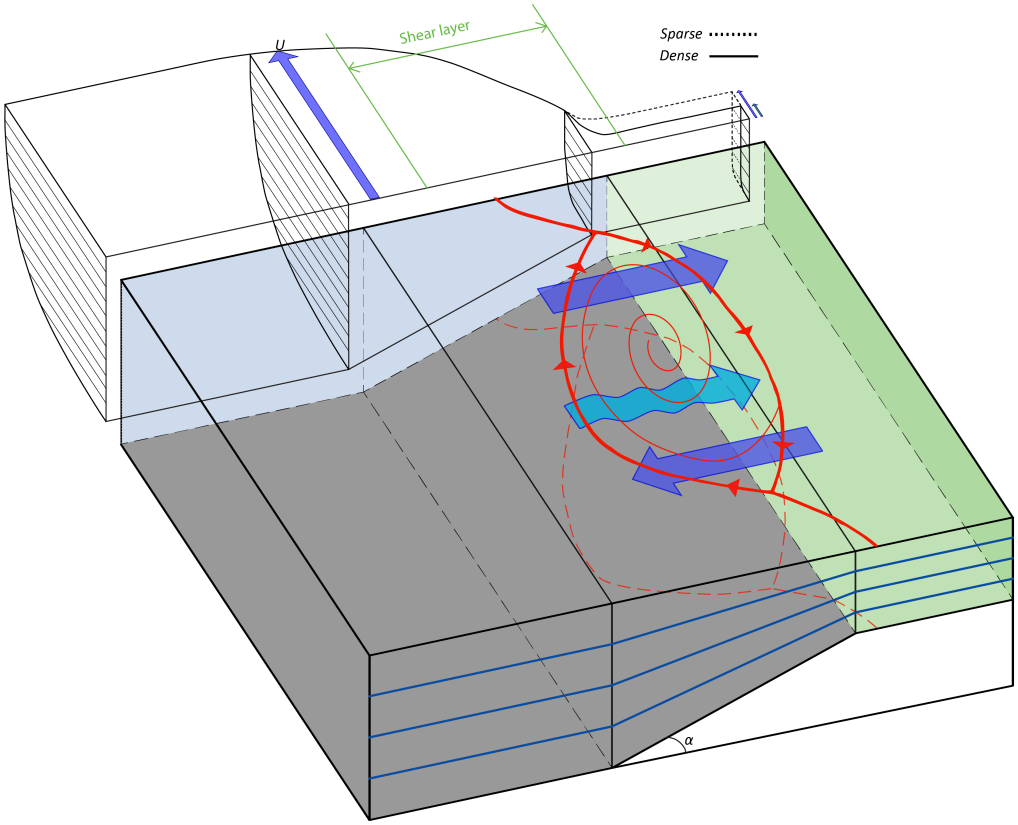


Figure 2.5: The processes governing flow in the a partly vegetated channel.

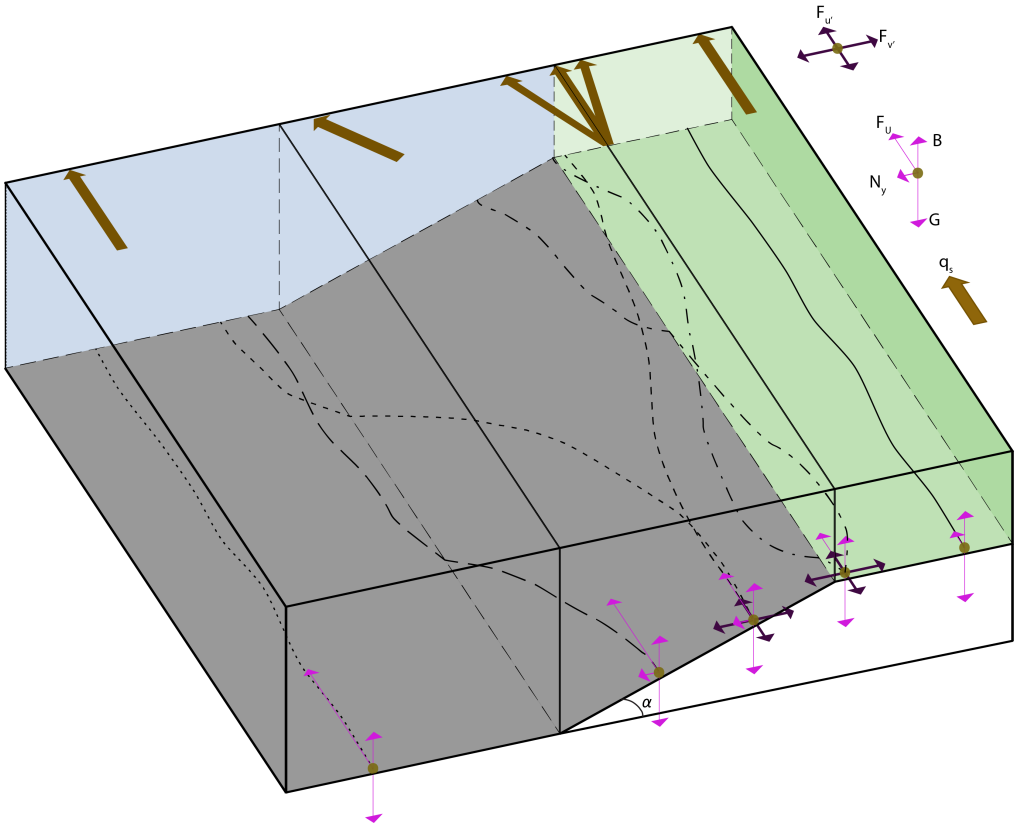


Figure 2.6: Hypothesized sediment transport directions in partly vegetated compound channel flows.

- The water depth on the floodplain is lower, which decreases the flow velocity;
- The vegetation on the floodplain increases the total friction on the flow, as the forcing is equal, same bed and surface gradients, flow velocity on the floodplain is lower than in the channel. Also, the flow profiles over the water depth are different because the vegetation drag acts over the total water column, resulting in a constant velocity over depth instead of a logarithmic profile without vegetation. The velocity inside the vegetation decreases when the vegetation density increases, which can be derived from the momentum balance in vegetated flows.

This results in the flow profile at the top of the figure, including flow profile over depth, where the flow in the channel is logarithmic and constant over depth within the vegetation.

Within the shear layer Kelvin-Helmholz like vortices govern the exchange of momentum (curved light blue arrow) and mass between (dark blue arrows) the floodplain and the channel. At the upstream end of the vortices the transverse velocity is directed from the channel towards the vegetation and is accelerated towards the floodplain as result of the transverse slope. At the downstream end the opposite holds. Streamwise momentum is transported from the channel towards the floodplain where it is dissipated. The vegetation density governs the penetration of the vortices into the vegetation as a higher density dissipates the incoming momentum faster.

On the transverse slope the flow towards the vegetation is converging, which may result in acceleration and increased bed stress.

The passing of a vortex through a point in the shear layer causes velocity fluctuations which may affect sediments at the bed. Through the forces acting on a particle the path could be derived, as shown in figure 2.6. The pink arrows indicate the static forces from gravity (G), buoyancy (B), transverse component of the bed-normal force (N_y) and the drag from the mean flow (F_U). For simplicity of the image the vertical component of the bed-normal force and the bed friction are not drawn. The dark purple arrows indicated the drag forces from the variable flow directions. The possible directions of the sediment transport are indicated with the brown arrows.

While the particle is located in the front of the vortex the drag force from the fluid is directed towards the vegetation. When this force is larger than the transverse component of the bed-normal force, the particle is accelerated towards the vegetation. The particle may be transported into the vegetation where the bed-normal force only has a component in the z-direction. For a particle located at the downstream end, the fluid drag and the transverse component of the bed-normal force have the same sign, reinforcing each other. Particles located outside of the influence of the vortices are transported into the flow direction of the parts with a horizontal bed and under an angle with the mean flow direction of the transverse slope.

The strength of the vortices near the bed has not been researched yet. Therefore it is hypothesized that the vegetation induced vortices are present near the bed, but are less strong due to bed friction. Particles near the bed may be transported up to a certain depth into the vegetation, which is related to the penetration of the vortices into the vegetation. The dashed red line in figure 2.5 is the assumed vortex projected on the bed, giving the maximum range of the influence of the vortex on the bed.

3

Methodology

The influence of the coherent vortices near the bed was measured in a series of flume experiments in the Environmental Fluid Mechanics Laboratory of Delft University of Technology. During the flume experiments, flows were measured in a partially vegetated compound channel.

The experiments aimed to obtain a better understanding of the flow patterns in a vegetated compound channel and to link the fluid motion, mainly the coherent structures, to the movement of particles on the bed. Therefore two types of flow measuring techniques were used; Acoustic Doppler Velocimetry (ADV) and Particle Tracking Velocimetry (PTV). During the experiments, two different vegetation densities were used.

This chapter describes the experimental setup and the data analysis methods in more detail.

3.1. Experimental setup

The experiments are carried out in a 3 m wide, 19 m long and 0.2 m high glass-walled flume with a horizontal bed in the streamwise direction. At the upstream end, water is pumped into the flume with constant discharge. With a valve, the discharge can be adjusted. At the downstream end, a weir is present over the full width to regulate the flow depth. Downstream the weir water flows back to the central water tank of the laboratory. The experimental setup is constructed over the first 13 m of the flume and only used 2 m of the total width. The flume has a rail on each side on which equipment can be placed, such that it can easily be moved over the length of the flume.

To remove initial distortions in the water level, due to the inflow structures, a flow smoothener is installed directly downstream the inflow point. This is a 1 m long, Styrofoam plate floating on the water surface over the full width of the experimental setup. At the downstream end of the flume, behind the weir, a sieve is installed to retrieve the tracer materials from the water without disturbing the flow.

The experimental setup is a compound channel of 2 m width. In the remaining 1 m of the flume, a construction has been made that does not allow for flow. The compound channel is divided into three zones, the channel, the transverse slope and the floodplain. A cross-section is shown in figure 3.1 with the dimensions in mm. The channel, the deepest part of the cross-section, is 70 cm wide. The transverse slope has a slope of 1:10 and over a width of 80 cm. This part is constructed out of concrete, and the surface is painted white. The floodplain is elevated 8 cm relative to the channel bed and had a total width of 50 cm. The bed of the floodplain was constructed such that model vegetation could be installed in two different staggered grid densities. Before the model vegetation was installed, the bed had been covered with duct tape to smoothen it. The bed roughness was measured in previous experiments to have a value of $c_f = 0.0027$ (Truong et al., shed). This value is an average value for the transverse slope and the channel.

The coordinate system assigned to the flume is as follows: x is positive in the streamwise direction, and $x = 0$ is at the upstream end of the vegetation, y is positive from the floodplain towards the channel and $y = 0$ at the interface between the vegetation and the slope, z is positive upwards and $z = 0$ is at the bottom of the channel. Figure 3.1 and figure 3.2 give a cross-section and a top view of the flume. Images of the setup and the measurement devices are given in appendix A.

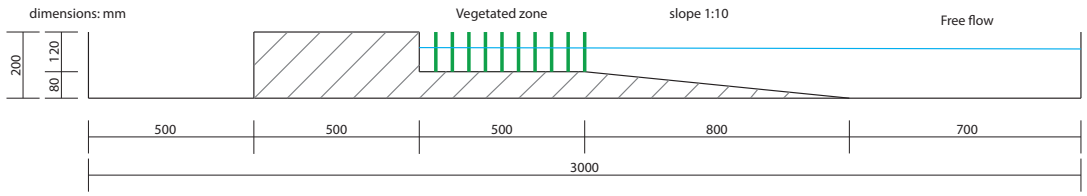


Figure 3.1: Cross-section of the flume

3.1.1. Vegetation

Rigid cylinders are used as model vegetation. These cylinders have a diameter of 1 cm and are emergent for each possible water depth in the flume.

The cylinders are placed in a uniform staggered grid, over the full width of the floodplain. For the sparse grid the heart-to-heart distance is 8.49 cm, and for the dense grid, this is 4.24 cm. The properties that can be assigned to the vegetation are given in table 3.1 and a top view is given in figure 3.3.

Table 3.1: The vegetation characteristics for the sparse and dense setup

		Sparse	Dense
Distance	ΔS (mm)	84.9	42.4
Cylinders/area	N (m^{-2})	139	556
Frontal area/volume	a (m^{-1})	1.39	5.56
Volume solid/total volume (porosity)	ϕ (-)	0.011	0.044

The vegetative drag coefficient for rigid cylinders is usually given as 1. This value is mostly used in modeling. With equations 2.2 and 2.3, the drag coefficients are calculated and have a value of 1.4 ± 0.2 and 1.6 ± 0.3 for the sparse and dense setup, respectively (Truong et al., shed). This results in values of $C_D a$ of 2.1 m^{-1} and 8.9 m^{-1}. The actual drag per meter, $C_D a$, can be calculated using equation 2.7 with the measured values of the spatially averaged flow velocity in the vegetation and the water surface slope.

3.1.2. Sediment

The bed installed in the flume is fixed and hydraulically smooth. Therefore no direct morphological activity could be measured. To study the possible effects of the coherent structures on sediments that are present around the interface another material had to be found. The criteria for the material were as follows:

- Detectable on images while below the water surface, for the PTV tracking
- Must represent bedload transport of sandy material
- Mobile in the experiment, at least on the full width of the transverse slope
- Uniform material, which makes it easy to assign mechanical and physical properties to the material

The first criterion gave that the material must have a distinct color in an RGB color image, preferably bright red or green, and must be larger than 1 pixel. In a picture of HD quality (1920x1080) pixels of an area of 3 by 2 meter (area of interest) gives a particle size of at least 2 mm, but preferably larger to ensure they are detectable in the water.

The second criteria, together with the result of the first criterion, results in scaling. Sandy particles are particles with a diameter between 63 μm and 2 mm since the particles must be larger than 2 mm scaling needs to be done with the density as both the Shields parameter and the Rouse number, parameters for mobility, both depend on the density and diameter of the particle. Therefore the density of the particle had to be larger than the density of water and smaller than the density of quartz sand: $1000 < \rho_p < 2650$ kg/m^3.

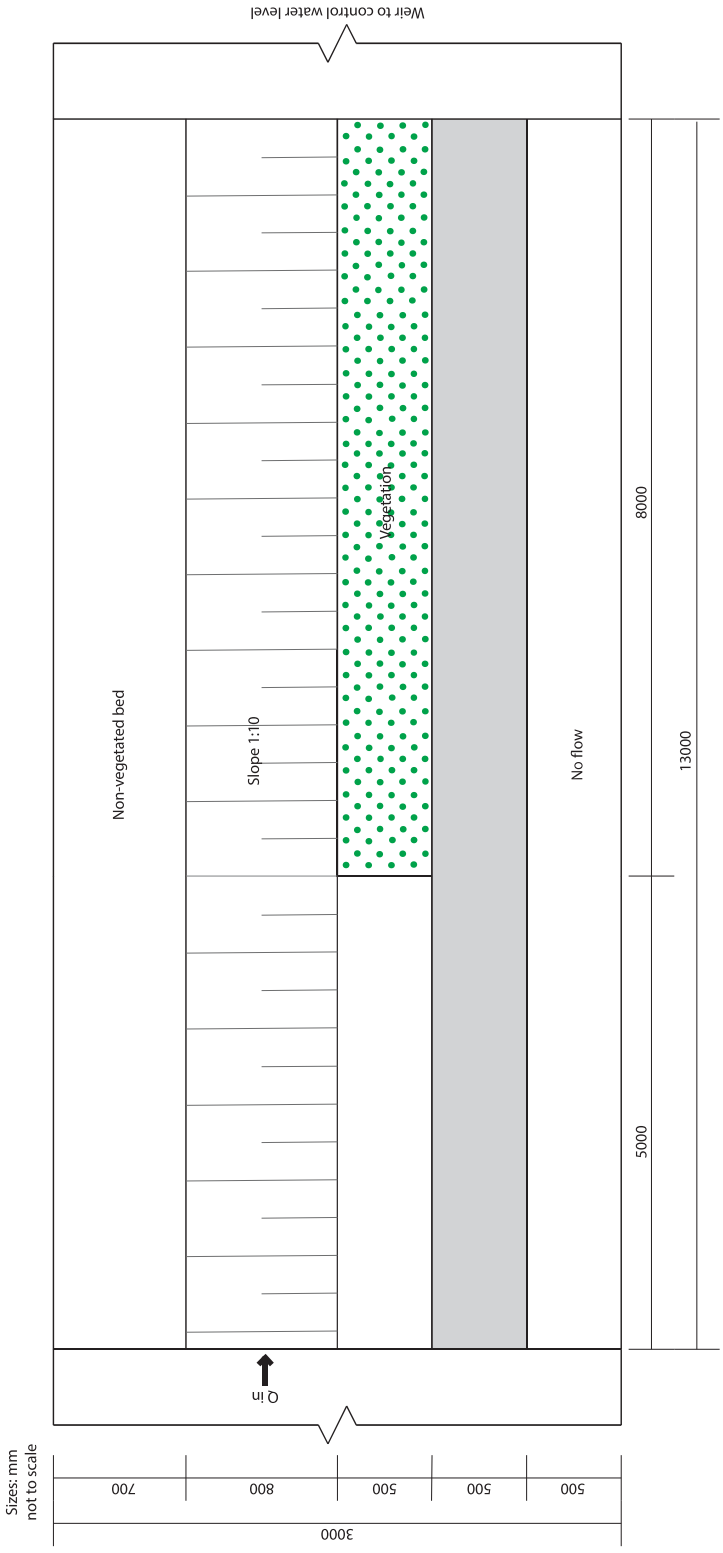


Figure 3.2: Top view of the flume

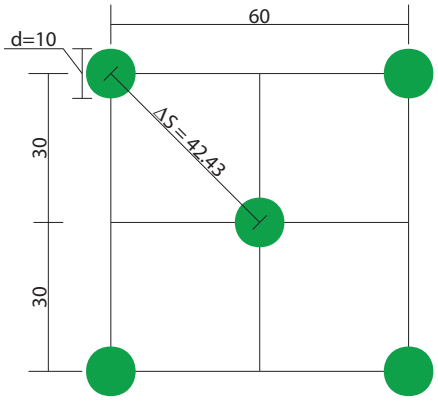


Figure 3.3: The geometric setup of the dense vegetation. The measurements are in mm

Regular sand is a granular material and is not available with only one diameter. Therefore the physical properties of the particles in sand are stochastic. A uniform bed material was consequently preferred to be able to track the particle motion and couple the movements to the governing flow field. This resulted in spherical particles.

The chosen material are bright red spheres, which are Bullet Balls for Airsoft guns. These are plastic balls with a diameter of $d_s = 5.9\,mm$ and a density of $\rho_s = 1050$ kg/m^3. Because the density of the balls is slightly higher than that of water ($\rho_w = 1000$ kg/m^3) they sink to the bottom.

The fall velocity of these spheres cannot be calculated with Stokes' law as the diameter is too large. The wake of the spheres is turbulent therefore the drag has to be taken into account resulting in equation 3.1. The theoretical drag coefficient for spheres is equal to 0.47; together with the density and the diameter of the spheres, this results in a fall velocity of 0.09 m/s.

$$w_s = \sqrt{\frac{3}{4}\frac{dg}{C_D}\frac{\rho_s - \rho_w}{\rho_w}} \tag{3.1}$$

3.1.3. Experimental conditions

For each vegetation density different combinations of water depth and discharge have been tested. These settings are chosen such that different water depths were tested with similar flow velocities in the channel, to see the influence of the water depth on the coherent structures and the movement of the particles. The different water depths are 12, 14 and 16 cm with a variation of ±0.1 cm. For each control depth at least 2 upstream discharges are tested. This results in 4 sets with similar channel flow conditions; set 2 and set 3 contain both vegetation densities and set 1 and 4 only have the dense vegetation.

Table 3.2 gives an overview of the different experimental settings that are tested.

3.2. Measurements

The measurements consist of two parts, first the point measurements with ADV and second the sediment transport or bed measurements with PTV. The point measurements are done to obtain insight into the flow properties at the middle of the water column and near the bottom. The bed measurements are done by tracking particles at the bottom of images. The combined data from the measurements can be used to obtain a good overview of the near-bed conditions of the flow and insight in the transport capacities.

The water depth is measured at two locations in the main channel. The upstream location is at $x = 4$ m and the downstream location is at $x = 8$m. This is done with two *optoNCDT 1302* lasers, these can measure the water level with an accuracy of ± 0.1 mm.

Table 3.2: Conditions for each experiment set

Experiment	Vegetation	Control depth cm	Discharge l/s			
			Set 1	Set 2	Set 3	Set 4
Ex1	Sparse	12		50	60	
		14		60	70	
		16		70	80	
Ex2	Dense	12		50	60	70
		14	50	60	70	80
		16	60	70	80	

The total discharge is measured with a discharge meter in the pipes downstream the valve. The discharge meter is a *PROline Prosonic Flow 93*, which has an accuracy of ±2l/s.

Zong and Nepf (2010) found that the coherent structures are fully developed at x = 5 to 6 m. They have done similar experiments however without the transverse slope. Truong et al. (shed) found that for the geometry of this setup the coherent structures were fully developed at the same location. Therefore the area of interest for the measurements is between x = 4.5 m and x = 7.5 m. To avoid the influence of the changing flow at the end of the setup, the last 0.5 m is not used. Additional images of the experimental setup and the measurement devices can be found in appendix A.

During the experiments, pink fluid, dissolved potassium permanganate, was injected into the flow to obtain a better insight into the development and structure of the coherent structures.

3.2.1. Acoustic Doppler Velocimetry (ADV)

Acoustic Doppler Velocimetry makes use of the Doppler shift of sound waves which scatter against small suspended particles in the flow. The observed Doppler shift is proportional to the velocity of that particle which is a measure of the flow velocity. During the experiments, a Nortec Vectrino 2D-3D Fixed Probe, which is a side looking ADV device, is used. The outputs are time series of the velocity components in the x, y and z direction. In appendix A the dimensions of the probe and a photograph of the setup can be found.

Because the water in the laboratory has not enough suspended particles for the sound waves to reflect on, gas bubbles are introduced into the flow with the hydrogen bubble technique developed by Clutter and Smith (1961). This technique is based on the creation of hydrogen bubbles by the electrolysis of water. A frame with thin platinum wires, diameter of 0.01 mm, is placed in the flow. This frame acts as cathode creating small bubbles from the wires. At another point in the flow, an anode is placed to complete the circuit. The sound waves from the ADV scatter against the hydrogen bubbles towards the four legs of the ADV. The signal is translated into velocity components in the 3 main axes. An image of the setup with the bubble screen is shown in figure A.5 appendix A .

The sampling volume has a diameter 5 mm, and the center of the sampling volume is located at 50 mm from the probe. The flow measurements in the experiments are done at a frequency of 25 Hz for 5 min per location, to capture the relevant turbulence levels and enough of the coherent structures.

The measurements are all done in the transect at x = 6.5 m. The near-bed measurements are taken at 3 mm above the bed and at mid-depth, which is defined as the middle of the water column at each point. The mid-depth location depends on the water depth and the corresponding y-coordinate of the measurement location. Assuming the water level is equal over the whole cross-section and using the bed profile the mid-depth location was calculated. The y-coordinates of the measurements are: 1.20, 0.90, 0.80, 0.70, 0.60, 0.50, 0.40, 0.30, 0.20, 0.10, 0.0, -0.05, -0.10 and -0.30 m. The measuring points are shown in figure 3.4.

3.2.2. Particle Tracking Velocimetry (PTV)

Particle Tracking Velocimetry is used to measure the velocity vectors of the spheres. PTV is based on following individual particles in a Lagrangian framework. From the PTV data, individual particle paths can be extracted as well as properties of the entire flow field. The PTV analysis consists of 3 main steps: 1.)Detecting the individual particles each image, 2.) determining the displacement of the particles between two consecutive frames by using autocorrelation over a beforehand specified interrogation area around each detected particle and 3.) data analysis. The data analysis includes the calibration, combination of the individual vectors to particle paths or instantaneous flow fields. The software that is used for the PTV analysis is called PTVlab 1.0,

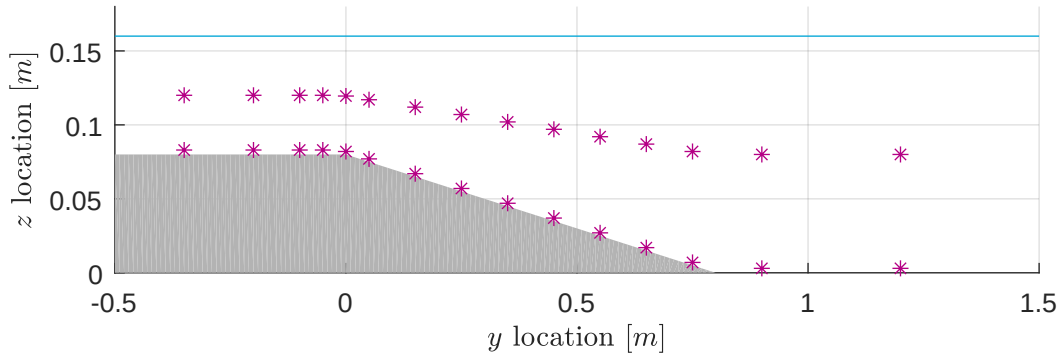


Figure 3.4: Locations of the ADV measurements, for a water depth of 16 cm. The z-coordinate of the mid-depth measurements scale with the water depth.

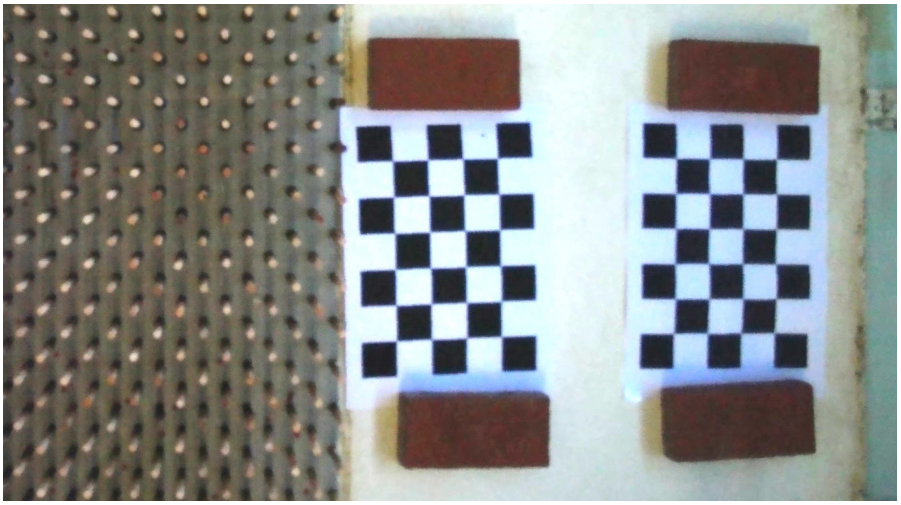


Figure 3.5: Calibration image with the chessboards located on the slope, each square is 5 by 5 cm in reality.

developed by Brevis et al. (2011). This package is run in *MATlab 2014a*.

The images for the PTV are made with a *Samsung NX1* camera with a *Samsung NX 16-50mm f/2-2.8 S ED OIS* lens and are the individual frames of short movies. The movies are taken with a frame rate of 24 frames per second and at a resolution of 1096 by 2160 pixels. The individual frames of the movies had to be extracted and preprocessed into black-and-white images before analysis with the PTV software, this was done with the *Free Video to JPG converter* of *Digital Wave Ltd.* and the *Image Processing Toolbox* in *MATlab* respectively. For each experimental setting, a movie of at least 5 minutes was made.

For the calibration of the real distance per pixel, calibration images were taken with a chessboard placed on the slope as shown in figure 3.5. As light breaks differently in water, the calibration images were taken for the three different water depths used in the experiment to test whether different calibration values should be used. No significant differences were found between the different water depths as well as on the slope itself for the calibration value. Therefore a constant calibration value for the whole image has been used, and the calibration images for the 14 cm water depth cases has been used. A new calibration image had to be taken each time the camera was removed from the setup to ensure the right settings.

The PTV tracers, the red spheres described in section 3.1.2, were released at the location $x = 2.5$ m over the width between $y = -0.3$ and $y = 0.5$ m. This was done with a dispenser shown in figure A.5 in appendix A. This to ensure that the spheres could reach the bottom and are in equilibrium with the flow before entering the area of interest. With the results from Truong et al. (shed), the maximum velocity was estimated to be approximately 0.5 m/s. Therefore the distance over which a particle is transported downstream before reaching the bed is in the order of 1 m. The particles were continuously released by a dispenser. For each setting, approximately 6000 spheres were released.

3.3. Data processing and analysis

The RAW data from the ADV measurements and PTV analysis have to be processed in such way that the results from both techniques can be compared and interpreted. The more complicated data processing and analyses are described in this section.

3.3.1. Image pre-processing

After the individual frames were extracted from the movies, each frame had to be converted to black and white images, leaving the spheres white on a black background. In the dense experiment, only the surface of the transverse slope was white. The surface between the cylinders was grey, and the cylinders had their original wood color. This complicated the process of extracting only the spheres from these images as they were less distinct within the vegetated area. In the sparse experiment, both the bed and the cylinders were painted white to enhance the visibility of the spheres.

For the image conversion, the fact that the spheres were bright red was used to single them out. Each pixel where the value of red was higher than the value of the blue and green (RGB) image was turned into a 1 (white), and all other pixels were turned into a 0 (black). These images were then used in the PTV software.

3.3.2. PTV

The output of the PTV analysis gave the locations in pixel number and displacements per image set of all the particles detected and identification numbers of those particles. The identification numbers are given to particles which are present in at least 2 consecutive image sets. For further analysis or the particle paths, only particles visible for at least 24 consecutive image sets were used.

To obtain information about the exchange of particles between the transverse slope and the floodplain, all the paths that cross the interface ($y = 0$ m) at least once are analyzed. The differences in the velocity vectors of particles entering and leaving the vegetation and the absolute amounts are extracted.

3.3.3. Velocity time series

The RAW ADV data are despiked using an algorithm of Mori et al. (2007). Next to despiking a standard deviation filter, which deleted all values of more than 3 times the standard deviations higher or lower than the mean, is used. For the statistical analysis the despiked, filtered data is used.

To extract the coherent motion from the time series, these are smoothed over 50 data points, corresponding to 2 seconds. This smoothing period showed to be sufficient to smooth the wiggles caused by the 3D turbulence without losing information about the coherent structures.

The ADV used in the experiments has a side looking probe, which needs to be installed such that the probe is looking perpendicular to the mean flow direction. If this is not the case, and the probe is rotated, it measures part of the streamwise velocity as part of the transverse component. Because the looking direction of the probe is installed visually, a small deviation of the looking angle is quite likely. In the first measurements, with the dense vegetation, this was solved within the data set, assuming the error in the looking angle was the same for all the points in the dataset.

From the RAW data, the rotation angle was determined such that the mean velocity profiles in the cross-section averaged over all the datasets for that setting resulted in a zero discharge. This lead to a rotation of 2^o around the z-axis. The rotated data was used for the analysis. For the sparse dataset, the angle of the ADV was tested at two locations in the channel, assuming the average value of the transverse component should be zero in that area, the looking direction of the ADV was adjusted until this value was obtained. The settings were checked every time a new profile was measured.

The rotation and the looking direction are based on the assumption that the total discharge through the cross-section should have been zero and mean transverse velocity in the channel was zero. However the velocity component in the transverse direction is strongly affected by the rotation.

4

Results

This chapter presents the results of the experiments and data analysis. First, some general observations, which were done during the execution phase of the experiments, and a brief overview of the relevant parameters are given. Afterwards, the results of the data analysis are presented, zooming in from the mean flow field through the Reynolds stress to the vortex structure, considering both near-bed as mid-depth flow. The last part gives an analysis of the particle paths of the PTV measurements.

4.1. General observations

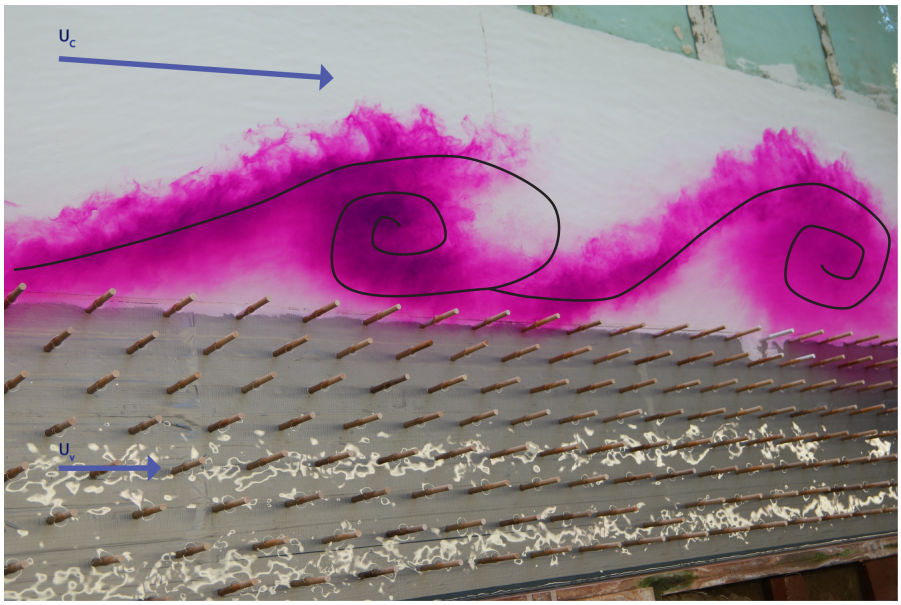


Figure 4.1: Vortex structure around the interface visualized with colored water.

During the experiments tests visualizing the flow were done with the colored fluid and the PTV-tracers as well. These tests gave insight into the flow structures present around the interface between vegetated and non-vegetated bed and their influence on the bed as shown in figure 4.1.

Adding the fluid at different locations in the cross-section showed the width of the mixing layer. When the colored fluid is injected near the interface, between $y = 0$ and $y = 0.1$ m, the coherent structures were visible. The width of the vortices on the non-vegetated bed was nearly constant for each setting, the intrusion of the colored fluid into the vegetation was larger for the sparse setup. Also, the length of the vortices changed with the vegetation density. In the sparse setup, the vortices were shorter and more frequent than for dense vegetation. The velocity at the interface was almost equal for both settings. Injection the colored fluid into

the vegetation, at $y = -0.25$ m, made the extent of the structures in the vegetation visible, showing ejections of fluid from the vegetation towards the channel.

The color added further away from the interface, at location $y = 0.6$, moved through the setup in a merely straight line, not much affected by the presence of the vegetation. Diffusion of the colored fluid in the transverse direction is caused by 3D turbulence only.

Inside the vegetation, the flow velocity was much smaller than in the channel, which resulted in a slow-moving 'blob' when colored fluid was injected in this area. This 'blob' slowed down and accelerated with the passing of the vortices at the interface. At a larger distance from the interface, the interaction with the channel became less visible. However, due to spreading of the fluid over the whole vegetated area, each passing vortex ejected colored fluid from the vegetation towards the channel. Mixing with the clear water injected during the sweeps, diluted the concentration of the colored fluid. The vortices cause strong mixing within the vegetation and the shear layer.

Most of the PTV-tracers released inside the vegetation eventually ended up on the slope. Only tracers released on the slope in the vicinity of the interface could be transported into the vegetation. This depended on the phase of the vortex wherein the tracers were released. Ejections showed a pattern similar to the colored fluid in the water column. However, tracers ejected onto the slope were transported towards the channel under the influence of the bed-normal force in the y-direction.

Within the dense vegetation, the streamwise transport of the tracers was much lower than within the sparse vegetation. The streamwise velocity component varied with the passing of the vortices. During ejections the streamwise velocity component of the tracers became negative in the dense setup. Where they only slowed down in the sparse setup.

Around the interface an exchange zone was observed when spheres were transported into the vegetation most of them crossed this area and stopped at a specific y-coordinate. Tracers which did not have enough momentum to be transported up to that point were transported out of the vegetation again in the first following sweep. This zone is further analyzed in subsection 4.5.3. In the sparse vegetation this location was nearer to the interface and less distinct, but still present.

Table 4.1 gives an overview of measured values for each setup. The data in each set has a similar magnitude of the channel velocity. For set 2 and 3, the both densities are measured, for set 1 and 4 only the dense vegetation is measured. The sets are sorted on the channel velocity. Where the channel velocities for each set have similar magnitudes, the Reynolds stress $\overline{u'v'}$ increases in absolute magnitude with increasing depth, the vortices in the middle of the water column are stronger for a larger water depth.

The vegetative drag $C_D a$ is calculated with equation 2.7, using the measured surface slope and U_V. Between the two vegetation densities, there is an order of magnitude difference of the value of the vegetative drag. Dividing these values by a, the value of C_D is of order 1 for the sparse set and order 10 for the dense setup. The total drag increases significantly with the density. Therefore more energy is dissipated by the dense vegetation.

4.2. Flow

Table 4.1 presents the differences between the channel velocity and the vegetation velocity. Within the vegetation the mean velocity at the bottom and in the middle of the water column had approximately the same value, giving a constant mean flow velocity in the vegetation above the bottom measuring point.

The dependency of the vegetation velocity differed for the two densities. In the sparse setup the mean flow velocity inside the vegetation, U_V, is a relatively constant percentage of the mean flow velocity in the channel, U_C, within each set. In the dense setup, the water depth influences U_V as well. An increasing water depth decreased the relative vegetation velocity, increasing the velocity gradient between these flows.

Deviations from the mean within the time series measured with the ADV technique represent the coherent structures. The time series are smoothed over a time span of 2 seconds to obtain the signal of the coherent structures. Figure 4.2 and 4.3 show the measured time series of the streamwise and transverse velocity components for the dense and sparse setup with the settings Q = 60 l/s H = 14 cm at 4 different locations in the cross-section. Figure 4.2 gives the velocity in the middle of the water column and figure 4.3 the near-bed velocities. The different locations were chosen such that each part of the compound channel and the interface is shown. The main difference between the velocity-time signals near the bottom and in the middle of the water column is the increased variability of the raw signal and more small-scale wiggles in the smoothed

Table 4.1: The flow properties of the different experimental setups

	Set 1: Dense		Set 2: Dense			Set 3: Dense		
	Q50H14	Q60H16	Q50H12	Q60H14	Q70H16	Q60H12	Q70H14	Q80H16
$Q\ [l/s]$	50	60	50	60	70	60	70	80
$i_s\ [*10^{-4}]$	1.39	1.56	3.25	3.08	2.48	3.17	4.55	3.76
$C_Da\ [m^{-1}]$	32.0	64.9	24.9	41.1	77.7	12.9	77.2	121.0
$H_c\ [m]$	0.14	0.16	0.12	0.14	0.16	0.12	0.14	0.16
$H_v\ [m]$	0.06	0.08	0.04	0.06	0.08	0.04	0.06	0.08
$H_rel\ [-]$	0.43	0.50	0.33	0.43	0.50	0.33	0.43	0.50
$U_{c,mid}\ [m/s]$	0.328	0.336	0.396	0.399	0.392	0.483	0.459	0.448
$U_{c,bot}\ [m/s]$	0.226	0.228	0.277	0.267	0.271	0.323	0.318	0.312
$U_{v,mid}\ [m/s]$	0.009	0.007	0.016	0.012	0.008	0.022	0.011	0.008
$U_{v,bot}\ [m/s]$	0.009	0.007	0.014	0.007	0.008	0.016	0.014	0.007
$U_{v,mid}/U_{c,mid}\ [-]$	0.028	0.020	0.040	0.030	0.020	0.045	0.023	0.017
$\overline{u'v'}_{0,mid}\ [*10^{-4}\ m^2/s^2]$	-4.27	-5.00	-4.40	-5.54	-7.16	-4.62	-8.63	-9.92
	Set 4: Dense		**Set 2: Sparse**			**Set 3: Sparse**		
	Q70H12	Q80H14	Q50H12	Q60H14	Q70H16	Q60H12	Q70H14	Q80H16
$Q\ [l/s]$	70	80	50	60	70	60	70	80
$i_s\ [*10^{-4}]$	6.00	4.81	4.13	4.17	5.37	9.52	4.12	4.96
$C_Da\ [m^{-1}]$	16.8	44.4	1.98	1.98	3.14	2.77	1.45	1.91
$H_c\ [m]$	0.12	0.14	0.12	0.14	0.16	0.12	0.14	0.16
$H_v\ [m]$	0.04	0.06	0.04	0.06	0.08	0.04	0.06	0.08
$H_rel\ [-]$	0.33	0.43	0.33	0.43	0.50	0.33	0.43	0.50
$U_{c,mid}\ [m/s]$	0.542	0.524	0.368	0.362	0.334	0.448	0.412	0.385
$U_{c,bot}\ [m/s]$	0.366	0.360	0.252	0.235	0.220	0.316	0.287	0.260
$U_{v,mid}\ [m/s]$	0.026	0.015	0.064	0.064	0.058	0.082	0.075	0.071
$U_{v,bot}\ [m/s]$	0.024	0.015	0.064	0.063	0.056	0.080	0.071	0.066
$U_{v,mid}/U_{c,mid}\ [-]$	0.049	0.028	0.174	0.177	0.173	0.259	0.260	0.274
$\overline{u'v'}_{0,mid}\ [*10^{-4}\ m^2/s^2]$	-7.02	-11.30	-4.07	-4.05	-5.68	-7.31	-7.82	-8.18

signal. The large-scale periodicity is most distinct near the interface.

Within the channel ($y = 0.9m$), the transverse component of the flow is merely constant. In the dense setup, there is some periodicity in the streamwise direction, but the variation is quite small and not distinct in the transverse component. Near the bottom the wiggles in the velocity profile are more random, and at first sight, no large-scale periodicity is present.

The mid-depth measurements at the interface ($y = 0$) show a clear difference between the dense and the sparse vegetation. The period of the vortices is larger for the denser vegetation while the mean flow velocity is similar. Also, the amplitude of the streamwise component is larger. At the same location near the bottom, there is still some periodicity in the velocity signal, however less distinct. Both near the bed and in the middle of the water column the transverse component has distinct sharp peaks and wide shallow troughs. The flow into the vegetation has a longer duration, but the magnitude of the velocity is smaller than for the flow out of the vegetation. At the interface both velocity components have a large amplitude and have a phase shift of 180^o.

The amplitude of the velocity signal inside the vegetation has a similar magnitude for both mid-depth and near the bottom. In the dense vegetation, the amplitude of the streamwise velocity is larger than the mean, resulting in negative velocities. In the sparse vegetation, the mean velocity is larger, and the amplitude is smaller. Therefore the velocity is small but always positive. Within the vegetation the phase shift between u and v is approximately 90^o.

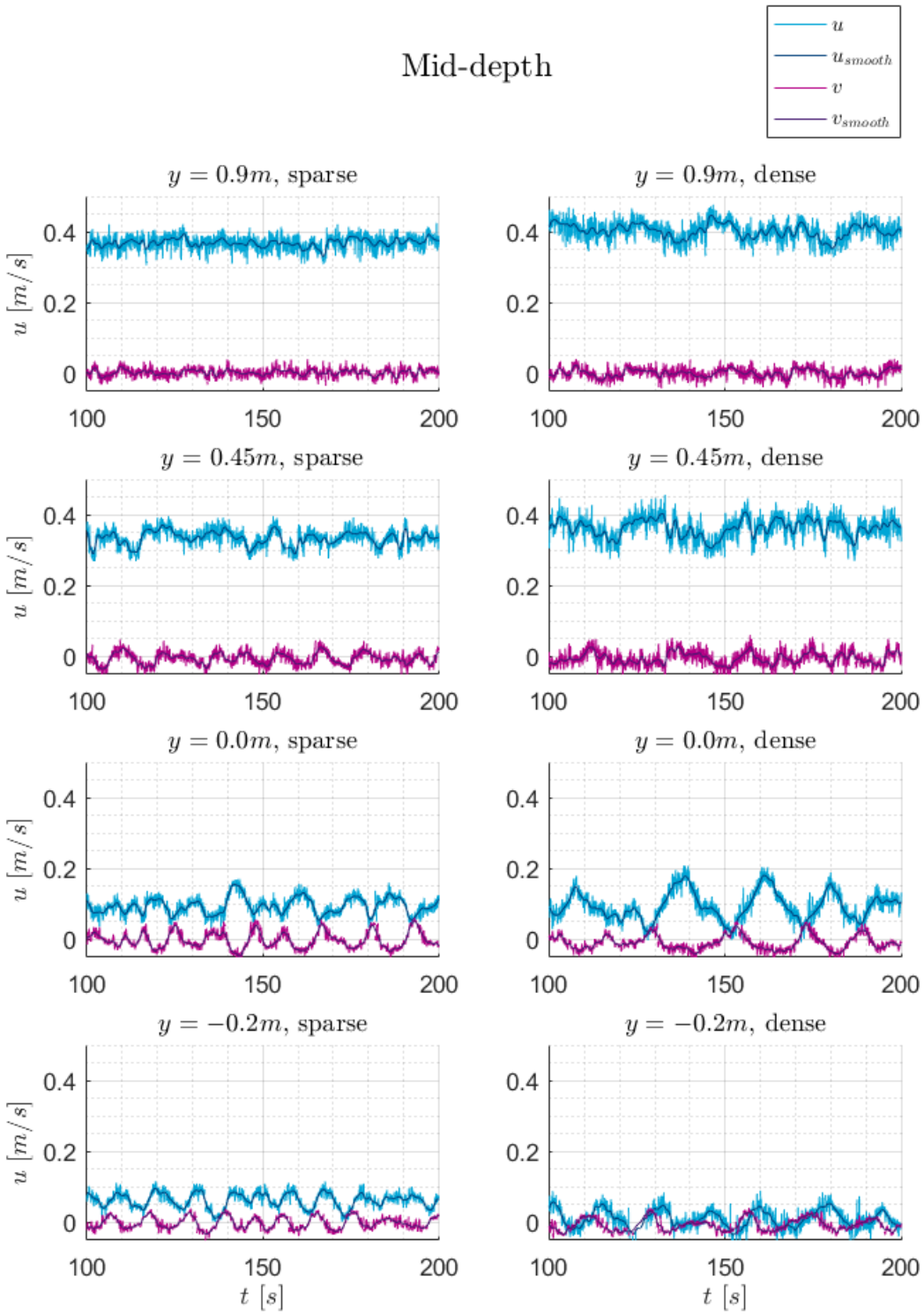


Figure 4.2: Time series for the sparse and dense setup for setting Q60H14 in the middle of water column. Top to bottom: in the channel $y = 0.9\ m$, on the slope $y = 0.45\ m$, at the interface $y = 0\ m$ and inside the vegetation $y = -0.2\ m$. The blue line is the streamwise component and the purple line the transverse component

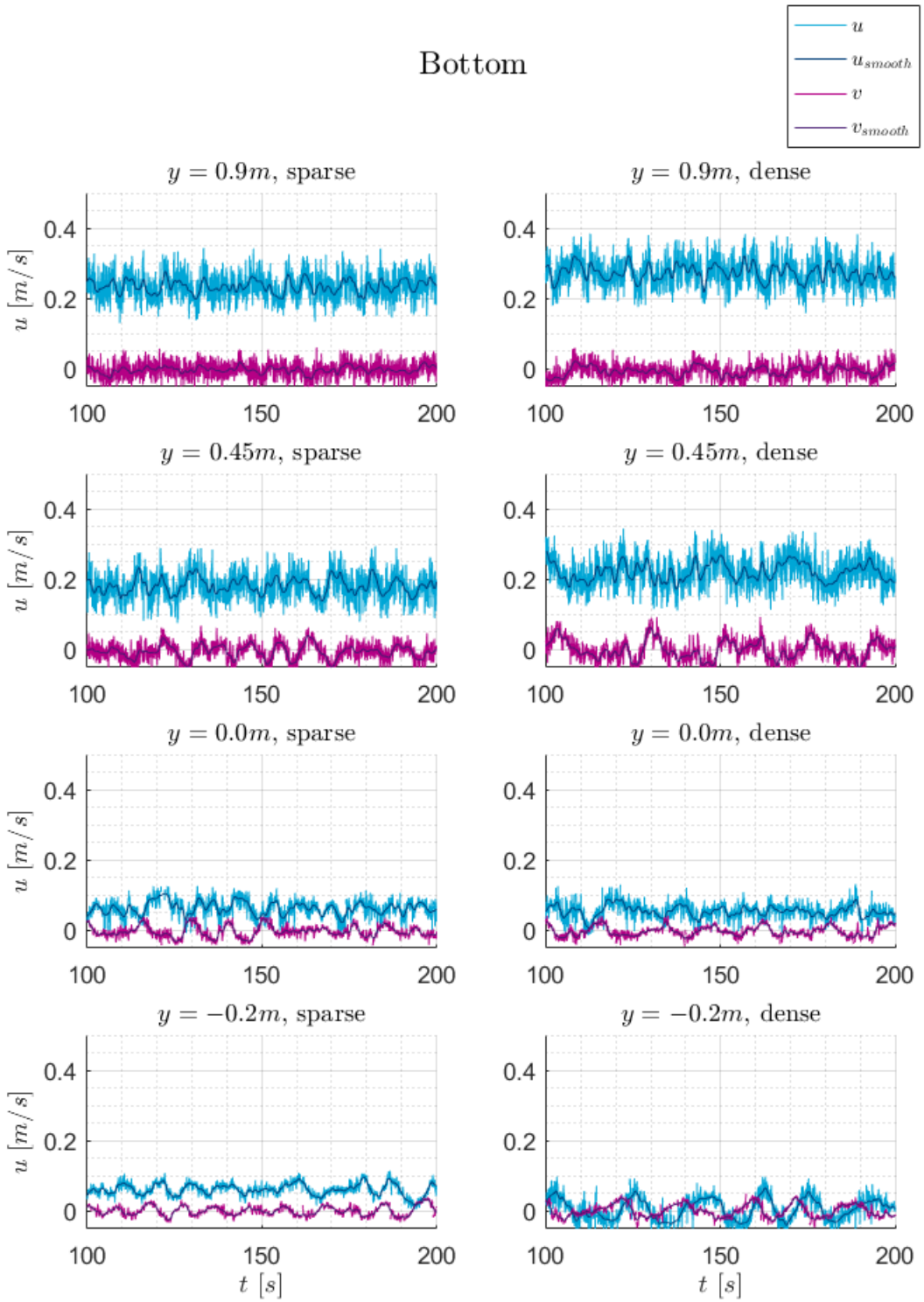


Figure 4.3: Time series for the sparse and dense setup for setting Q60H14 near the bottom. Top to bottom: in the channel $y = 0.9\ m$, on the slope $y = 0.45\ m$, at the interface $y = 0\ m$ and inside the vegetation $y = -0.2\ m$. The blue line is the streamwise component and the purple line the transverse component

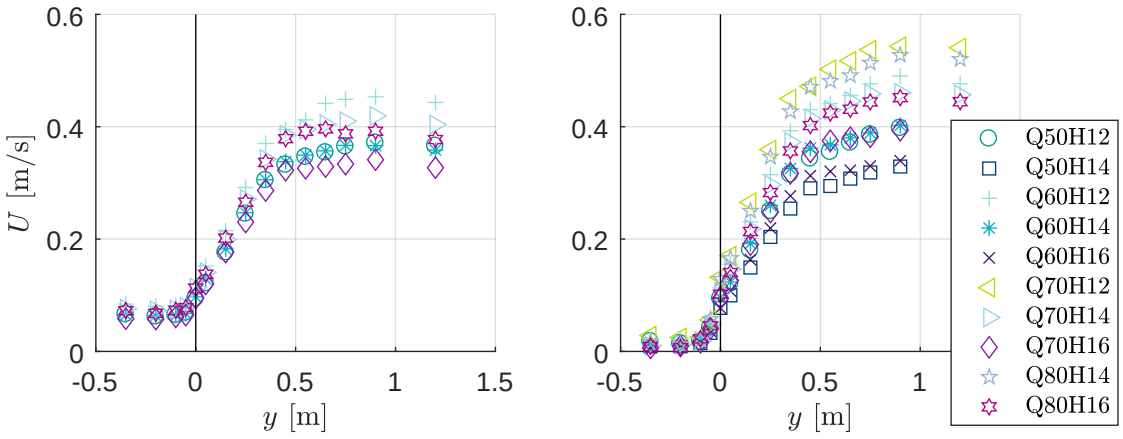


Figure 4.4: Mean streamwise velocity profiles in the cross section at mid-depth. Left the profiles for the sparse setup. Right the profiles for the dense setup. The same channel velocity gives similar profiles for the different depths. The black line indicates the location of the interface

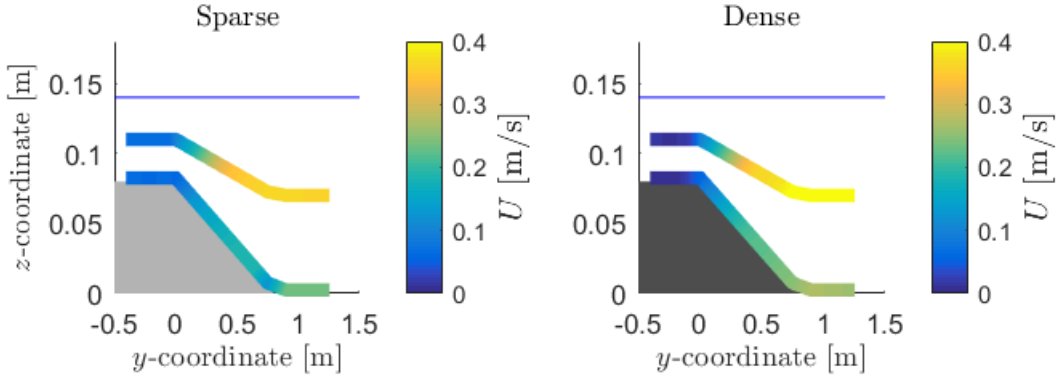


Figure 4.5: U for $Q = 60\,l/s$ and $H = 14\,cm$ in the sparse (left) and dense (right) setup.

4.2.1. Mean streamwise velocity component

The mean streamwise velocity component follows an S-shaped curve (figure 4.4), which is divided into two parts corresponding to the vegetated flow, the inner region, and the non-vegetated flow, the outer region. The length scale of the shear layer is different in both regions, order estimates for these length scales are 0.05 m in the inner region and 0.5 m in the outer region.

The difference between the bottom velocity and the velocity at mid-depth were visualized in figure 4.5. The profile near the bottom and at mid-depth have a similar S-shape. Inside the channel, $y > 0.8$, the velocity profile follows a logarithmic profile, which can be determined by the law of the wall and inside the vegetation the velocity is constant except for the first 4 mm above the bed. Above the transverse slope, the vertical velocity profile cannot be determined from the measured data. Near the bed, the vertical velocity gradient is larger. Therefore the measurements are more sensitive to the exact distance above the bed.

Each velocity profile has been normalized by the mean channel velocity in the middle of the water column, left pane of figure 4.6. This shows that the channel velocity determines the shear layer of the outer region. To determine the length scale of the outer layer, δ_0, the outer region profile was fitted to the equation 4.1. The matching point $y_m = 0.05$m, with the corresponding $U_m = U(y_m)$. The resulting thickness is displayed in table 4.2. This table shows that the velocity the outer region is solely dependent on the channel velocity, U_C, when considering the channel velocity as a given constant. The value of the outer layer thickness is equal for all settings at $\delta_O = 0.37\ m$.

$$U_O(y) = U_m + (U_C - U_m)\left[\frac{y - y_m}{\delta_O} - \frac{1}{4}\left(\frac{y - y_m}{\delta_O}\right)^2\right] \tag{4.1}$$

The velocity in the inner region depends on the vegetation density. The velocity in the sparse vegetation

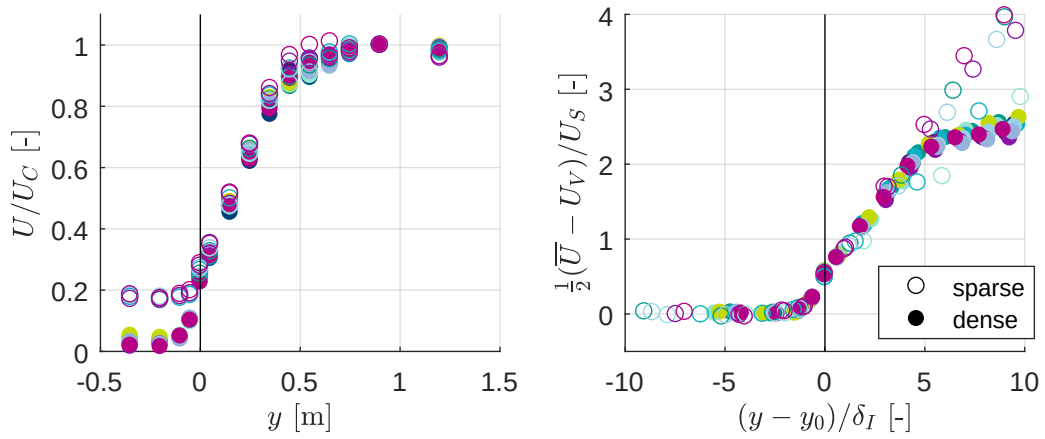


Figure 4.6: Normalized velocity profiles. Left) The velocity normalized by the mean mean channel velocity. Right) The profiles scaled by the inner layer thickness δ_I and velocity normalized by the slip velocity.

is approximately 20% of the channel velocity, while this is between 2% and 4% in the dense vegetation (figure 4.6, left pane). The inner region profile scales with the inner layer thickness and the vegetation velocity, U_V, according to a hyperbolic tangent, which has its inflection point at the interface, $y_0 = 0$. The length scale of the inner layer, δ_I was found by fitting the inner region to equation 4.2. These values are given in table 4.2. As shown in the right pane of figure 4.6, the velocity profiles of the inner region collide when the velocity is scaled to the channel velocity, U_C, and the velocity at the interface, $U(y_0)$, and the y-coordinate is scaled with δ_I.

$$U_I(y) = U_V + U_S\left(1 + \tanh\left(\frac{y - y_0}{\delta_I}\right)\right) \tag{4.2}$$

The inner layer thickness increases with increasing total water depth and is also larger for a larger vegetation density. As the difference between the velocity at the interface and within the vegetation increases with increasing density the shear increases, therefore, the shear layer is smaller for the sparse vegetation than for the vegetation. However, the vortices, observed with the colored fluid, go further into the sparse vegetation than into the dense vegetation. Irrespective of the flow velocity, depth and vegetation density the outer layer thickness is constant.

Table 4.2: Thickness of the inner and outer layer as calibrated with equations 4.1 and 4.2

Set 1			Set 2			Set 3			Set 4		
dense	δ_I	δ_O	dense	δ_I	δ_O	dense	δ_I	δ_O	dense	δ_I	δ_O
			Q50H12	0.074	0.37	Q60H12	0.064	0.37	Q70H12	0.067	0.37
Q50H14	0.079	0.38	Q60H14	0.078	0.37	Q70H14	0.079	0.37	Q80H14	0.080	0.37
Q60H16	0.082	0.36	Q70H16	0.081	0.37	Q80H16	0.081	0.37			
sparse			sparse			sparse			sparse		
			Q50H12	0.039	0.36	Q60H12	0.025	0.37			
			Q60H14	0.032	0.36	Q70H14	0.041	0.36			
			Q70H16	0.047	0.35	Q80H16	0.050	0.34			

4.2.2. Transverse velocity component

The profiles of the mean transverse velocity, V, over the cross-section are given in figure 4.7. Thes plots show similarities in shape between the sparse and dense vegetation. However, the discharge in the cross-section is non-zero for all dense profiles. The flume has two closed walls at either side. Therefore the total discharge in the transverse direction should be zero.

When the profile for the dense vegetation is transposed in such way the total discharge through in the transverse direction is zero, the velocity shows a pattern. V is positive inside the vegetation and increasing

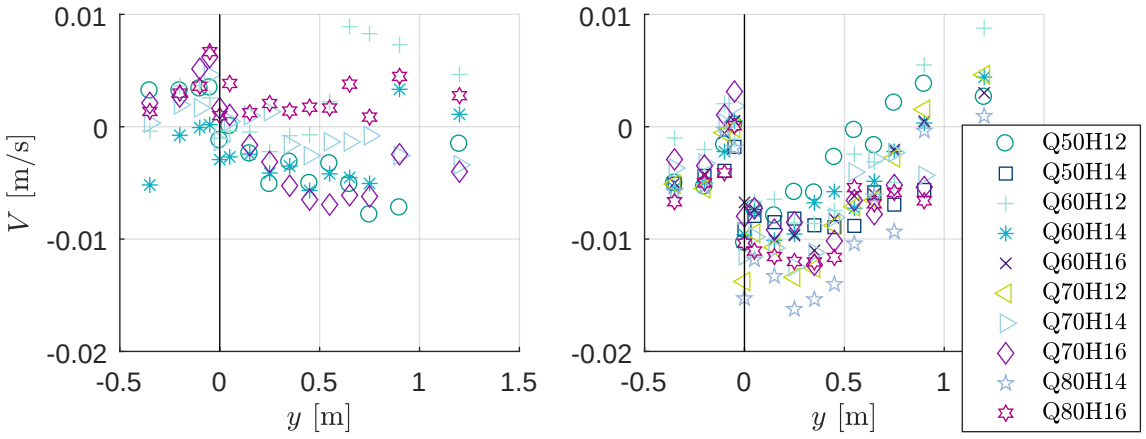


Figure 4.7: Comparison of the mean transverse velocity component, V. Left the profiles for the sparse vegetation. Right the profiles for the dense vegetation. The black line indicates the location of the interface

towards the interface. At the interface V becomes negative and starts to increase over the channel. The sparse vegetation V-profile shows a similar step in the velocity at the interface, however, this step is smaller.

The near-bed profile of the mean transverse velocity does not give a consistent profile, although it still varies around 0.

The transverse profiles of all the mean velocity components can be found in appendix B. There both the near-bed and mid-depth profiles are given.

4.3. Reynolds stress

For the analysis of the Reynolds stresses the components in the horizontal plane are considered: the deviations in the streamwise and transverse direction, $u' = u - U$ and $v' = v - V$. These deviations and the correlation of the deviations between the different axes give the properties of the strength of the coherent structures. The Reynolds shear stresses are defined as the mean of the product two perpendicular deviations: $\overline{u'v'}$, $\overline{u'w'}$ and $\overline{v'w'}$. The normal stresses are divined as the mean of the square of one component: $\overline{u'u'}$, $\overline{v'v'}$ and $\overline{w'w'}$. The Reynolds shear stress indicates the strength and direction of exchange of momentum in the indicated plane.

4.3.1. Reynols shear stress

The Reynolds shear stress is the mean of the product u' and v' and is an indication of the redistribution of momentum over the cross-section, in this case, the distribution of x-momentum in the y-direction. The shear stress profile in the cross-section is shown in figure 4.8. The peak shear stresses are located at the interface, and the order of magnitude is 10^{-4}. The magnitude of the shear stress decreases rapidly inside the vegetation, becoming relatively constant. In positive the y-direction the shear stress is decreasing slowly and approaches zero between 0.3 and 0.5 cm from the interface, which is approximately outer layer thickness.

For equal the channel velocities and mean velocity profiles, the absolute magnitude of the peak of the shear stress and the width of the shear stress profile are more significant for larger water depth. Increasing depth also increases the maximum absolute shear stress as well as the shape of the profile. The maximum shear stress at the interface is not equal for these situations. When the depth increases, the absolute value of the shear stress increases and also the width of the peak increases. The increase of the channel velocity between set 2 and set 3 results in a larger absolute peak shear stress at the interface. The shape of the profiles for the different water depths is similar.

The vegetation density has a small influence on the magnitude of the shear stress, has a significant influence on the mean shear stress inside the vegetation. Within the sparse vegetation the shear stress is negative and one order of magnitude smaller than in the shear layer, while the shear stress in the dense vegetation is merely positive.

However, the flow structure in the upper water column influences the structures found on the bed; there are some differences between the shear stress at the bottom and the middle of the water column. Near the bottom the shear stress profile wiggles around zero as can be seen in figure 4.9. Two distinct peaks can be

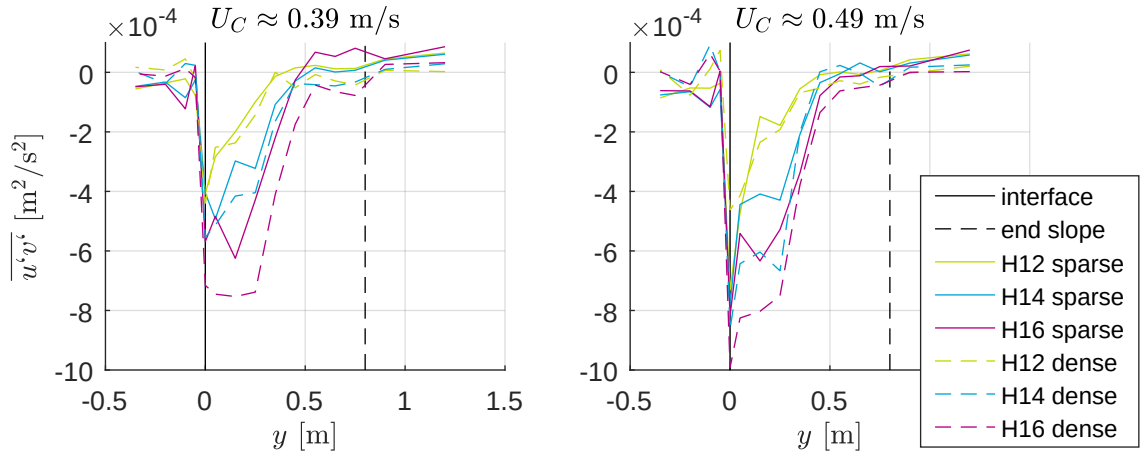


Figure 4.8: Reynolds shear stress, $\overline{u'v'}$, in the middle of the water column. Left) the shear stress profiles for set 2, $U_C \approx 0.4 m/s$. Right) the shear stress profiles for set 3, $U_C \approx 0.45 m/s$. The solid lines indicate sparse vegetation and the dashed lines the dense vegetation

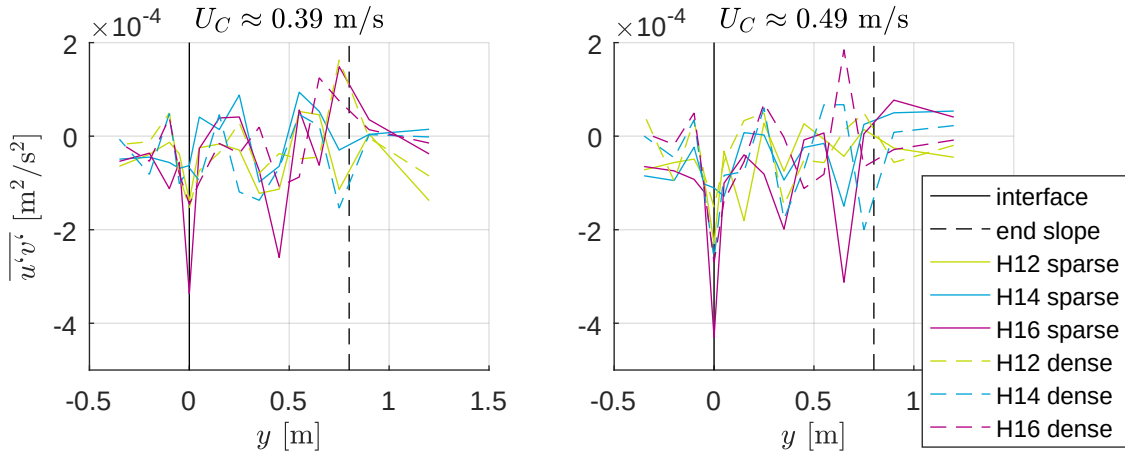


Figure 4.9: Reynolds shear stress, $\overline{u'v'}$, near the bottom. Left) the shear stress profiles for set 2. Right) the shear stress profiles for set 3. The solid lines indicate sparse vegetation and the dashed lines the dense vegetation

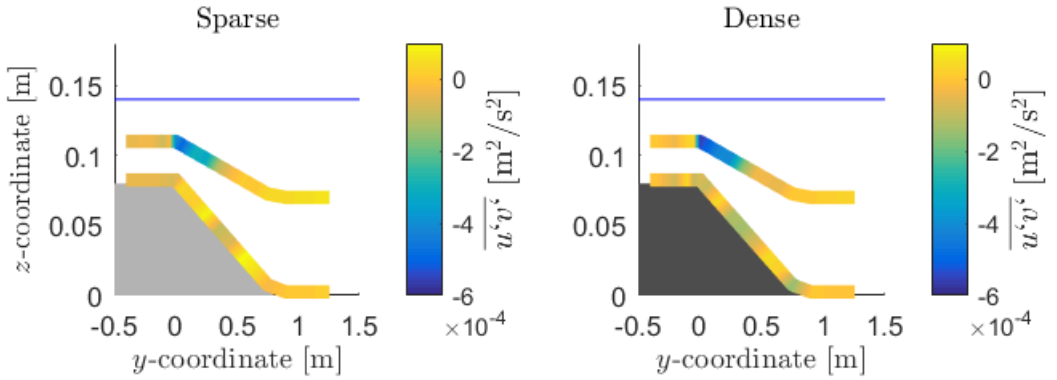


Figure 4.10: $\overline{u'v'}$ for $Q = 60\,l/s$ and $H = 14\,cm$ in the sparse (left) and dense (right) setup. The profile of the Reynolds stress is similar for both setups, however the magnitude at the interface is larger for the dense vegetation.

identified in each profile. Around the interface the first peak is visible, this one is at the same location as the peak found in the middle of the water column, but is smaller by a factor 3 to 5. Also, the width of this peak is smaller. A second peak is found around $y \approx 0.4$ m. This one smaller than the peak at the interface but appears in all the profiles around the same location. At the same place as where the shear stress at mid-depth becomes constant.

Within the vegetation, the difference between the shear stress at the bottom and in the middle of the water column is zero. As with the flow velocity, the decrease in shear stress within the vegetation depends only on the vegetative drag.

Shear stress profile in the cross-section

Figure 4.12 shows the comparison between the shear stresses near the bottom and at mid-water depth in more detail. As can be seen, the second peak of the bottom shear stress is located in the middle of the slope. Also, the influence of the dense vegetation is shown with the darker shade near the interface. Within the vegetation, the lines have the same color. The vegetation governs not only the velocity but also the shear stress over the whole water depth.

4.3.2. Normal stresses

The depth and channel velocity are governing for the outer layer, the vegetation density more so for the inner layer. Into the vegetation, the Reynolds stress drops within 10 cm towards the value of the vegetative Reynolds stress. This which is mainly determined by the vegetation density, influencing the velocity and the amount of turbulence. $\overline{u'u'}$ as a similar drop inside the vegetation. This decrease, however, is not as steep as for $\overline{v'v'}$. These two values give insight into the strength of the velocity fluctuations, the square root of $\overline{u'u'}$ and $\overline{v'v'}$ give the RMS of the velocity amplitude.

The fluctuations on the slope are stronger in the streamwise direction than in the transverse direction. Also the peak of $\overline{v'v'}$ lies further away from the interface than the peak of $\overline{u'u'}$. However, they have the strongest negative correlation at the interface. In the outer layer, the Reynolds stress profiles show dependency on the water depth. Maximums of $\overline{u'u'}$ and $\overline{v'v'}$ increase with increasing water depth.

At the bottom, it appears that there are two regions, a region influenced by the vegetation, the peak at y=0 and a region where the channel affects the lateral shear. At lower elevations the slope causes differences velocity at that specific depth, these do not penetrate into higher elevations as there the difference with the vegetation becomes more important. This is not important for the upper part of the water column as there the velocity and structures are merely determined by the presence of the vegetation. The mean velocity at the bottom follows the velocity at mid-depth, governed by the momentum present in the upper part of the water column.

4.3.3. Contribution of the coherent structures vs. 3D turbulence

After the time series had been smoothed over a time interval of 2 s, contributions to the Reynolds shear stress from the vortices and the 3D turbulence were identified. Within the region of shear, around the interface, the contribution of the vortices is one order of magnitude larger than the contribution of the 3D turbulence,

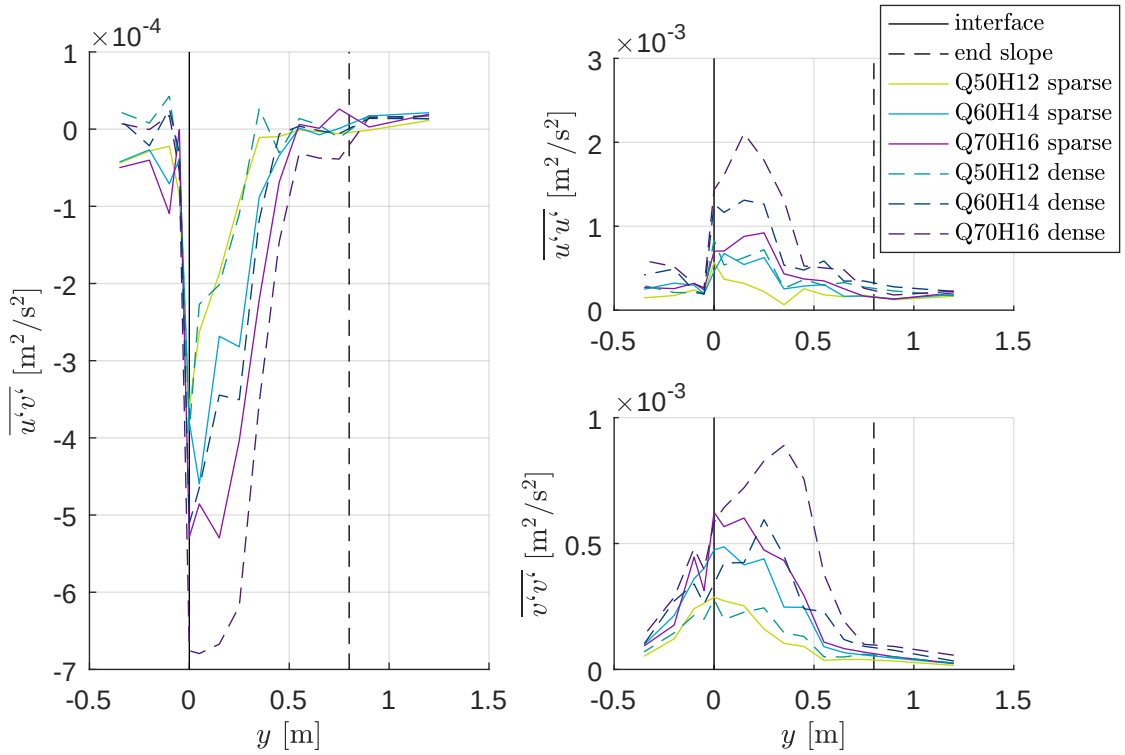


Figure 4.11: Comparison between $\overline{u'v'}$, $\overline{u'u'}$ and $\overline{v'v'}$, for set 2 in the middle of the water column. The full lines indicate the sparse vegetation, the dashed lines indicate the dense vegetation.

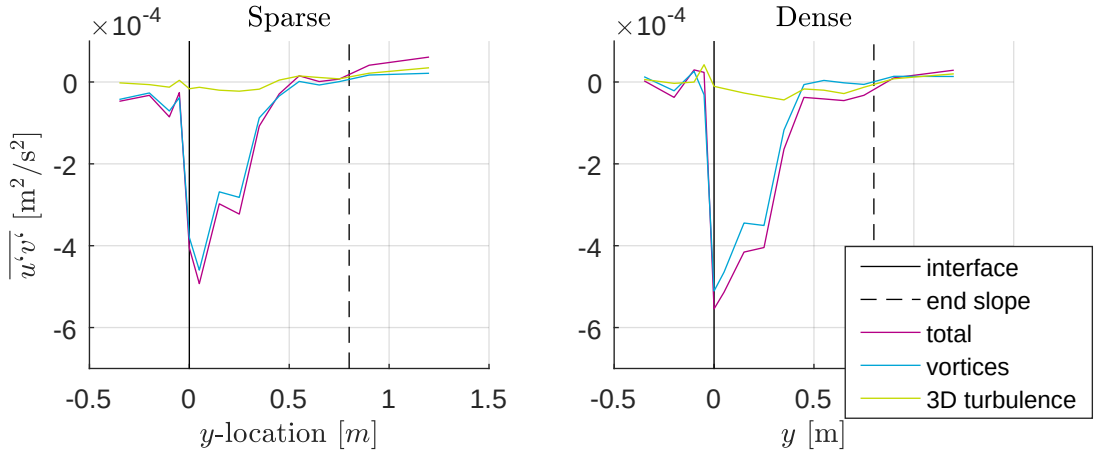


Figure 4.12: Contributions to the Reynolds stress $\overline{u'v'}$ for $Q = 60 l/s$ and $H = 14\ cm$ in the sparse (left) and dense (right) setup. The largest part of the Reynolds stress is determined by the vortices. Outside the shear layer the 3D turbulence is more important.

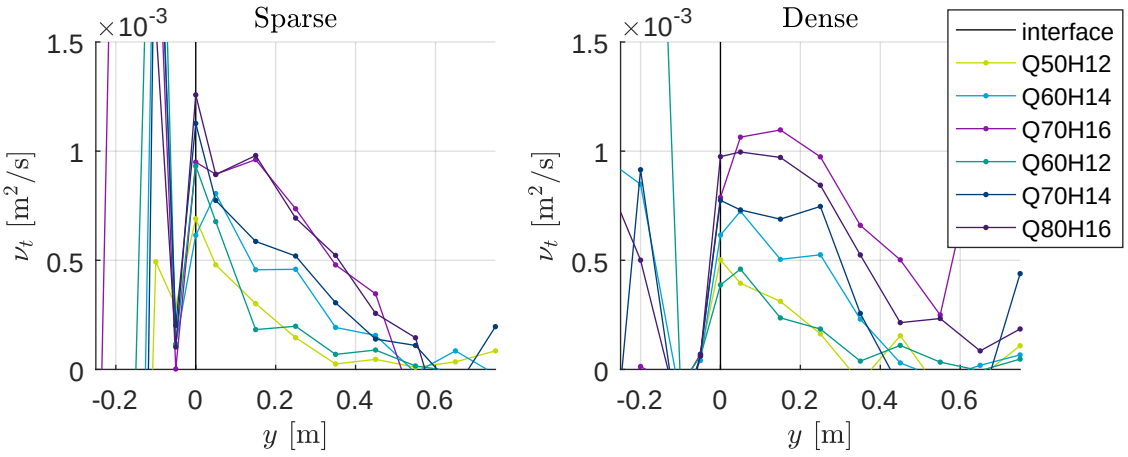


Figure 4.13: ν_t in the sparse (left) and dense (right) setup.

$1e-4$ and $1e-5$ respectively. In the channel, outside the zone of influence of the vortices, the 3D turbulence is dominant.

The shear caused by the 3D turbulence is constant over the total cross-section. Considering sediment transport, 3D is important for initiation of motion, while the larger structures distribute particles further over the cross-section.

The 3D turbulence is constant for y>0 and less strong inside the vegetation. The shear stress at location y = 0.05 m has a small positive peak; this peak is related to the smaller scale vortices created by a single cylinder. These vortices have a shorter length scale and are positively correlated. The characteristics of these vortices are related to the shape and location of the individual plants.

In the dense setup, 3D turbulence governs $\overline{v'v'}$ in the channel. However, the difference in the locations of the peak of $\overline{u'u'}$ and $\overline{v'v'}$ does not change. The maximum values of the deviations from the mean V are located at a location further away from the interface than the maximum value of the deviations from U. Now looking at the difference between the different vegetation densities results in similar strengths of $\overline{v'v'}_{vortices}$, but the difference lies in the 3D turbulence component.

4.3.4. Turbulent viscosity

For most modeling purposes a turbulent viscosity is needed for turbulence closure in the flow. The Boussinesq equation (equation 4.3) can be used to calculate the turbulent viscosity at each measuring location, and the mixing length can be calculated with equation 4.3.

$$\nu_t = -\overline{u'v'} / \frac{\partial \overline{U}}{\partial y} \tag{4.3}$$

For each profile dU/dy was calculated with the central differences method from the measured data, the value of $\overline{u'v'}$ was derived directly from the measured data using only the contribution of the vortices to the Reynolds stress. The results for the turbulent viscosity are shown in figure 4.13. When the velocity gradient is approaching zero, the value of the turbulent viscosity explodes. The turbulent viscosity is not defined when there is no gradient. Therefore the plots only cover the area of shear, $-0.25 < y < 0.75$.

The turbulent viscosity has a distinct peak at the interface with the sparse vegetation, while the peak at the dense interface is broader. The turbulent viscosity increases with water depth, and each depth shows the same profile of for the different velocities. The location where the turbulent viscosity approaches zero increases with depth and varies between $y = 0.4$ and $y = 0.6$. The flow velocity in the channel does not influence the profile. As the influence of the channel velocity and the gradient in the shear region is represented in dU/dy, as well as in the influence in the on the shear stress.

The order magnitude of the turbulent viscosity is $1e^{-3}$. The order magnitude of the turbulent viscosity in the vertical, a result from the bed turbulence, $1/6\kappa u^* h$, is similar to the turbulent viscosity resulting from the shear in the transverse direction. However the length scale in the vertical is much smaller, 10 cm versus 50 cm.

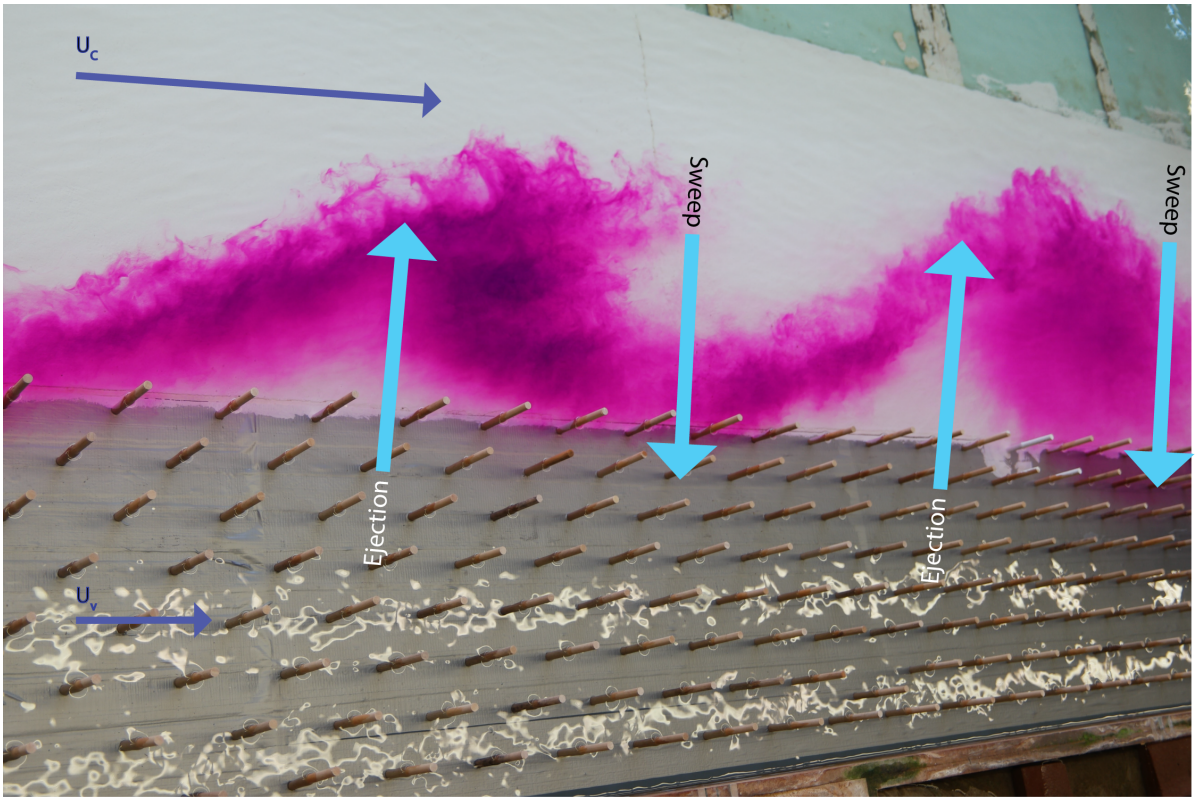


Figure 4.14: Sweep and ejections, visualized with colored fluid in the water. The blue line indicates the mean flow direction.

4.4. Vortex structure

The coherent vortices are the main contributor to the Reynolds stress and the mixing processes. The characteristics of the vortices are analyzed in this section to get a better insight into the vortex structure and the possible effects on sediment transport properties.

4.4.1. Sweeps and Ejections

As observed in the ADV measurements the shear stress in the zone where the vortices are present is negative. This indicates vortex structures that consist of sweeps, u' positive and v' negative, and ejections, u' negative and v' positive. The directions of the sweeps and ejections in the flow are visualized with color fluid in figure 4.14. The visualized vortex negative transverse velocity at the downstream end, followed by the positive transverse velocity at the upstream end.

The pattern of the sweeps and ejections at the interfaces is shown in figures 4.15 and 4.16. The upper panels show the deviations from the streamwise and transverse velocity components, the lower panels their products. Also, the Reynolds stress is plotted in the figures. The peaks of the stress in the middle of the water column are a factor 3 larger than the time mean.

Sweep ejection pattern is stronger and more regular at mid-depth than at the bottom. At mid-depth $u'v'$ is almost always negative while at the bottom the negative peaks are smaller and more often also positive, this because the velocity deviations in both directions are less regular and are shifted in phase to each other. Still, there are strong vortices are reach the bed.

In the middle of the water column, the ejections are in general shorter in duration but have a lower minimum value than the sweeps. The ejection has almost always a smaller minimum than the sweep it follows, with a factor 1.5.

Near the bottom the pattern is less regular and between a sweep and ejection the value of $u'v'$ becomes positive, due to the phase shift between both velocity components. Still, for the dense vegetation, the sweeps tend to be less strong but longer in duration than the ejections.

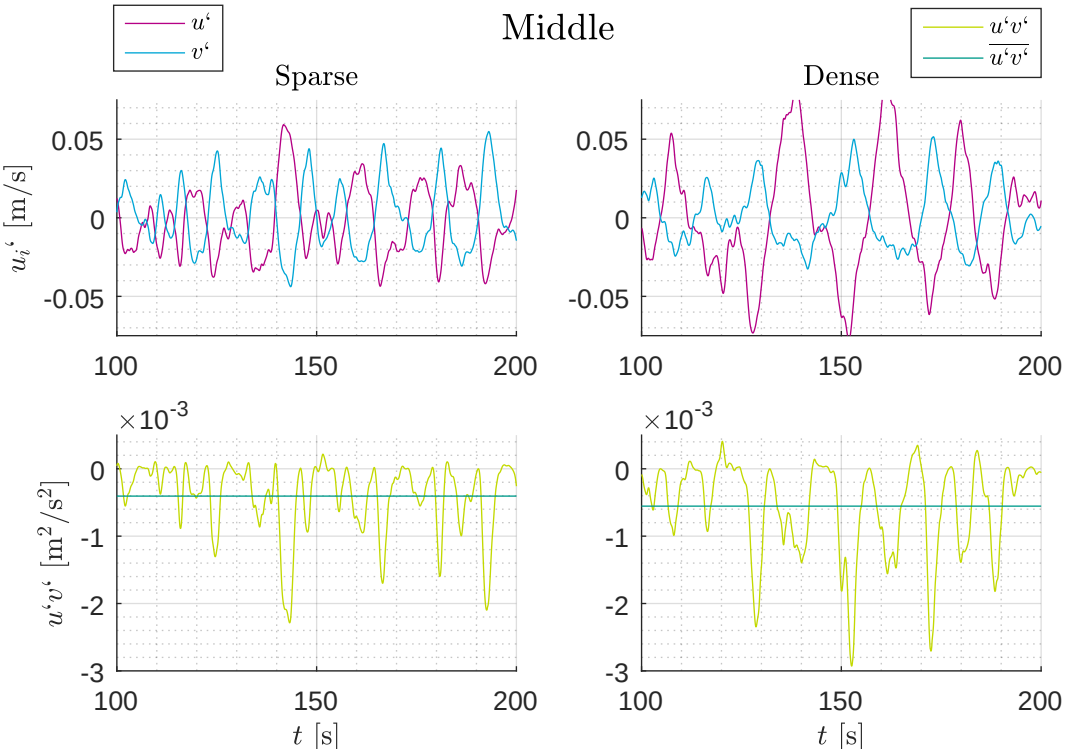


Figure 4.15: Sweep and ejections in the middle of the water column for Q60H14. The dark green line in the lower panels give the Reynolds stress

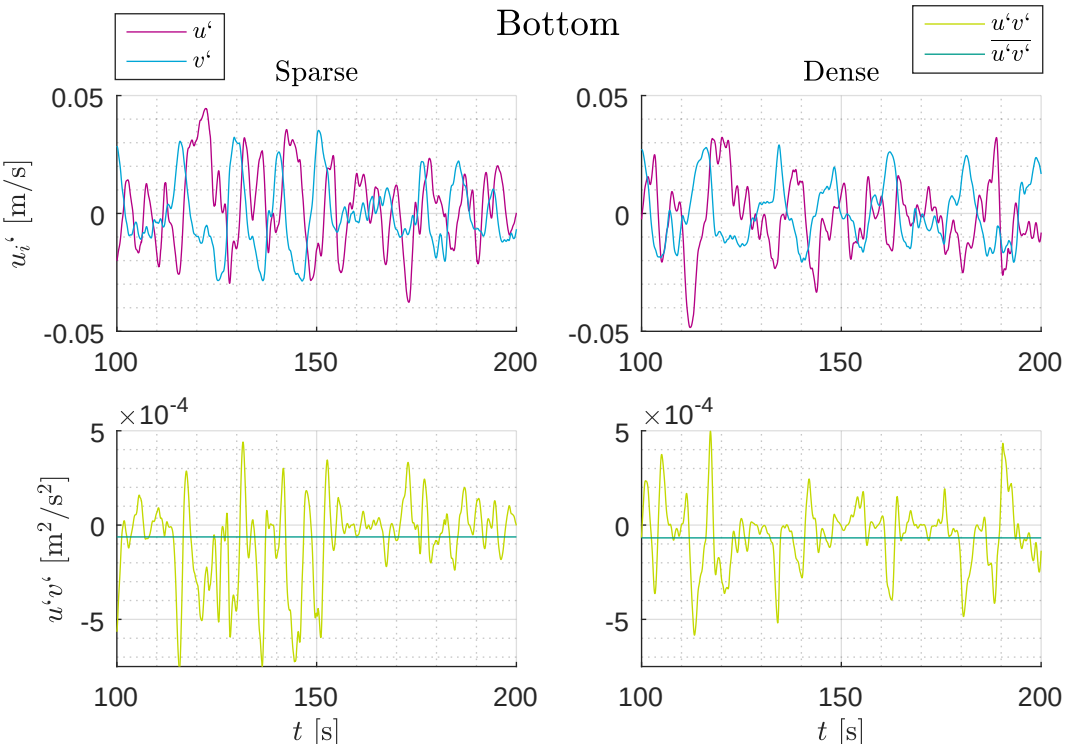


Figure 4.16: Sweep and ejections at the bottom for Q60H14. The dark green line in the lower panels give the Reynolds stress

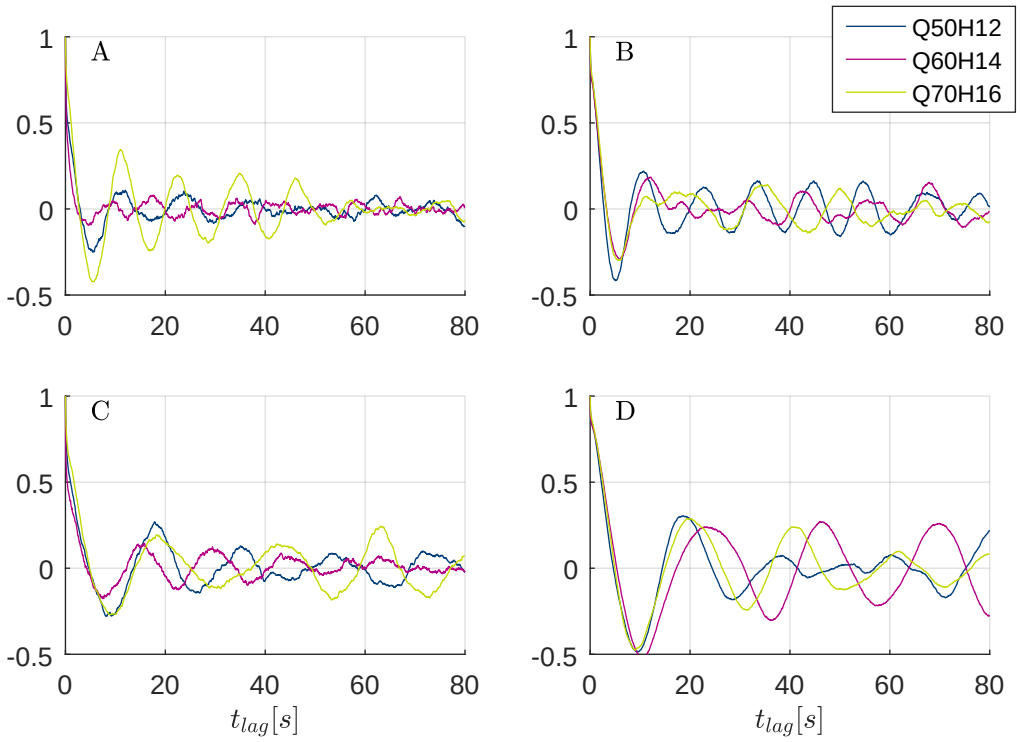


Figure 4.17: Autocorrelation of the time signals at the bottom and at mid depth on $y = 0$ for different water depths with similar channel velocities $(U_{c,mid} \approx 0.4\ m/s)$ (set2). A) At the bottom with sparse vegetation. B) At mid-depth with sparse vegetation. C) At the bottom with dense vegetation. D) At mid-depth with dense vegetation. For the sparse vegetation, the first time autocorrelation changes sign is around $t_{lag} \approx 3\ s$. The lower panel shows the autocorrelation for the dense vegetation, the first time autocorrelation changes sign is around $t_{lag} \approx 5\ s$.

4.4.2. Autocorrelation

Figure 4.17 shows the autocorrelations for the time series in set 2. The influence of the coherent structures is visible in the decreasing sine which starts after a steep drop in the first quarter second. The drop can be assigned to the random 3D turbulence. Within the first quarter second the autocorrelation drops, for larger t_{lag} the autocorrelation function changes into a decreasing sinusoidal signal. The quick drop can be assigned to the 3D turbulence, and the sinusoidal part can be assigned to the coherent motion. The timescale of the coherent motion is ≈ 1.5 times larger for the dense vegetation.

At the bottom the peaks of the autocorrelation are lower and dampen faster than at mid-depth. However, the vortices have the same frequency. The upper part of the water column determines the motion of the total water body, which is still felt at the bottom. However, friction plays a role in the dissipation of the coherent motion, making it less structured than at the middle of the water column. Also, the 3D turbulence is of more important, because the slope of the autocorrelation plot for the first two time steps is steeper near the bottom.

At the bottom the peaks of the autocorrelation are lower and dampen faster than at mid-depth. However, the vortices have the same frequency. The total water body moves with the same frequency. A larger water depth gives a larger autocorrelation at the bottom.

4.4.3. Energy density spectrum

The autocorrelation gives insight in the strength and the similarity of the coherent structures; the spectral analysis gives more information about the frequencies of the structures the rate of energy dissipation to smaller turbulence structures. For the calculation of the energy density spectra, each time series was divided into five equal sections for which the energy density spectrum was derived. The energy density spectrum of the whole time series has been determined by taking the mean of the five subspectra. Figure 4.18 shows the energy density spectra derived from u' and v' at the interface for set 2. This figure shows the importance of the different variables for the frequency of the vortices and the energy these frequencies store. This is related to the momentum exchange by the vortices. The peak in the low frequency gives the main frequency of the coherent vortices. The slope of the spectrum towards the higher frequencies scales with the frequency to

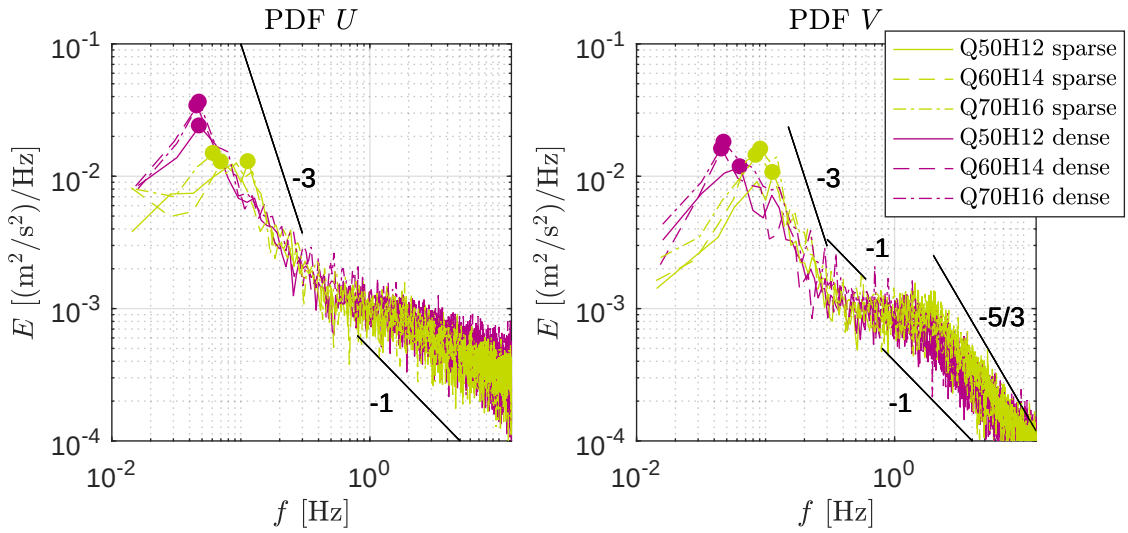


Figure 4.18: Energy density spectra derived for set 2. Left) energy density spectrum of the streamwise velocity component. Right) energy density spectrum of the transverse velocity component. The green lines indicate the sparse vegetation and the purple lines the dense vegetation. The different water depths are presented as follows: solid line (-) 12 cm, dashed line(–) 14 cm and dash-dot line (-.) 16 cm.

the power -3, which indicates the energy transfer to higher frequencies through 2D coherent motion. In the high-frequency tail, the slope of the spectrum scales to the power $-5/3$ (for u'), which is the slope for the energy cascade in the 3D random turbulent motion. Therefore the smoothing of 2 seconds for the time series is a good value to filter the turbulence.

The main frequency for the dense vegetation varies between 0.046 and 0.077 Hz, corresponding to periods of 13 to 22 seconds. For the sparse vegetation, the frequency varies between 0.092 and 0.123 Hz, which corresponds to smaller periods between 8 and 11 seconds. For an increasing water depth, the frequency decreases and with an increasing channel velocity the frequency increases. The top frequency is constant over most of the cross-section. The influence of the coherent structures is present over almost the full cross-section. For the dense vegetation case only with a water depth of 12 cm the time series in the channel have different frequencies, for the other two depths frequency of the coherent structures is constant over the full width. With the sparse vegetation the coherent structures are persistent up to $y \approx 0.7 \pm 0.1$. A larger water depth creates larger coherent structures that reach further into the channel.

The channel does not influence the coherent structures while at y = 0.45 m and lower the peak of the energy density spectrum is at the same frequency and power as at the interface (figure 4.19. While the Reynolds shear stress is already one order magnitude smaller at this location than at the peak. The same is valid for the location y = -0.2. The coherent motion is still active at this location. However, the redistribution of streamwise momentum in the transverse direction is almost zero.

With the the found frequency and the momentum thickness (values given in Appendix B),

$$\Theta = \int_{\infty}^{-\infty} \left[\frac{1}{4} - \left(\frac{U - \overline{U}}{\Delta U} \right)^2 \right] dy \tag{4.4}$$

the Strouhal number of the vortices, equation 4.5, has been calculated. The momentum thickness was calculated using the trapezoidal rule for discrete integration and the frequency at the interface was taken. The calculated Strouhal number was 0.044 ± 0.007 for the sparse vegetation and 0.031 ± 0.003 for the dense vegetation in the middle of the water column.

$$St = f\Theta/\overline{U} \tag{4.5}$$

Near the bottom the frequencies are equal to the frequency at mid-depth, but the energy contained in that frequency is lower, decreased with 25% to 60%. Also, the depth and the velocity influence those two parameters and determine the momentum which is available in the water column. The vegetation density is of lesser importance for the energy contained in by the max frequency. The energy contained in the peak frequency is related to the $\overline{v'v'}$ as the power is the square of the velocity components.

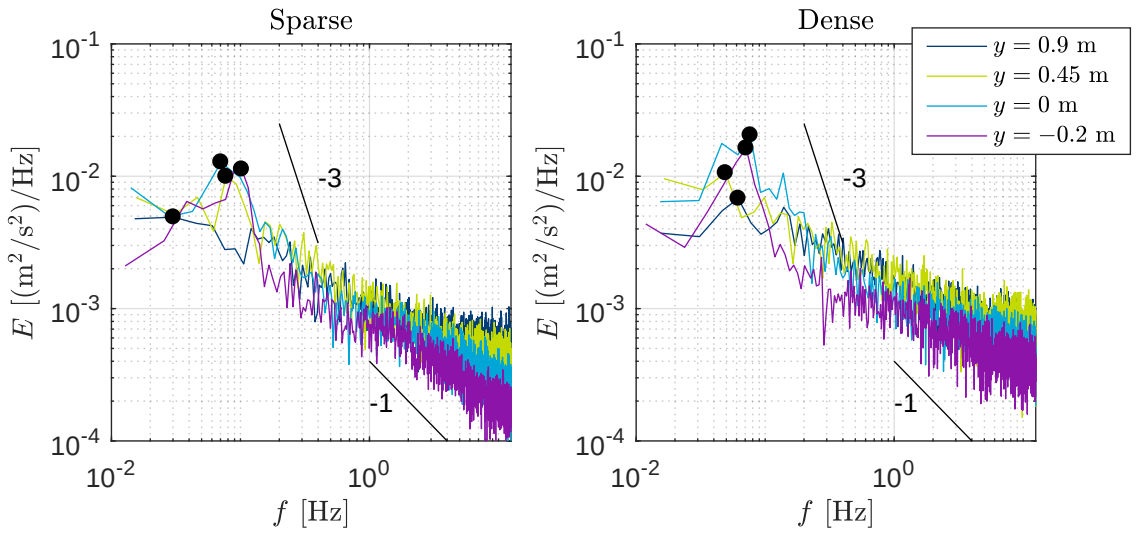


Figure 4.19: Energy density spectra derived for set Q = 60 l/s and H = 14 cm at four locations in the cross-section. Left) sparse vegetation. Right) dense vegetation

4.4.4. Instantaneous flow field

The instantaneous flow field was derived from the measured vector field from the PTV analysis, using interpolation between the different vectors. Two flow fields are shown in figures 4.20 and 4.21, both in a different phase of a passing vortex. The upper panel of these figures shows the magnitude of the streamwise component and the lower of the transverse component. The arrows give the velocity vector of each detected tracer in that frame. The negative y is within the vegetation and the positive on the slope.

Considering the streamwise component, it is observed that, the velocity in the vegetation has its minimum while the velocity on the slope is at its maximum. Indicated by dark blue and bright yellow respectively in the upper panels of the two figures.

The transverse component has its positive maximum at the moment when the streamwise velocity deviation changes sign, as can be seen at $x_{ref} = 0.8m$ in figure 4.20. The positive maximum of the transverse velocity is quite concentrated in the x-direction. However, the negative minimum transverse velocity spreads over a greater length and has a smaller magnitude, see figure 4.21. When the streamwise velocity in the channel is at its minimum in the vegetation, the transverse velocity is almost zero. Comparing this to the measured time series of the velocity for these settings, as can be found in appendix C. At the interface, the maximum streamwise component occurs at the same time as the minimum transverse component, however, within the vegetation this the maximum and minimum streamwise velocity occur while the transverse component is approaching zero.

4.5. Transport

In the process to extract the particle paths from the videos, color detection was used to distinguish the red spheres from the bottom and the cylinders. In the experiment with the dense vegetation, the slope was white while the bed between the cylinders was grey, also the cylinders had a woody color. This complicated the process to detect the red particles inside the vegetated zone properly and therefore to extract paths for this area.

For the experiment with the sparse vegetation, the bed and the cylinders in the observation area were painted white. This resulted in a better visibility inside the vegetated area. The lower density of the vegetation also enhanced the visibility of the particles.

Only the particle paths that could be tracked for longer than 1 second, at least 24 image pairs, are taken into account in the further analysis. Some spheres have a water bubble attached to it and start to float; this happens mostly inside the vegetation. The floating particles move faster than the rolling particles. At the bed the driving force consists of the flow velocity and the profile is still developing for most of the diameter of the spheres. Therefore the driving force is lower at the bottom. At the bottom, the particles are influenced by friction as well.

The main difference between the paths in the sparse and dense vegetation is that they move with a con-

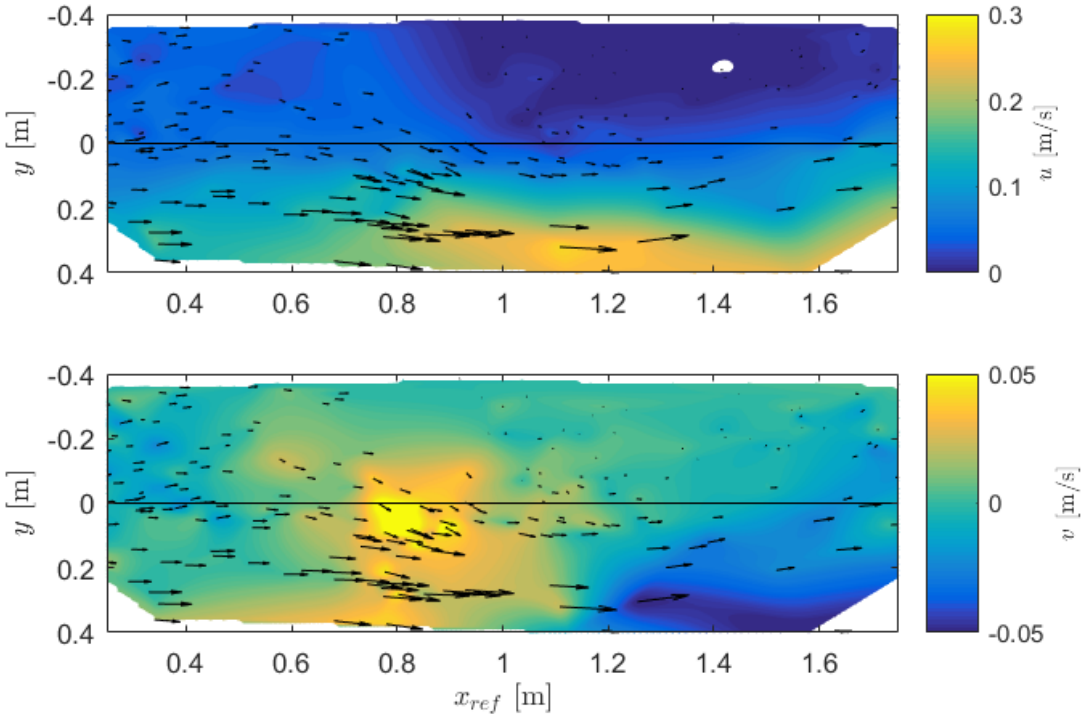


Figure 4.20: The instantaneous flow field at for frame 2241 of the Q60H14 dataset. Left) The streamwise component of the flow. Right) The transverse component of the flow. The arrows indicate the velocity vector of the detected tracers

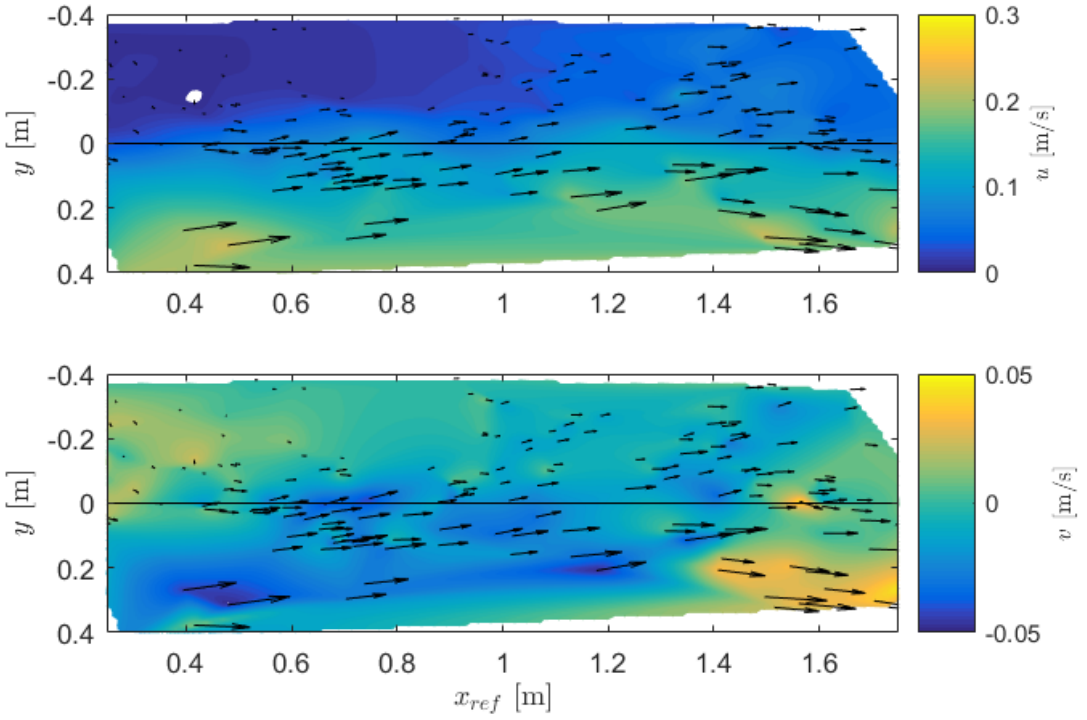


Figure 4.21: The instantaneous flow field at for frame 2100 of the Q60H14 dataset. Left) The streamwise component of the flow. Right) The transverse component of the flow. The arrows indicate the velocity vector of the detected tracers

siderably lower mean velocity within the dense vegetation, as well as moving in opposite direction to the mean velocity during ejections. Within the sparse vegetation, a decrease of the streamwise velocity towards zero was observed during the ejections. However, in none of the sparse test settings, the streamwise velocity component became negative. This observation is consistent with the observed time series with the ADV measurements (Appendix B). During a period the streamwise velocity component varies around the mean and becomes negative in the dense setting. The variable velocity changes the direction of the drag force exerted on a particle over a period.

4.5.1. Qualitative observations PTV movies

At higher velocities the tracers started to saltate, this happened on the slope and influenced the eventual path of the particles. While the tracers are touching the slope the bed-normal force, resulting from the gravity, has a component in the positive y-direction. During a sweep, the drag force in y-direction on the tracer is decreased by this value. Therefore the particle has a smaller acceleration in the upslope direction. The tracer touching the slope will need more time to be transported over the same distance as a tracer located on a horizontal bed. Moreover, the effect of the ejections is enhanced by the gravity, bringing the tracers further downslope in one ejection event.

The location where tracers started to saltate, increased with increasing channel velocity. Within the first 10 cm from the interface, the tracers were all touching the bed. Tracers transported into the vegetation first accelerated as result of the decrease of the y-component of the bed-normal force while the drag remains constant. Within the vegetation, the transverse velocity decreases and resulting in deceleration of the tracers. The maximum distance tracers were brought into the vegetation depends on the vegetation density.

The effect of the ejections and sweeps is visible over the full width of the vegetation, however near the wall this is most visible in acceleration and deceleration of the streamwise velocity component. Near the interface, the variation in the transverse velocity component appears to be stronger.

If particles are more than 20 cm away from the interface, there is only a slight chance for them to eventually end up in the vegetation. In the area between $y = 0.15$ and 0, the chance of interaction with the canopy increases.

More particles leave the vegetated area than that enter it. Also, the transverse velocity component is stronger in the positive direction for the spheres. This is counter-intuitive with the idea of the convergent flow into the vegetation but can be explained by the influence of gravity on particles on a slope. Especially in the dense setup, strong ejections are responsible for large accelerations in the transverse velocity, pulling almost all the particles nearby the interface out of the vegetation. It is estimated that around half of these particles will stay on the slope and the other half will stay in the exchange zone.

The difference between the dense and sparse vegetation can be characterized the flow characteristics and length scales related to the shear layer.

1. Tracer velocity inside the vegetation: related to the mean flow velocity in the vegetation, the deviations from the mean velocity inside the vegetation and the period of the vortices.

2. Length scale over which interaction between the vegetation and channel is possible: related to the strength of the vortices in the inner region (vegetation side) and the outer region(channel side).

In the dense setup, there are test settings for which a negative streamwise velocity component is observed inside the vegetation. This appears to be stronger for larger water depths and higher channel velocities. For larger streamwise velocities the peak in the Reynolds stress is higher, while for a larger water depth the peak is wider. No negative transport directions were observed in the sparse vegetation.

The interaction between the sparse vegetation and the channel was larger than for the dense vegetation. Within the dense setup the area around the interface only served as an exchange area. Tracers were passing through this area from the channel towards the vegetation or vice-versa. In the sparse setup, tracers were present in the exchange zone for more extended periods of time and transported over long distances in the streamwise direction while situated in the area of exchange.

4.5.2. Particle paths

When a tracer could not be tracked within two consecutive frames, it was assigned a new particle number by the PTV software the next time it was visible. Therefore some particle paths could not be tracked throughout the complete area of interest. This frequently happened inside the vegetated area where tracers moved through the image shadow of the cylinders. Because the sparse setup has fewer cylinders, fewer tracers are

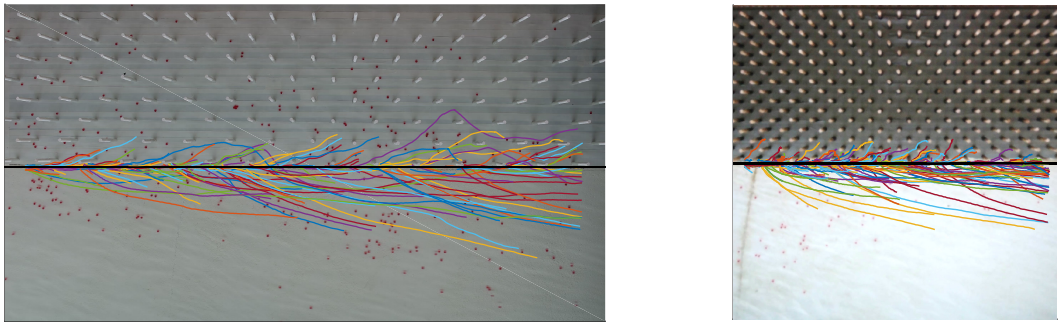


Figure 4.22: Tracked particle paths originating at the interface. Left) Sparse. Right) Dense. The scaling of the images is the same.

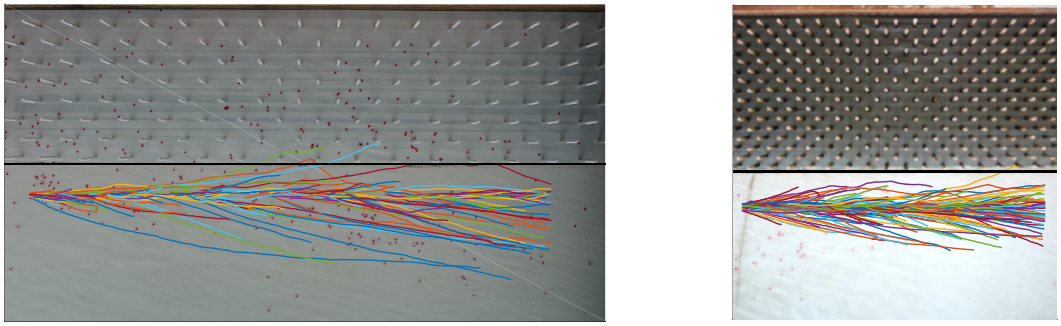


Figure 4.23: Tracked particle paths originating at 10 cm down slope of the interface. Left) Sparse. Right) Dense. The scaling of the images is the same.

passing the image shadow, increasing the traceability of the tracers. Also, the increased contrast after the adjustments to the flume increased the visibility of these particles. Therefore direct comparisons between the sparse and dense setup are hard to make.

Figures 4.22 and 4.23 show tracer paths originating in the interface and at 0.1 m from the interface respectively. Particles are entering the vegetation at a small angle with the interface direction, but the angle increases afterward. This effect is stronger within the dense vegetation where the angle of the path changes to more than 45^o. In the sparse setup, this effect is visible as well, but path angles are still moderate.

The influence of the slope is visible in the broader spreading towards the channel than towards the vegetation. Also, the mean transverse velocity is positive for the whole cross-section, indicating a downslope transport. During the experiments it was observed that more particles left the vegetation than entered it, a positive V is consistent with these observations.

Although the mean transport was downslope, the vortices were still able to transport tracers up the slope. However, the original location determines the maximum distance a particle can penetrate into the vegetation.

4.5.3. Exchange

The exchange region is defined as the region around the interface where PTV tracers entering the observation area within these bounds can be transported across the interface within a downstream distance of ≈ 1 m. The exchange zone is divided into two areas, the vegetated and non-vegetated, which are indicated by two different length scales. The part within the vegetation ($y < 0$) is the inner exchange region, $\delta_{e,I}$, and the part of

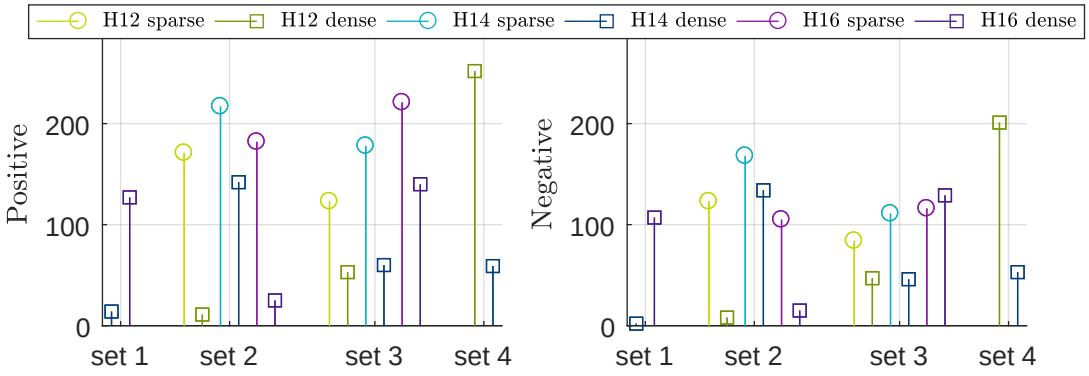


Figure 4.24: The amount of observed crossings, these are the total amount of crossings extracted from the PTV data. A positive crossing is in the positive y-direction, out of the vegetation. A negative crossing is in the negative y-direction, into the vegetation

the transverse slope ($y > 0$) is the outer exchange region, $\delta_{e,O}$. These length scales have been estimated from the movies made for the PTV analysis together with the data from the PTV analysis, using only the data was not sufficient as paths had gaps when particles were not detected in two consecutive frames. The exchange region thicknesses are displayed in table 4.3.

In general, a higher vegetation density reduces the exchange region and a larger water depth or mean flow velocity increases this region. The depth influences the thickness of the inner layer, especially for the set with the higher velocity. In this case, the particles penetrate further into the vegetation. When they reach the maximum intrusion depth, they are transported out of the vegetation by the ejection.

Table 4.3: Exchange regions for the different comparable sets. The set numbers relate to the set numbers in table 4.1, the channel velocities for each set are approximately equal.

Set 1			**Set 2**			**Set 3**			**Set 4**		
dense	$\delta_{e,I}$	$\delta_{e,O}$	dense	$\delta_{e,I}$	$\delta_{e,O}$	dense	$\delta_{e,I}$	$\delta_{e,O}$	dense	$\delta_{e,I}$	$\delta_{e,O}$
			Q50H12	0.1	0.06	Q60H12	0.1	0.06	Q70H12		
Q50H14			Q60H14	0.1	0.08	Q70H14	0.1	0.10	Q80H14		
Q60H16			Q70H16	0.12	0.12	Q80H16	0.14	0.12			
sparse			sparse			sparse			sparse		
			Q50H12	0.13	0.14	Q60H12	0.14	0.12			
			Q60H14	0.14	0.16	Q70H14	0.14	0.14			
			Q70H16	0.14	0.12	Q80H16	0.2	0.16			

Inside the exchange region, the number of tracers leaving the vegetation was larger than the amount entering, decreasing the total number of tracers in the vegetation in all experimental settings (figure 4.24). Extrapolating this could indicate a net erosion within the exchange region as an initial response to a similar bathymetry. However, this experiment as the critical shear stress for the tracers is negligible does not take the effect of incipient motion into account. The observed velocity magnitudes, $u * v$, figure 4.26, and velocity angles, figure 4.25, when the particles crossed the y-axis.

When a particle on the slope approaches the vegetation, it slows down as result of the decreasing flow velocity. Also because the variation in the vertical velocity is smaller the force to bring particles upslope during a sweep becomes lower. With the higher vegetation density, the time to reach the vegetation in during one sweep is longer, but the momentum of the particle is lower when the interface is reached, exchange region for the inner layer is smaller for the dense vegetation.

The three properties on which the velocity magnitude and angle can be compared are the vegetation density, water depth, and the channel velocity. Only the data sets with more than 40 crossings in both directions are considered sufficient for further analysis. Measured velocity magnitudes above the 0.25 m/s are deemed erroneous as these are not consistent with the ADV data and are far outside the 95% confidence limits of the box plots.

Tracers were transported into the vegetation on an angle which was twice as small as the angle of the tracers leaving the vegetation: particles are transported into the vegetation more perpendicular to the in-

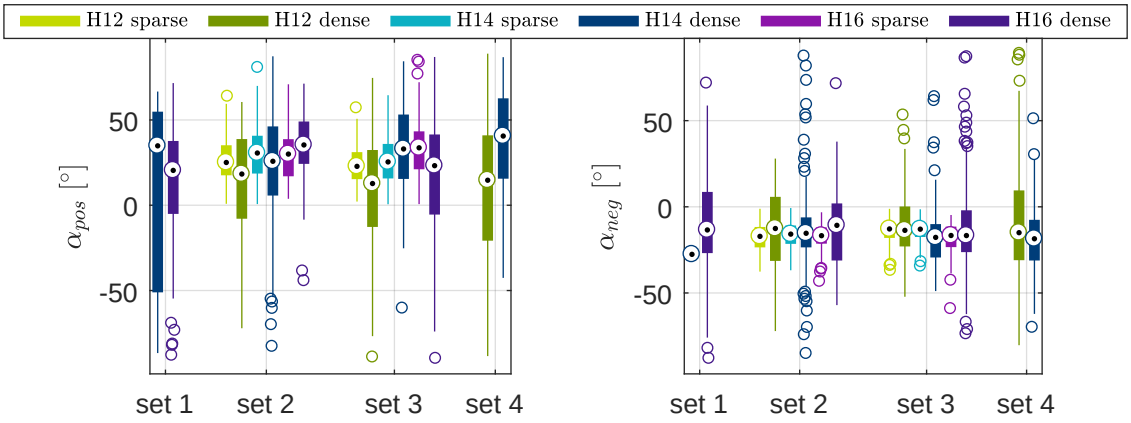


Figure 4.25: The velocity angles, α, at the moment the particles cross the y-axis. The different sets correspond to the sets shown in table 4.3 with similar channel velocities

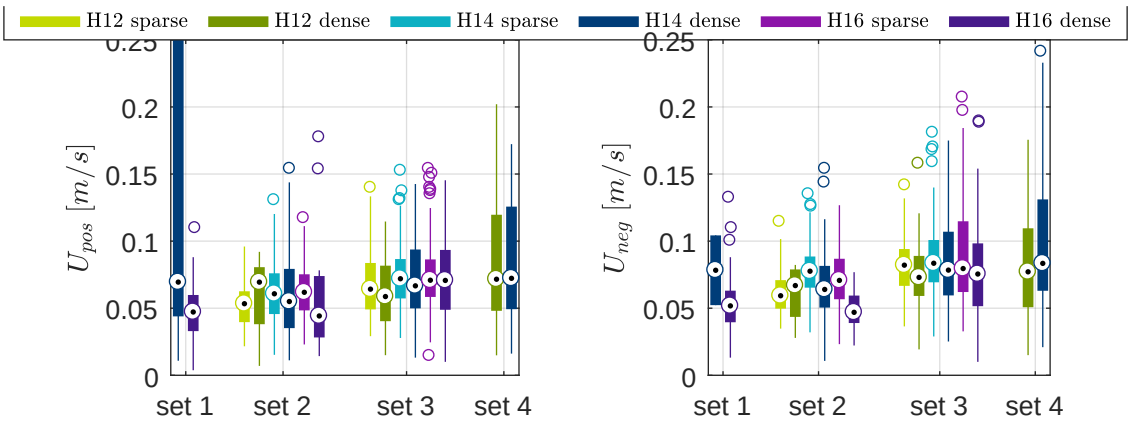


Figure 4.26: The velocity magnitudes, $U = \sqrt{u^2 + v^2}$, at the moment the particles cross the y-axis. The different sets correspond to the sets shown in table 4.3 with similar channel velocities

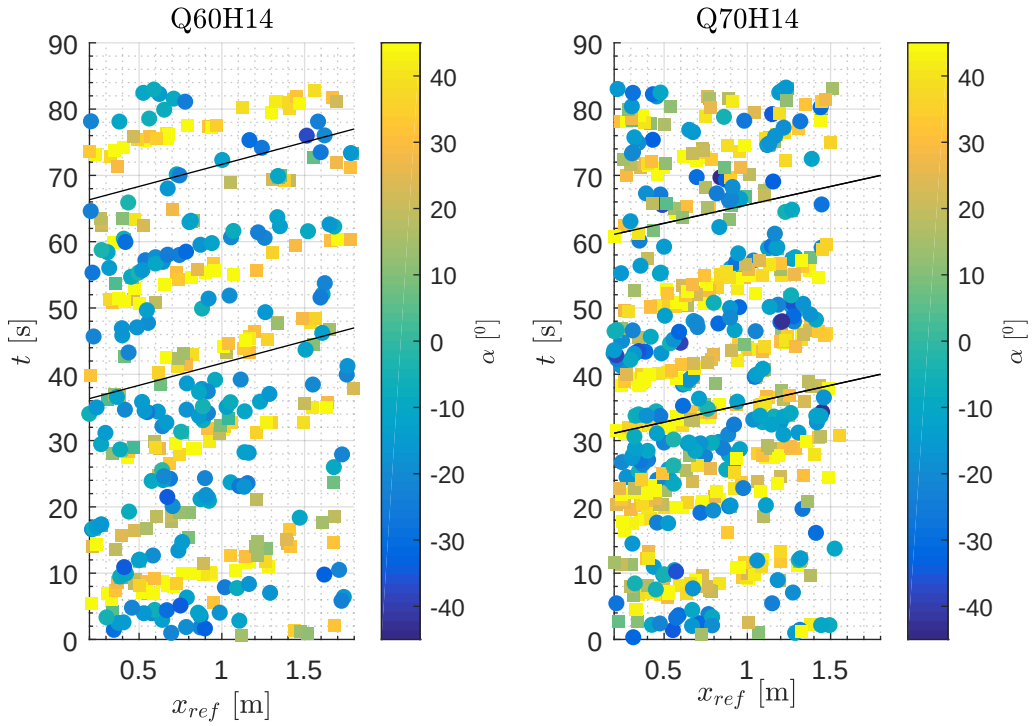


Figure 4.27: $X-t$ plot of the crossings of the interface. Each dot indicates a negative crossing, each square a positive crossing. The color indicates the angle. The black line indicates the propagation of a vortex. Left) Setting Q60H14. Right) Setting Q70H14

terface. The calculated angles and the differences in angles are consistent with the observations during the experiments and in the movies. For a larger depth, and therefore a larger shear, the outgoing angle increases, while the angle the particles entering the vegetation is the same for each depth. The influence of the channel velocity on the angle is inconclusive.

For the velocity magnitude, the difference between the ingoing and outgoing tracers is small, but because the angles are different the magnitude of the two velocity components is different. The relative importance of the streamwise component is larger for the tracers entering the vegetation. The tracers leaving the vegetation come from a location with a low streamwise mean flow which increases towards the interface. The velocity magnitude increases with increasing mean velocity.

The influence of the vegetation density on the angle is inconclusive as the positive angles of set 2 H14, set 3 H12 and set 3 H16 have a mean value which is smaller for the dense setup, but for set 3 H14 the opposite holds. The other sets have too little interface crossings for the dense setups to give meaningful results. The negative angle is equal for both dense and sparse, driven only by the velocity and velocity gradient on the transverse slope which is independent of the vegetation density. The velocity magnitude, in both directions, is larger for the sparse vegetation.

All the interface crossings for setting Q60H14 and Q70H14 are plotted in figure 4.27, while for each crossing the time and location were determined. Each positive crossing happens during an ejection and a negative one during a sweep. The propagation speed of the vortex at the interface was determined by plotting straight lines through the plots, this resulted in propagation speeds of the $U_{prop} = 0.15 \pm 0.1$ and $U_{prop} = 0.18 \pm 0.1$ m/s. This is larger than the streamwise component at mid-depth for these locations, which are $U_0 = 0.097$ and $U_0 = 0.114$ m/s respectively but smaller than the mean of the channel and vegetation velocity. This plot could only be constructed for the sparse settings as within the dense setup, not enough tracers were crossing the interface during the passing of one vortex.

5

Discussion

In this chapter, the results of the experiments are discussed as well as the relevance of the experimental setup. The experiments aimed to obtain insight into the flow structures in the shear zone around the interface of vegetated bed and non-vegetated bed, and their strength and effects near the bed. In the experimental setup, the effects of both a complex bed topography and vegetation together are measured.

5.1. Experimental setup and methods

The experimental setup is limited to rigid emergent vegetation with a uniform density. Also, the bed was relatively smooth and not mobile. Therefore morphological changes could not be measured or observed. Only the implications of the flow for erosion and deposition could be deducted.

The particle Reynolds number, $Re_p = Ud/\nu$ of the cylinders in the vegetation was of $O(10^3)$ for all settings. Therefore the flow velocity inside the vegetation could be assumed to be turbulent and constant over depth. The Strouhal number at the location of the measurements had a similar value as found by White and Nepf (2007), for the position where the shear layer had reached its equilibrium state. Therefore the measurement locations were located far enough downstream from the start of the vegetation.

5.1.1. Particle tracking

The idea of flow measurements through particle tracking is not revolutionary. However, the application for measuring near-bed velocities and movements is still a challenge as the availability of tracers compliant with the required properties is small. Tracers near the bed need to be visible and stay at or in close vicinity of the bed while following the flow. These criteria are conflicting. Therefore the choice of the tracers in this study was a compromise between the visibility and the ability to track the flow. The specific weight was large enough, so the tracers moved in close vicinity to the bottom, also because the larger total weight made full suspension by the flow was not possible. However, at higher velocities, the tracers started to saltate/jump over the bed. Within the experimental setup, the vertical component of the flow was small. However, when the vertical motion increases, it may capture the tracers and bring them in suspension. Therefore the tracers used in this experiment are only suitable for flows without strong vertical structures.

The tracers were also large enough to cover multiple pixels in the images. Larger tracers are not able to visualize the turbulence of scales smaller than their diameter, but for the aim of these experiments, to capture the large-scale motion, the size was sufficiently small.

The visibility of the tracers depended on the background color and inside the vegetation on the density. During the sparse vegetation runs, the bed within the vegetation was gray, which had a negative influence on the detectability of the red tracers as the color spectra were more overlapping. Before the sparse vegetation runs, the bed was taped with white tape, and the cylinders were painted white in the area of the observations, creating a uniform background color with a distinct color spectrum. This enhanced the ability to track the tracers. The higher vegetation density complicated the tracking of the particles due to the shadows on the bed as a result of the viewing angle of the camera. Also less light could reach the bed, making the contrast between the tracers and the bed even smaller.

When this technique is applied again, it is recommended that a uniform background color should be used. Also, the choice of camera and camera settings may be reconsidered, especially with high-density vegetation.

For this type a camera lens with a small looking angle is preferable. This implies that the camera should be situated higher above the flume to obtain a similar captured area.

Some bias in the measurements may be caused by the number of tracers in specific parts of the vortices. On the slope, more tracers were present in the ejections than in the sweeps. This may have contributed to a bias towards the ejection. However, it was also observed that tracers were more easily transported out of the vegetation than into it. This could explain the preference of tracers towards the ejections too.

The PTV analysis itself was quite a laborious process. First, the individual frames of the movies had to be extracted; whereafter the images were preprocessed for the PTV software. Especially the videos taken during the dense setup runs needed color enhancing and increasing of contrast for the Matlab scripts to identify the individual tracers. Still not all the tracers in the vegetation were captured in the black-white images which were used in the PTV analysis. The images taken in the sparse runs had enough contrast between the colors of the bed and the tracers and therefore did not need additional image preparation before the black-white images were extracted. This leads back to the visibility of the tracers.

The PTV analysis was mainly used to track the movement of the tracers on the bed and to obtain insight into the effect of the coherent structures near the bed. The mean flow field could be extracted. However, with the low number of particles the distances over which the velocity is interpolated is relatively large. To extract flow and vortex properties near the bed a larger tracer density is needed, this, however, increases the analysis time and therefore PIV should be a better method. Coupling the structure near the bed and in the water column could also give more insight into 3D components of the structures. To do that a 3D PTV or PIV technique is needed, as when tracers are followed on the bed and in the water surface, the bed tracers are overshadowed by the surface tracers.

5.1.2. ADV

The measurements of the ADV depend on the suspended particles in the water column on which the sound waves can reflect. Because no suspended matter was present in the water discharged into the flume, a bubble screen creating hydrogen bubbles was installed 30 cm upstream of the probe. Near the bed, the screen produced fewer bubbles than in the middle of the water column. Therefore a larger sampling volume needed to be used to obtain a correlation larger than 85% which is the minimum for relevant observations. The lower amount of bubbles still resulted in more noise.

When strong ejections passed the ADV, a sudden drop in the correlation and an increase in noise was detected. This was strongly related to the distance between the bubble screen and the sampling volume. When the bubble screen was located closer to the sampling volume this effect was reduced. During the ejections, the streamwise velocity was at its minimum while the transverse velocity was at its maximum. Within the distance between the bubble screen and the sampling volume, the bubbles were already transported towards the channel and not crossing the sampling volume. This mechanism was strongest in the vegetation where the streamwise velocity also reached negative values. For future experiments which use ADV for measuring coherent structures, other ways to introduce some turbidity into the water should be considered. For example using suspended Chinese clay, which eliminates the effect of the bubble screen structure on the flow and provides a more constant distribution of particles also in the vegetation.

For near-bottom measurements, an ADV with a side looking probe is less suitable. Near bottom measurements were taken while the probe was just touching the bed. This implied that the probing volume was located approximately 4 mm above the bed in the area where there was no transverse slope. In the zone with the transverse slope, this distance was lower as the sampling volume was approximately 5 cm away from the probe itself. However, in this first 5 mm the gradient in the vertical velocity is strong and small differences in the location of the velocity measurements relative to the bed lead to large variations in measured velocity. The velocities measured at the locations y = -0.35, -0.20, -0.10, -0.05, 0.90 and 1.2 m are taken at a larger distance from the bed than the measurements on the slope. Therefore these cannot be compared directly. This problem could be solved with the use of a down looking ADV, which measures at several locations near the bed and can detect the bed as well.

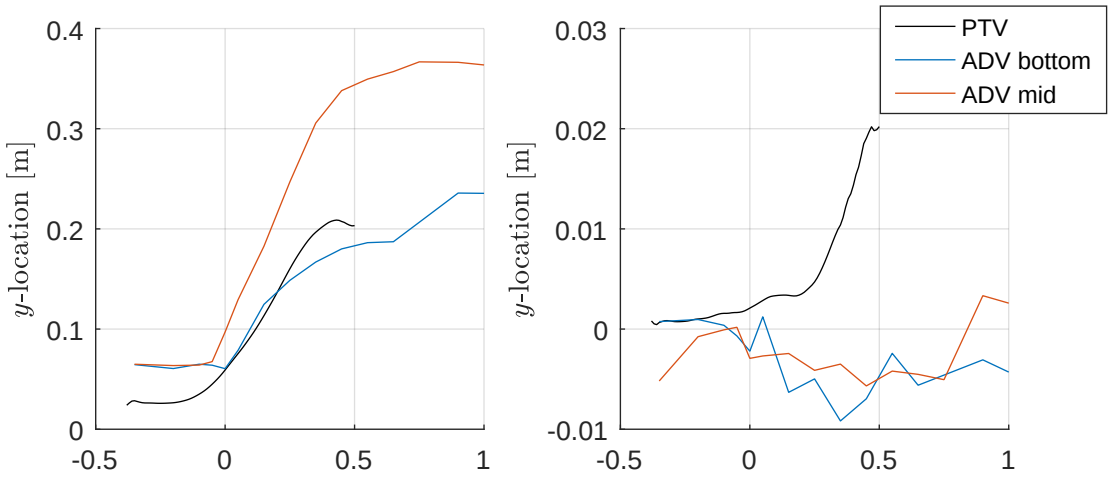


Figure 5.1: Comparison between the mean velocity profiles obtained with the ADV technique and the PTV technique, for dataset Q60H14 with sparse vegetation. Left) the mean streamwise velocity. Right) Mean transverse velocity

5.1.3. Flow profiles

The mean velocity profiles measured with the ADV and extracted from the PTV analysis are shown in figure 5.1. This figure shows the measured profiles for the setting $Q = 60$ l/s and $H = 14$ cm with sparse vegetation. Between $y = 0$ and $y = 0.15$ m the near-bed profile from the ADV measurements and the PTV measurements overlap. However, inside the vegetation, the mean velocity of the spheres is smaller than the mean measured velocity with the ADV. For $y > 0.15$ m the velocity measured with the PTV is larger than the one measured with the ADV. The differences within the vegetation could be explained by the location of the sampling volume relative to the bed, as discussed in the section above.

The larger velocities measured with the PTV can be explained from strong vertical velocity gradients near the bed. While taking the movies for the PTV analysis, it was observed that at higher flow velocities the tracers started jumping over the bed instead of rolling. When a particle jumps, it obtains the velocity of the new location in the water column which is faster.

The PTV and ADV data are also different for the transverse velocity component. Since further downslope, tracers on the bed also had to overcome the resulting force of the gravity to follow the flow upslope. Another explanation is a bias towards the ejection part of the vortices, as in general, more tracers were present in this part of the vortex than in the sweep. Within the ejection the transverse velocity component is positive (downslope) leading to a larger contribution of these values to the mean.

5.2. Flow and turbulence

Different aspects of the flow have been measured during the experiments focusing on the contributions of the vegetation and the complex topography. Both aspects result in velocity differences caused by differences in friction. However, the main difference between the flow through a partly vegetated channel and compound channel with complex topography is the influence of the friction over the full depth. In the latter, the flow in the shallow part of the flow can develop in a logarithmic profile, while inside vegetation the flow is constant over the whole water depth. The influence of both features on the mean flow and turbulence features is further discussed in this section.

5.2.1. Mean flow

The difference in drag between the channel and vegetation governs the difference in mean flow velocity and the development of the coherent vortices. With increasing vegetation density the difference between the two constant flows increases, increasing the strength of the shear. This is measured in the larger peak shear stress at the interface for the dense vegetation. The influence of the transverse on the shear layer can be derived with the results of previous studies from White and Nepf (2007, 2008) and Buckman (2013), shown in table 5.1. These studies are done with similar vegetation densities simulated by wooden cylinders. Buckman (2013) has used wooden cylinders with a diameter of 1 cm (same as in this study) and the cylinders of White and Nepf (2007, 2008) had a diameter of 0.6 cm.

Table 5.1: Momentum thickness and inner and outer layer thicknesses found in the current research compared to results from flat-bed experiments

		Buckman (2013)		White and Nepf (2007)			Current	
		Sparse	Dense	Sparse	Sparse	Dense	Sparse	Dense
ϕ		0.01	0.04	0.02	0.02	0.045	0.011	0.044
H_C	[cm]	13.6	13.6	13.8	6.8	6.6	14	14
U_C	[m/s]	0.327	0.410	0.240	0.177	0.174	0.362	0.399
U_V	[m/s]	0.081	0.026	0.019	0.022	0.013	0.064	0.012
θ	[m]	0.042	0.052	0.062	0.051	0.048	0.092	0.113
δ_I	[m]	0.086	0.112	0.062	0.037	0.026	0.032	0.078
δ_O	[m]	-	-	0.199	0.160	0.167	0.37	0.37

The momentum thickness of the three most comparable cases is taken to see the effect of the transverse slope. With the transverse slope present, the non-vegetated part attracts more flow than without transverse slope, lowering the flow velocity in the vegetation. The momentum thickness of the sparse and dense vegetation are doubled in the situation with the transverse slope relative to the setup of Buckman (2013), while the water depth in the channel and velocities are similar. The difference may be assigned to the transverse slope.

The results of (White and Nepf, 2007, 2008) show an opposite relation between the vegetation density and the values of the inner layer thickness and the momentum thickness. This difference may be caused by the setup, where the cylinders in this study have a larger diameter, fewer cylinders per square meter are needed to obtain the same vegetation density as with the smaller cylinders. As the maximum turbulence and the interference of the wakes is governed by the distance between the cylinders,

5.2.2. Near-bed Reynolds stress

Although the velocity profile at the bed follows the same curve as the velocity in the middle of the water column, the Reynolds shear stress profile has a completely different profile. The only similarity is the peak at the interface with the same order of magnitude, $O(10^{-4})$, as the Reynolds shear stress peak in the middle of the water column. In the middle of the slope, a second peak is found which is not appearing in the mid-depth profile. At larger distances from the interface, Reynolds shear stress is less related to the presence of the vegetation and more to the transverse slope and the bed shear stress.

Within the vegetation, the value of the Reynolds shear stress is the same as at mid-depth. Therefore in together with the equal mean flow velocities, this results in constant flow characteristics over the depth. The vegetation, cylinders, are uniform. Therefore, their influence on the flow is equal to the whole flow depth.

Also, the influence of 3D turbulence is larger near the bed, related to the initial fast drop of the autocorrelation profile at the interface. After the drop, the autocorrelation follows a decreasing sine function, with lower peaks than the autocorrelation in the middle of the water column. The vortices near the bottom are less self-similar as result of the influence of the bottom shear stress.

5.2.3. Secondary circulation

The net flux towards the interface can be explained by secondary circulations, which are also described by White and Nepf (2007). The argued that the vortices rotating around a stable node at the bottom and an unstable node at the water surface. This should result in an upward flux near the interface and a flux downwards at the edges of the vortices. Also, a depression would be measured at the location of the interface. During the experiments, the water level was only measured at two locations to measure the water level and the surface slope. This should be verified by more extensive water surface measurements which are linked to instantaneous flow fields.

Secondary circulation could also explain the second peak in Reynolds stress near the bottom. This peak may be the result of the downward flux from the coherent motion or a result of the slope. As Shiono and Knight (1991) found that in compound channels a secondary circulation is present, with one cell from the toe at the bottom of the channel up to approximately half of the height of the slope, and another at the in the upper layer, from half the slope height onto the floodplain. It should be noted that the experiments by Shiono and Knight (1991) were done a compound channel with a transverse slope of 1:1 instead of a slope of 1:10. The location of the second peak is also at half the slope height.

Prooijen et al. (2005) have found that the secondary circulation did not contribute to the Reynolds stress and only to mass fluxes. Therefore the magnitude of the second peak is fairly large. However, the peak is

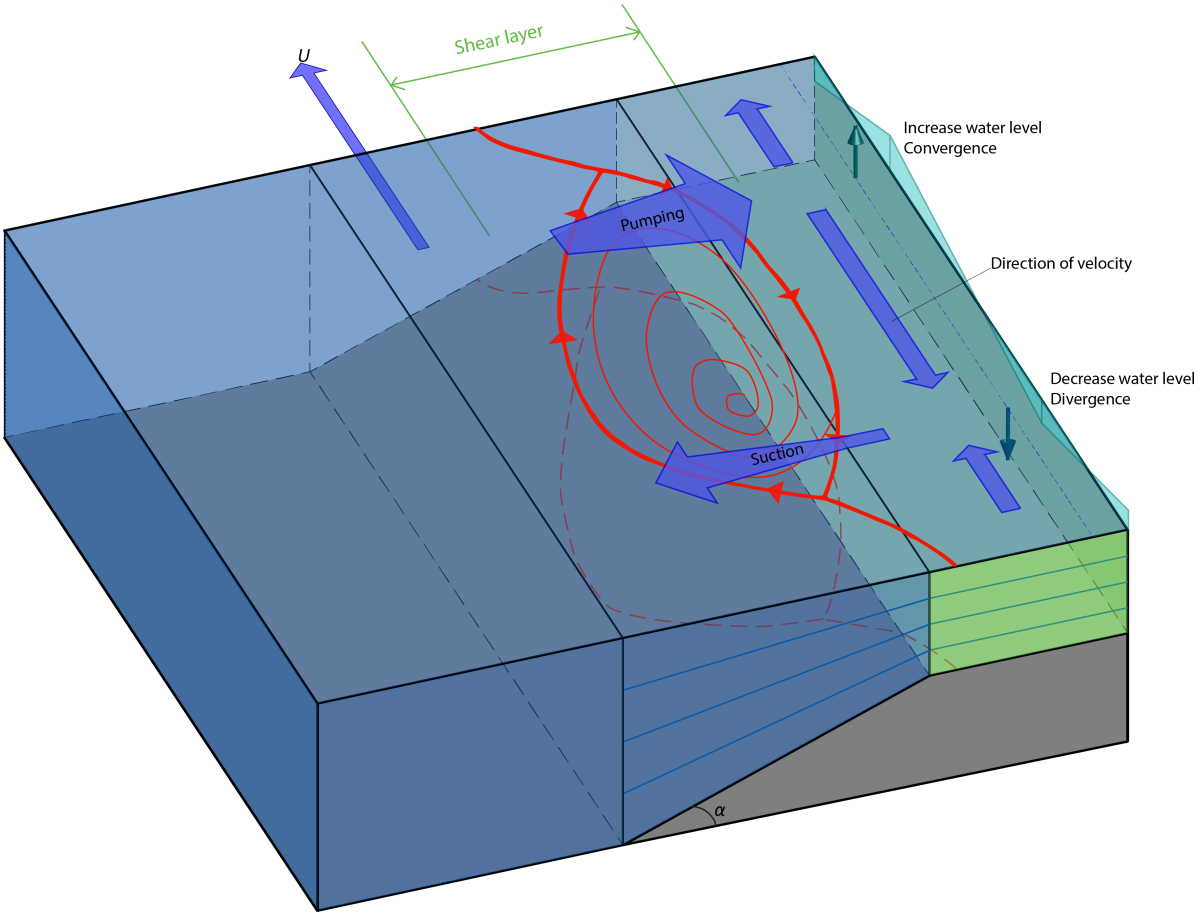


Figure 5.2: Concept of the flow where momentum and mass exchange governing the strength of the vortices

present in each profile at approximately the same location and a similar order of magnitude.

5.3. Momentum and mass exchange

The shear layer found in the experiments has characteristics similar to the coherent structures found in other shear flows affected by either vegetation or bed level differences or both (Dupuis et al., 2017; Prooijen et al., 2005; Shiono and Knight, 1991; White and Nepf, 2007). The strength and the size of the can be explained from the exchange of momentum and mass between the channel and floodplain.

Streamwise momentum is transported through the shear layer from the high momentum transport towards the low momentum transport flow. This happens in the vortices throughout the range where the turbulent viscosity is defined. However the momentum thickness is larger within the dense vegetation, the width over which this takes place is equal for both densities. The momentum exchange is limited to the area between $y \approx 0.4$ m, depending on the water depth, and $y \approx -0.1$ m, depending on the vegetation density. Color fluid injected at the interface indicated that vortices spread over this area, rotating around a point around $y \approx 0.15$ m.

Where the height of a vortex is decreased vorticity increases, this is the result of the consideration that the amount of potential vorticity, linked to the total energy and momentum, is constant. As the water depth is changing over the width of a vortex, this should mean that the vortex is wider and rotates slower in the shallow part and faster and smaller in the deep part. This is not directly visible in the measurements. However, in the front of the vortex, the transverse velocity component is smaller than in the back, where the depth increases. However, the transverse velocity is larger near the interface than at the deeper parts, indicating an increase of vorticity in the shallow part. This cannot be explained with the momentum balance only.

In this specific setup, a compound channel with a vegetated floodplain and a transverse slope between the floodplain and main channel, the mass balance is important for the shape and strength of the vortices.

Figure 5.2, shows the directions of mass and momentum exchange as well as their effects on the vortex.

In the ADV measurements as well as the PTV measurements also outside of the zone of the momentum exchange oscillatory motion was measured, especially inside the vegetation. Considering the vortices as only a result of the momentum exchange this oscillatory motion cannot be explained. In this case, the exchange of mass between the vegetation and channel can explain the

In the front of the vortex, the downstream end, the velocity component is directed inwards. From the outer edge of the vortex, the water depth decreases, considering the mass balance either the flow has to accelerate, or it has to increase in width and water level. On the slope acceleration of the vortex is possible. However, when this flow enters the vegetation, it slows down.

The excess mass, transported from the slope into the vegetation, pushes the water outside the vortex further into the vegetation patch. At that location a wall is present leaving the free surface as the only place to store this excess mass, increasing the water level. At the upstream end of the vegetation the opposite happens, the flow is directed from the vegetation towards the channel and is diverging on the slope. The vortex pulls the water out of the vegetation, resulting in a drop of the water level inside the vegetation.

The differences in the free surface elevation over the length of a single vortex creates surface slopes, generating flows. Thus the pumping of the vortex creates the oscillatory movement inside the vegetation at the locations where there is no shear. As was measured with the ADV the u and v velocity components in this area are 90^o out of phase. Which is in line with this analysis.

As the free surface level has not been measured during the experiments, this cannot be verified. However, the measured flow velocities and the movement of the PTV tracers are in line with the theory of vortex strengthening by pumping mass in and out the vegetation. Measurements of the surface elevation in a cross section simultaneously with flow measurements should be done to verify this.

5.3.1. Width of the vegetation

During the experiments with the dense vegetation, there were settings for which the tracers were transported a significant distance upstream during sweeps. This movement upstream was stronger at larger flow velocities and larger flow depths.

At larger flow velocities the vortices were stronger, resulting in a larger exchange of mass through the interface. During the sweeps, the mass flowing into the vegetation could create a locally higher water surface, while the ejection does the opposite. This could create a positive surface slope which increases the effect of the vortices inside the vegetation. As is described above, this vortex strengthening was also found by Truong et al. (shed) in experiments where the width of the vegetated area was decreased. A smaller width increased the strength of the vortices, predominantly in the vegetation zone.

The width of the vegetation between the interface on the channel side and an impermeable wall on the other side influences the strength of the vortex. While the width is larger than the inner layer shear zone, it would have no significant effect on the momentum exchange, as the differences in velocity are governed equally. However, the extra width functions as a basin for the pumping mechanism described above. A larger width equals a smaller change is water level due to the mass exchange during the passing of a vortex, decreasing the changes in surface slope which.

5.3.2. Periodicity

In the sparse vegetation, the effect of the sweep did not cause the tracers to move upstream. They only decelerated to a minimum which was still in positive x-direction, hereafter they accelerated again. This may be because of the higher frequency of the vortices along the sparse vegetation. Therefore there is less time to build up mass and the subsequent surface slope.

The period of the coherent motion was larger for the dense vegetation. Together with the larger deviations from the mean velocity the total exchange of mass within one period of the vortex increases. This influences the total mass brought into the vegetation. The larger mass fluxes in and out the dense vegetation could explain the influence of the width on the strengthening of the vortices for larger velocities and depths. Therefore the strong fluctuations in the horizontal velocity components throughout the entire vegetation.

The periodicity together with the value of the momentum thickness resulted in Strouhal numbers between 0.031 for the dense vegetation and 0.044 for the sparse vegetation. Indicating the vortices are mainly 2D phenomena. This is consistent with values found for other vegetated shear layers (Dupuis et al., 2017; White and Nepf, 2007).

When the water mass is flowing in and out of the vegetation, also the suspended materials flow in and out the vegetation. Depending on the period of the vortices and the settling velocity the suspended sediments may settle in the vegetation. And the strengthening also creates higher near-bottom velocities increasing the possibility of incipient motion of bed load inside the vegetation and therefore erosion.

5.4. Transport mechanisms

The setup of the experiments made the influence of the vegetation on the flow and the consequential flow patterns clear. Also, the observations from the PTV tracers have resulted in insight in the strength of the structures near the bed. This information could be used to derive the influence of the vegetation on the transport mechanisms near the bed as well as in the water column.

5.4.1. Bed load transport

The tracers in the PTV experiments were able to be transported into the vegetation. The location of origin of the tracers and the phase within a vortex determined the probability of a particle being transported into the vegetation. The thickness of the outer exchange layer was observed to be smaller for the dense vegetation, while the difference in the outer layer shear thickness was similar for both vegetation densities. However, the outer layer exchange region increased with increasing depth. The net transverse transport of the PTV tracers was in the positive transverse direction, downslope, and increasing as the shear stress in the vertical direction increased.

Tracers entering the vegetation dense ended up at the location at ≈ 0.1 m distance from the interface. At this location, they stopped moving, or were transported a small distance upstream. Most tracers remained there until the following ejection. This effect was less strong in the sparse vegetation as the tracers were always in motion. Translating these observations to actual sediment transport should be done with care, as the spherical particles on a smooth bed have a critical shear stress of almost zero, but transport of angular material and on a rough bed needs higher bed shear stresses to be transported.

The net transport on the transverse slope should be downslope, as was observed in the experiments and is consistent with literature, cited in section 2.6.2. Outside the influence zone of the shear layer on the slope, the transport would only be influenced by the slope angle. Within the shear layer, however, the sweeps and ejections could result in a wider spreading in the direction of individual particles. Near the interface, only small particles would be mobile due to the smaller flow velocity, when a particle is picked up by the flow the phase of the vortex will determine the direction of the transport. In general particles on a transverse slope need a smaller force to be transported downslope than upslope, which may result in that only small particles could be transported upslope.

The shear stress, dependent on the turbulent kinetic energy near the bed, inside vegetation under the conditions measured, is lower in the dense vegetation (Yang et al., 2016). If sediment is transported into the vegetation by a sweep, the dense vegetation could retain smaller grains. But they will end up at a smaller distance from the interface.

5.4.2. Diffusion

The main focus of this research is on bed load material, some of this material might be brought in suspension in the channel and transported into the vegetation. Therefore this section diffusion is dealt with.

At the head of a long patch of vegetation advection by incoming flow is the dominant transport mechanism for both bed load and suspended sediment. Depending on the settling velocity, suspended material settles within the vegetation at a specific distance downstream from the head of the vegetation (Zong and Nepf, 2010). The transport capacity within the vegetation also decreases rapidly within the vegetation (Nepf, 2012a; Yang et al., 2016). Sediment transport at locations further downstream depends on the influence of the mixing through the interface, by the coherent structures in the shear layer. For diffusive transport of suspended sediments the main drivers are the diffusivity ε in the transverse and vertical directions, the settling velocity w_s and the gradients in concentrations, as give in equation 5.1.

$$w_s \frac{\partial C}{\partial z} + \frac{\partial}{\partial y}\left(\varepsilon_y \frac{\partial C}{\partial y}\right) + \frac{\partial}{\partial z}\left(\varepsilon_z \frac{\partial C}{\partial z}\right) \tag{5.1}$$

The eddy diffusivity scales with the turbulent viscosity, which depends on the gradients and the Reynolds shear. Inside the vegetation, the turbulent viscosity in the vertical direction is expected to be low based on the decrease in turbulence and the absence of gradient in the mean flow velocity (Nepf, 2012a; Yang et al.,

2016). Therefore suspended sediments should settle faster in the vegetation than in the channel leading to transverse gradients in sediment concentration.

Results from experiments with suspended sediments done by Sharpe and James (2006) show a dependence of the transverse deposition of suspended sediments on the vegetation density. They found that the deposition increased in the dense vegetation, the total amount as well as the distance from the interface. The larger amount of mass transfer through the vegetation due to the stronger ejections and sweeps as well as the lower frequency could explain this. As more mass is transported through the interface and it stays longer inside, the sediment has more time to settle before leaving the vegetation again. This only holds if there is a concentration gradient over the interface. It should be noted that in the experiments done by Sharpe and James (2006) every particle that settled was not eroded again as a result of the choice of an 'absorbing' bed material. The particles could only stay there if the bed shear stress is small enough, which is more probable further inside the vegetation where lower velocities are measured.

6

Conclusion and recommendations

The objective of this research was to obtain a better insight into the flow and transport mechanisms at the interface between vegetated and non-vegetated flow. The research questions stated in section 1.2 are repeated and answered in this chapter. Recommendations for further research and implications for engineering practice are given in the second section of this chapter.

6.1. Conclusions

What are the factors influencing the shear layer in vegetated flow?

In a partly vegetated channel the shear layer in the flow transverse direction, caused by the difference in drag between the non-vegetated and vegetated bed, can be divided into two regions: one inside the vegetation, the inner region, and another in the non-vegetated part, the outer region. This division is founded on the principal governing parameters which determine the shear profile in that region. Based on literature these parameters are the vegetation density and the channel velocity respectively. The flow in the shear layer is characterized by large coherent structures which cover the total shear layer and are responsible for the momentum transport from the channel towards the vegetation, indicated by a negative Reynolds shear stress which has a peak at the interface.

The inner shear layer has a smaller width than the outer shear layer, because of the fast dissipation of momentum due to the presence of vegetation. Denser vegetation has higher drag and is more efficient in the dissipation of momentum. Within the vegetation, the Reynolds shear stress decreases to zero within 10 cm from the interface.

The outer layer shear profile is mainly governed by the channel velocity, which is responsible for the gradient. The mean velocity profile in the outer layer is not dependent on water level and vegetation density. The Reynolds shear stress in the outer layer, however, depends on the bathymetry and the flow velocity. A larger water depth in the channel, increases the width of the Reynolds stress peak in the middle of the water

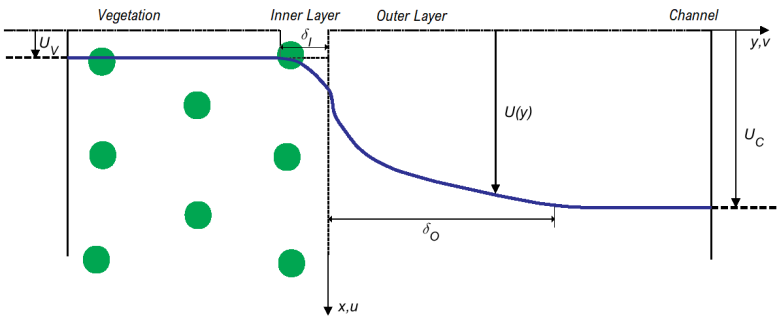


Figure 6.1: Inner and outer layer within a partly vegetated flow

column, creating a more extensive region of maximum exchange of momentum. Also the outer layer with the transverse slope of 1:10 shows a broader shear region than partly vegetated flows without a transverse slope.

Near the bottom, the mean velocity profile follows the profile measured at the middle of the water column. The Reynolds stress, however, does show a different pattern. The peak at the interface is still present, but approaches zero faster with distance from the interface. Near the bottom, on the transverse slope, the influence of the vegetation is less strong as the bed level is located below the level of the vegetation. Although the exchange of momentum is low, there is still mass exchange near the bottom.

The maximum turbulent viscosity in the middle of the water column increases with increasing water depth and is similar for both tested densities. The maximum value is of order $O(10^{-3})$ at the interface and decreases towards zero on both parts of the shear layer. The factors influencing the shear layer are the vegetation density, channel velocity and its driving forces, water depth and the presence and angle of a transverse slope.

How can an experiment be designed to make relevant observations on sediment transport in and around vegetation?

To make relevant statements on sediment transport first the driving mechanisms need to be understood and described well. For sediment transport, these are the flow characteristics, especially near the bed. The direction of the near-bed velocity is essential for the direction of sediment transport and 3D turbulence is governing entrainment of particles from the bed. As the mean velocity component in the middle of the water could be measured more easily, relations between the mean flow and the near-bed conditions are needed.

The combination of using the ADV point measurements and the PTV field measurements results in a relatively complete set of flow characteristics, especially for the near-bed conditions. Flow visualizations with colored fluid give insight into structures and order of magnitude of diffusion and is a valuable tool to obtain a concept of the flow and what to expect from measurements.

When using particle tracking the tracer color should be chosen with care, taking into account the background color. The best way to ensure visibility is using a white background with bright colored tracers. Painting the individual cylinders and the total bed may cost more time during construction of the setup, but the increased visibility decreases the time needed for image preparation. The chosen particles followed the flow well and could be used in other experiments where the flow near the bed needs to be observed, however in flows with strong vertical mixing other materials need to be found.

The near bed measurements made clear that the presence of a transverse slope influences the coherent structures and has a profound effect on the near-bed conditions. The installed slope resulted in unexpected flow features, which could be studied in this setup and resulted in new insights. Also, a slope between a floodplain and a channel is a more natural situation.

What is the influence of the vegetation density on sediment transport mechanisms in the transition zone?

Because no actual sediment transport was measured, implications for transport mechanisms are deducted from the flow characteristics related to sediment transport. The PTV tracers near the bed were tracked to observe possible effects of the sediments.

The primary mechanism transporting sediments in and out of the vegetation is the coherent vortices resulting from the velocity shear around the interface. The vortices have two phases, sweeps and ejections. Sweeps are characterized by a positive streamwise flow deviation and a negative transverse flow deviation, which is directed into the vegetation. Sweeps transport mass into the vegetation including the sediments. As the frequency of the vortices in the presence of the dense vegetation is smaller, the total amount of mass transported into the vegetation is larger than in sparse vegetation. Sediments can settle more efficiently within the vegetation because of the lower velocity and are therefore more likely to deposit in the vegetation.

Within the sparse setup, sediments can be transported further into the vegetation because of the higher velocity inside the vegetation. This also means that sparse vegetation attracts coarser sediments than dense vegetation. Because the strength of the vortices decreases with distance into the vegetation sediments with a larger d_{50} may settle closer to the interface than the fines. This results in a bed with coarser sediments near the interface which becomes finer with distance from the interface. In denser vegetation, the sediment will become finer more rapidly.

Without a transverse slope sweeps will be able to transport sediment up to the critical size into the vegetation, there the transport capacity will be lower, and the sediment will settle. The location of deposition could be related to the inner layer exchange width observed in the PTV movies. During the ejection, the flow must be stronger to transport sediments out of the vegetation.

Including the transverse slope in the outer layer implies stronger sweeps are needed to transport sediment upslope and into the vegetation. Only the smaller grains may be transported upslope, while larger grain sizes follow the transport direction governed by the slope angle and the size of the grain. The duration of the sweeps is longer for denser vegetation, while the transverse velocity component has a similar magnitude for both the sparse and dense vegetation. Therefore, dense vegetation may attract more sediments during a sweep into the vegetation. But the opposite holds for ejections which transport sediments towards the channel from the area around the interface where the sediment is still mobile. Only when sediments are transported to a location in the vegetation where they are not mobile, they will deposit and contribute to accretion.

Is it possible to explain bank growth patterns from vegetation density?

As the experiments were done with a fixed bed, only the initial response of such setting could be derived. Within both vegetation density settings of the experiments, the tracers transported into the vegetation ended up at a specific distance from the interface. Between a sweep and the subsequent ejection, tracers collected at this location, which was further from the interface for sparser vegetation.

Transport of bed material depends on the ratio of the actual bed shear stress to the critical shear stress. The tracer material used in the experiments was spherical. Also, the bed was smooth which resulted in an infinitely small critical shear stress. Therefore, the tracers were always mobile. However, when real sediment is considered the bed shear stress would become important. Where sediments are mobile in the channel, they might not be inside the vegetation. Therefore the net erosion seen with the spherical tracers is less likely to occur with real sediment.

From the experimental results and the discussion, it could be hypothesized that:

- The initial response of vegetation added to a floodplain increases the retention of fine sediments in the inner layer of the vegetation, this effect is stronger for dense vegetation as the flow velocities are smaller and.
- Vegetation can capture fine sediments; larger sediments will stay at the outer edges of the vegetation patch, protecting the inner part. The d_{50} should decrease with distance into the vegetation.
- After planting vegetation on a floodplain, a dune will form near the edge of the vegetation patch. This dune will grow until a certain equilibrium is reached, depending on the vegetation density, governing water depth, sediment grading and the initial angle of the slope between the floodplain and the channel.

To test these hypotheses further research is needed.

6.2. Recommendations

Based on the results of the experiments and experiences from the experiments recommendations for both engineering practices as further research on this topic are done.

6.2.1. Engineering vegetated flows

For only discharge or flow modeling the drag and the flow profile are sufficient. However when sediment transport near elongated vegetated patches needs to be modeled, the coherent vortices are important. Therefore around the interface more detailed calculations should be done. The adjustment of a grid in a numerical model can help. Choosing the viscosity in the for the horizontal plane with care can help to obtain better approximations of the real flow. When the shear layer and the coherent structures can be modeled, transport can follow. If the effect of the shear layer is not modeled, mixing effects may be neglected resulting in different transport.

Using a small grid increases the calculation time. Therefore a special diffusivity parameter may be introduced. This parameter could be dependent on the flow characteristics, the bed topography, vegetation characteristics and sediment grading. Taking into account the different locations where sediment may end up. To derive such a parameter more research on sediment grading and the influence of the bed topography should be done.

Replanting vegetation on banks should be done with care. Depending on the effect that is desired the density of the vegetation is important. A higher density will attract more fine materials which may erode fast.

Sparser vegetation could be planted first to attract coarser sediment. One could use vegetation or stems or imitation vegetation to initiate the process and create an environment to obtain the right bed elevation and grading. Piles or other imitation vegetation could serve as an incubator to reach the a required bed level. When the right state is reached trees, shrubs or grass could be planted in that area.

6.2.2. Further research

This study has only looked into the interaction between flow and vegetation in a compound channel. Directions for sediment transport are estimated by using Particle Tracking Velocimetry with particles on the bed. Therefore this study gives only insight into the processes that may play a role in the transport of bed material. Further research is needed to determine the exact effect of these processes.

Mass exchange

The pumping mechanism, mass exchange through the interface, described in the discussion needs to be validated. As is argued in the discussion this mechanism strengthens the vortices. This mechanism should still be tested. This can be done with measurements of the water surface combined with flow measurements. Coupling changes in water level elevation to the flow velocity may give proof for this mechanism. If the oscillations in water level elevation correlate with the flow velocity, this may also be a good way to do field measurements.

Slope

In this experiment, the slope was fixed on 1:10. The convergence and divergence of the transverse component of the vortex have shown to influence the shape of the vortex and the exchange of mass between the channel and floodplain. The literature on compound channels gives that the slope angle and the difference in water depth between the floodplain and channel are important for the strength of the vortices. The effect of the steepness of the slope on the pumping mechanism and the strength of the vortices is needed to obtain a complete overview of the parameters influencing the flow.

Sediment transport and morphology

In future experiments, the focus should be on the strength of the vortices and the ability to transport sediments into the vegetation and where they are deposited and eroded. This could be done with a similar setup where sediment with small median grain sizes, fine sand, is added to the flow. Measurements on the grading over the slope and within the vegetation could be done to validate the conclusions of the first research question. Adding suspended sediments to the water could give a better insight in the diffusion and the ability of vegetation to capture suspended sediments from the flow.

The roughness of the bed and the angularity of sediment has a large influence on the critical shear stress. Experiments with real sediments are therefore important to test whether the sediments stay in the vegetation.

Sediment transport governs the morphological changes. When the influence of the vegetation on the sediment transport is clear, the knowledge of morphology follows. In a test with morphology, the interaction between the vortices and morphology could be studied. As the vegetation density determines the grading and the amount of sediment deposited in the vegetation patch, morphological features depend on the type of vegetation.

It should be researched to what extent the morphology, vegetation density, and governing hydraulic conditions coexist. Whether there is an equilibrium which is stable and whether there are general characteristics in that equilibrium.

Scale

River flows are on a much larger scale than the experiments done in the flume. While the Reynolds and Froude number are scaled such that the flow is turbulent and subcritical, the scaling of the vortices needs to be researched. On a small scale the velocity fluctuations in the shear zone are significant respective to the mean flow velocities. When this is still so in vegetated flows in naturally occurring scales, these features may influence the bedload transport. However, if the relative strength decreases the impact on the bed may be much smaller than observed in the small-scale tests.

References

Armanini, A., Righetti, M., and Grisenti, P. (2005). Direct measurement of vegetation resistance in prototype scale. *Journal of Hydraulic Research*, 43(5):481–487.

Baptist, M. J., Babovic, V., Uthurburu, J. R., Keijzer, M., Uittenbogaard, R. E., Mynett, A., and Verwey, A. (2007). On inducing equations for vegetation resistance. *Journal of Hydraulic Research*, 45(4):435–450.

Belcher, S., Jerram, N., and Hunt, J. (2003). Adjustment of a turbulent boundary layer to a canopy of roughness elements. *Journal of Fluid Mechanics*, 488:369–398.

Brevis, W., Niño, Y., and Jirka, G. H. (2011). Integrating cross-correlation and relaxation algorithms for particle tracking velocimetry. *Experiments in Fluids*, 50(1):135–147.

Buckman, L. J. (2013). *Hydrodynamics of partially vegetate channels: stam dreag forces and application to an in-stream wetland concept for tropical, urban drainage systems.* Msc thesis, Delft University of Technology.

Buckman, L. J., Uijttewaal, W. S. J., Penning, W. E., and Dijkstra, J. T. (2014). Spatially varying stem drag forces in vegetated mixing layers. *Proceedings of the International Conference on Fluvial Hydraulics, RIVER FLOW 2014*, pages 543–551.

Camporeale, C., Perucca, E., Ridolfi, L., and Gurnell, A. (2013). Modeling the interactions between river morphodynamics and riparian vegetation. *Reviews of Geophysics*, 51(3):379–414.

Clutter, D. and Smith, A. (1961). Flow visualization by electrolysis of water. *Aerospace Engineering*, 20(1):24–27 and 74–76.

Costanza, R., d'Arge, R., De Groot, R., Farber, S., Grasso, M., Hannon, B., Limburg, K., Naeem, S., O'neill, R. V., and Paruelo, J. (1998). The value of the world's ecosystem services and natural capital. *Ecological economics*, 25(1):3–16.

Coulthard, T. J. (2005). Effects of vegetation on braided stream pattern and dynamics. *Water Resources Research*, 41(4).

Curran, J. C. and Hession, W. C. (2013). Vegetative impacts on hydraulics and sediment processes across the fluvial system. *Journal of Hydrology*, 505:364–376.

Dupuis, V., Proust, S., Berni, C., and Paquier, A. (2017). Mixing layer development in compound channel flows with submerged and emergent rigid vegetation over the floodplains. *Experiments in Fluids*, 58(4):30.

ECRR (2014).

Gurnell, A. (2014). Plants as river system engineers. *Earth Surface Processes and Landforms*, 39(1):4–25.

Gurnell, A., Corenblit, D., García de Jalón, D., González del Tánago, M., Grabowski, R., O'Hare, M., and Szewczyk, M. (2016). A conceptual model of vegetation–hydrogeomorphology interactions within river corridors. *River Research and Applications*, 32(2):142–163.

Ikeda, S. and Kanazawa, M. (1996). Three-dimensional organized vortices above flexible water plants. *Journal of Hydraulic Engineering*, 122(11):634–640.

Jammers, S. (2017). *Sediment transport over sills of longitudinal training dams.* Msc thesis, Delft University of Technology.

Koch, D. L. and Ladd, A. J. (1997). Moderate reynolds number flows through periodic and random arrays of aligned cylinders. *Journal of Fluid Mechanics*, 349:31–66.

López, F. and García, M. (1998). Open-channel flow through simulated vegetation: Suspended sediment transport modeling. *Water resources research*, 34(9):2341–2352.

Millar, R. G. (2000). Influence of bank vegetation on alluvial channel patterns. *Water Resources Research*, 36(4):1109–1118.

Mori, N., Suzuki, T., and Kakuno, S. (2007). Noise of acoustic doppler velocimeter data in bubbly flow. *Journal of Engineering Mechanics, American Society of Civil Engineers*, 133,(1):122–125.

Nabi, M., Vriend, d. H., Mosselman, E., Sloff, C., and Shimizu, Y. (2013). Detailed simulation of morphodynamics: 2. sediment pickup, transport, and deposition. *Water resources research*, 49(8):4775–4791.

Nepf, H. M. (2012a). Flow and transport in regions with aquatic vegetation. *Annual Review of Fluid Mechanics*, 44:123–142.

Nepf, H. M. (2012b). Hydrodynamics of vegetated channels. *Journal of Hydraulic Research*, 50(3):262–279.

Prooijen, B. C. v., Battjes, J. A., and Uijttewaal, W. S. J. (2005). Momentum exchange in straight uniform compound channel flow. *Journal of Hydraulic Engineering*, 131(3):175–183.

Rominger, J. T., Lightbody, A. F., and Nepf, H. M. (2010). Effects of added vegetation on sand bar stability and stream hydrodynamics. *Journal of Hydraulic Engineering*, 136(12):994–1002.

Schoelynck, J., de Groote, T., Bal, K., Vandenbruwaene, W., Meire, P., and Temmerman, S. (2012). Self-organised patchiness and scale-dependent bio-geomorphic feedbacks in aquatic river vegetation. *Ecography*, 35(8):760–768.

Sekine, M. and Parker, G. (1992). Bed-load transport on transverse slope. i. *Journal of Hydraulic Engineering*, 118(4):513–535.

Sharpe, R. G. and James, C. S. (2006). Deposition of sediment from suspension in emergent vegetation. *Water SA*, 32(2):211–218.

Shiono, K. and Knight, D. W. (1991). Turbulent open-channel flows with variable depth across the channel. *Journal of Fluid Mechanics*, 222:617–646.

Tal, M., Gran, K., Murray, A. B., Paola, C., and Hicks, D. M. (2004). Riparian vegetation as a primary control on channel characteristics in multi-thread rivers. *Riparian vegetation and fluvial geomorphology*, pages 43–58.

Talmon, A. and Wieseman, J. (2006). Influence of grain size on the direction of bed-load transport on transverse sloping beds. In *Third International Conference on Scour and Erosion*.

Talmon, A. M., Struiksma, N., and Vanmierlo, M. (1995). Laboratory measurements of the direction of sediment transport on transverse alluvial-bed slopes. *Journal of Hydraulic Research*, 33(4):495–517.

Tanino, Y. and Nepf, H. M. (2008). Laboratory investigation of mean drag in a random array of rigid, emergent cylinders. *Journal of Hydraulic Engineering*, 134(1):34–41.

Truong, S. H., Uijttewaal, W. S. J., and Stive, M. J. F. (unpublished). Flow field and exchange processes in floodplain vegetated channels: applications to squeeze mangrove vegetated banks. Unpublished Work.

Uijttewaal, W. S. J. (2014). Hydrodynamics of shallow flows: application to rivers. *Journal of Hydraulic Research*, 52(2):157–172.

Vargas-Luna, A. (2016). *Role of vegetation on river bank accretion.* Doctoral thesis, TU Delft.

Vargas-Luna, A., Crosato, A., Calvani, G., and Uijttewaal, W. S. J. (2016). Representing plants as rigid cylinders in experiments and models. *Advances in Water Resources*, 93, Part B:205–222.

Vargas-Luna, A., Crosato, A., and Uijttewaal, W. S. J. (2014). Effects of vegetation on flow and sediment transport: comparative analyses and validation of predicting models. *Earth Surface Processes and Landforms*, 40(2):157–176.

White, B. L. and Nepf, H. M. (2007). Shear instability and coherent structures in shallow flow adjacent to a porous layer. *Journal of Fluid Mechanics*, 593:1–32.

White, B. L. and Nepf, H. M. (2008). A vortex-based model of velocity and shear stress in a partially vegetated shallow channel. *Water Resources Research*, 44(1).

Yang, J. Q., Chung, H., and Nepf, H. M. (2016). The onset of sediment transport in vegetated channels predicted by turbulent kinetic energy. *Geophysical Research Letters*, 43(21):11,261–11,268.

Zong, L. and Nepf, H. (2010). Flow and deposition in and around a finite patch of vegetation. *Geomorphology*, 116(3–4):363–372.

A

Experimental setup figures and dimensions



Figure A.1: Photo of the flume setup, viewing direction is downstream. In the front is a working platform from where the flume could be overseen, followed by the tracer dispenser and in the end the frame on which the camera was installed

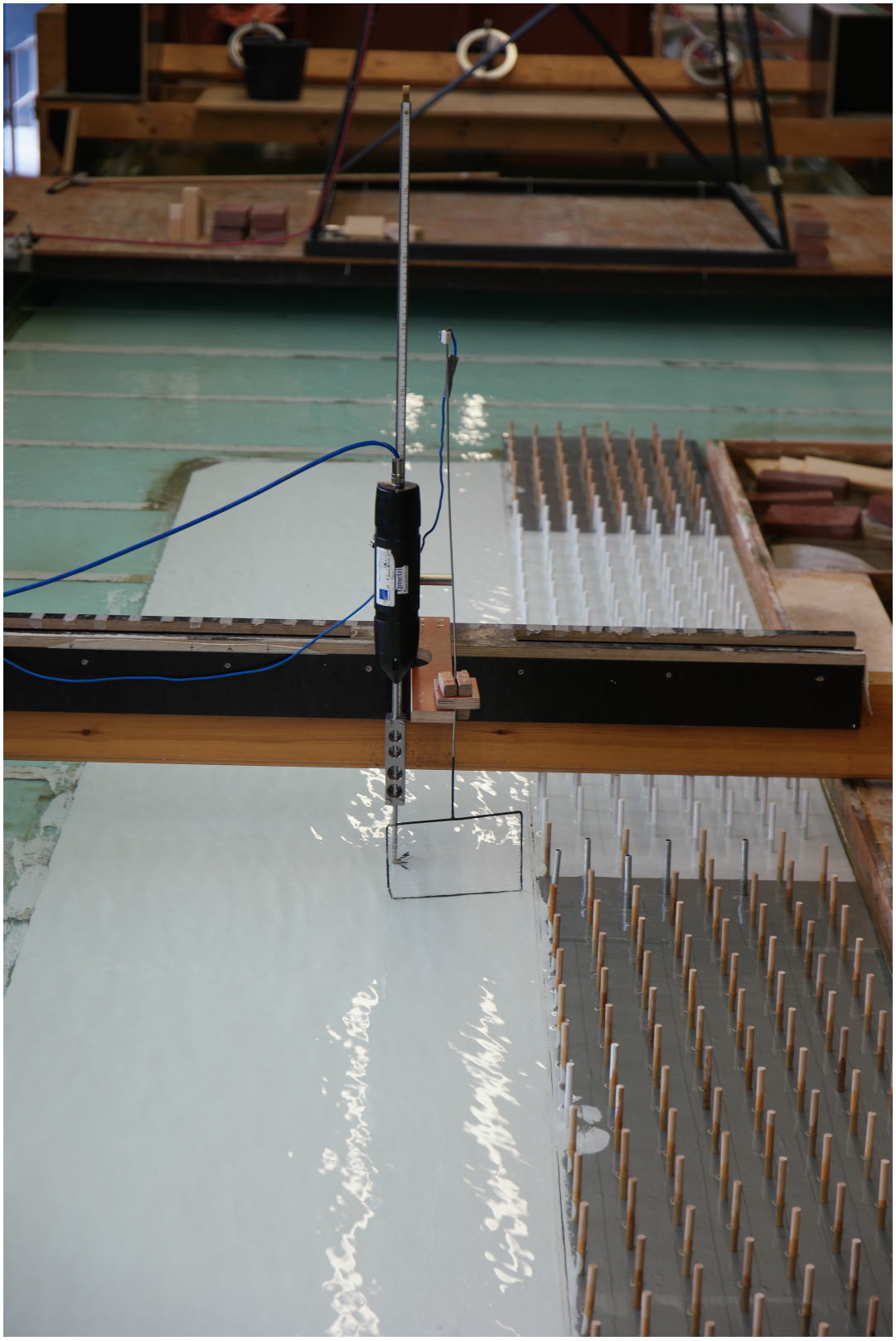


Figure A.2: The *Vectrino* ADV device with a bubblescreen installed upstream of the probe

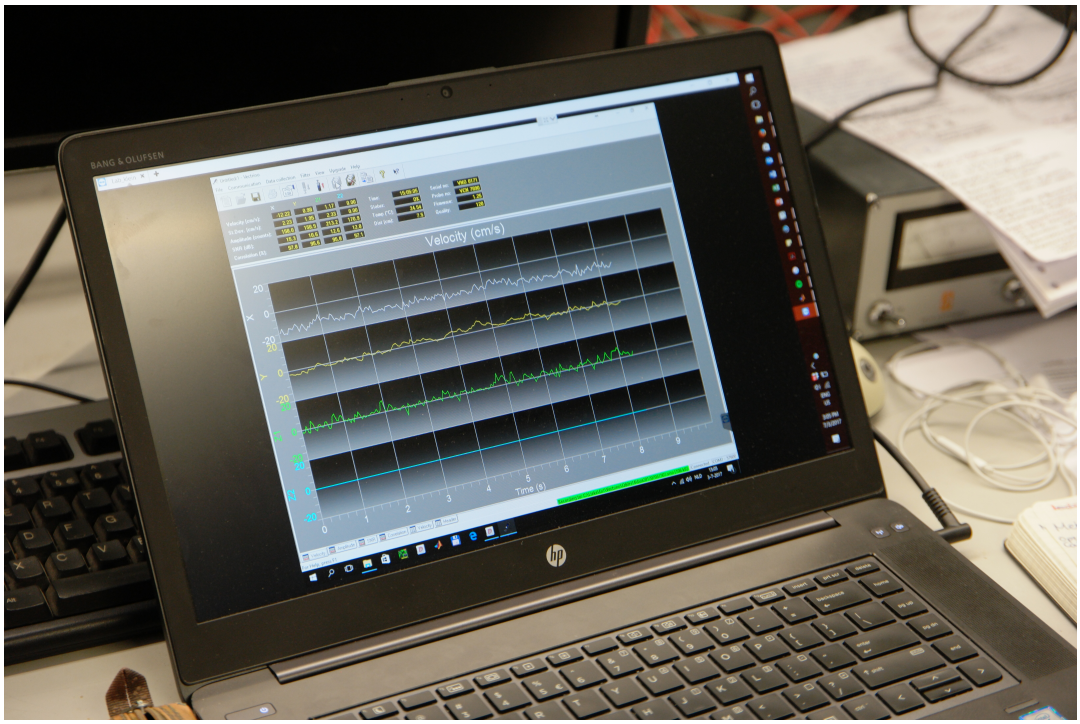


Figure A.3: The screen on which the RAW ADV data is gathered

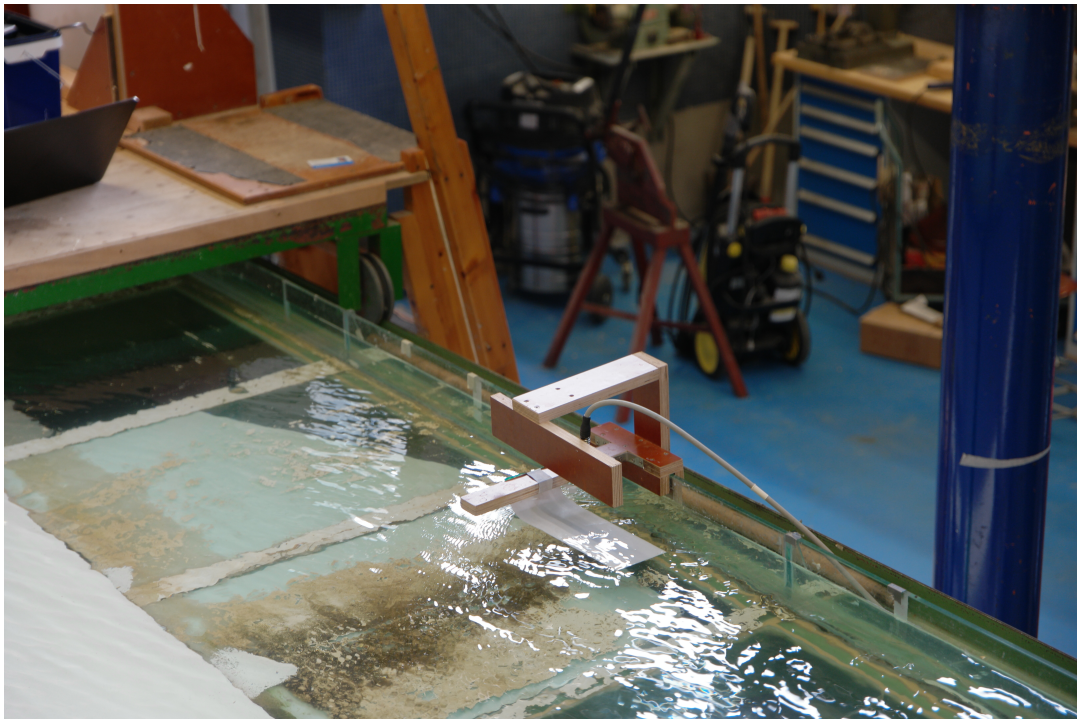


Figure A.4: The construction in which the depht measuring lasers are placed. The laser reflects on a floater measuring the water depth

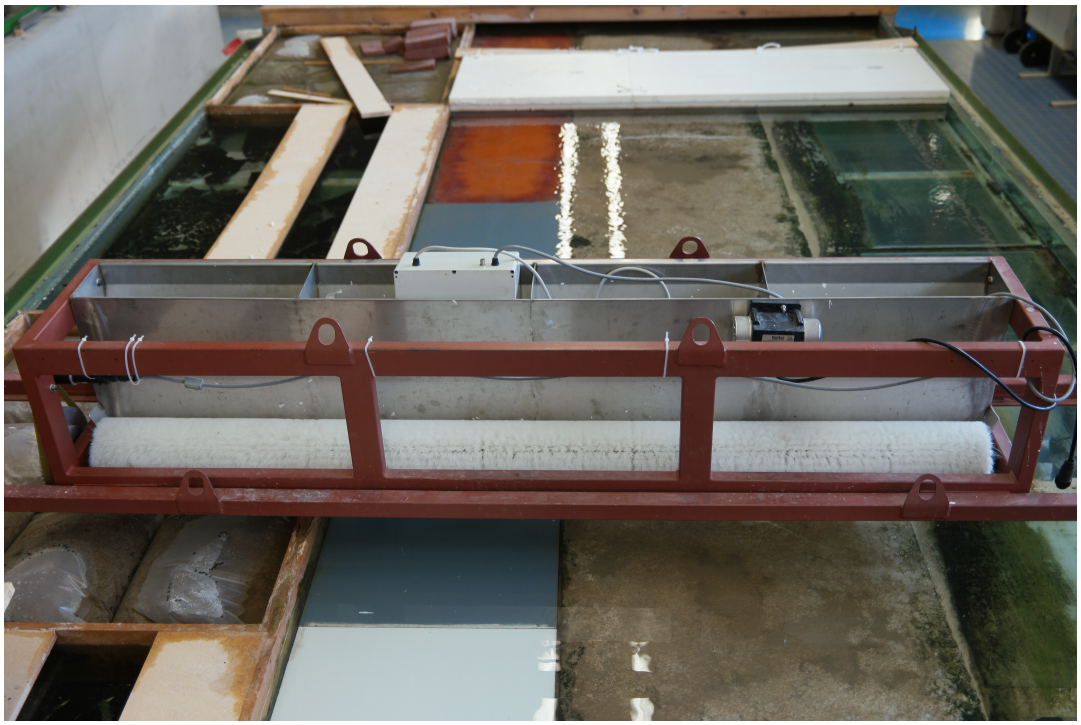


Figure A.5: The tracer dispenser. Tracers are stored in the metal storage. The round brush sweeps the tracers into the water

B

Supporting result figures

Momentum Thickness

Table B.1: Values of the momentum thickness in m.

Set 1		Set 2		Set 3		Set 4	
dense	Θ	dense	Θ	dense	Θ	dense	Θ
		Q50H12	0.122	Q60H12	0.114	Q70H12	0.113
Q50H14	0.122	Q60H14	0.113	Q70H14	0.108	Q80H14	0.110
Q60H16	0.107	Q70H16	0.111	Q80H16	0.115		
sparse		sparse		sparse		sparse	
		Q50H12	0.103	Q60H12	0.102		
		Q60H14	0.092	Q70H14	0.094		
		Q70H16	0.089	Q80H16	0.072		

Velocity profiles

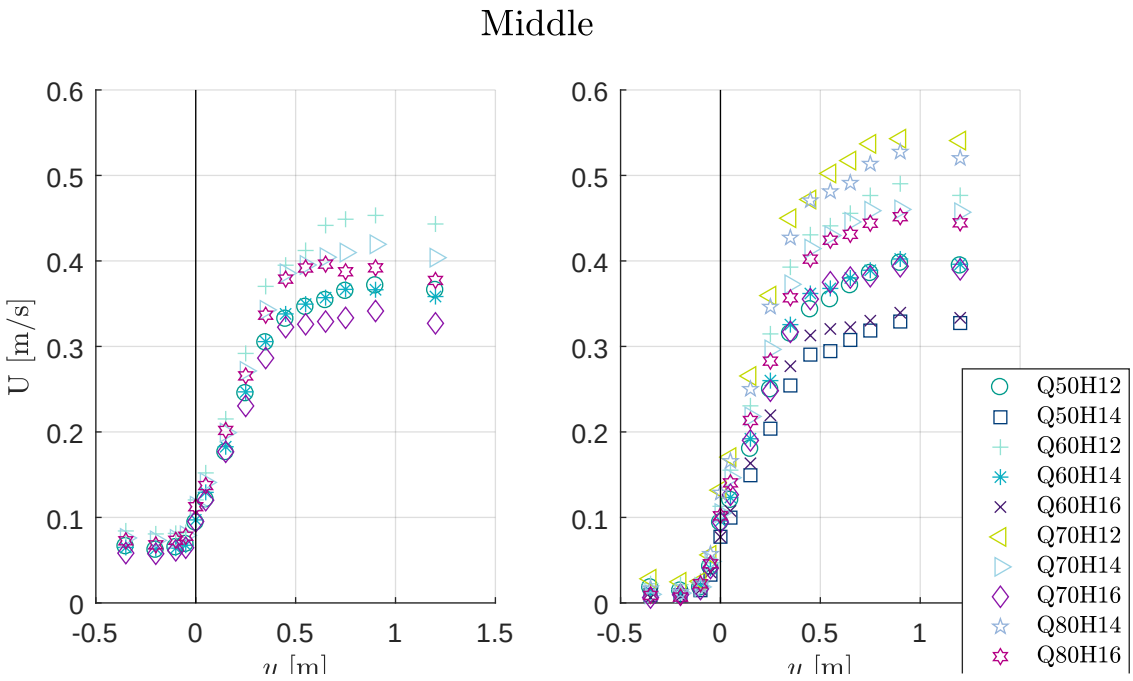


Figure B.1: Mean U profiles at mid-depth

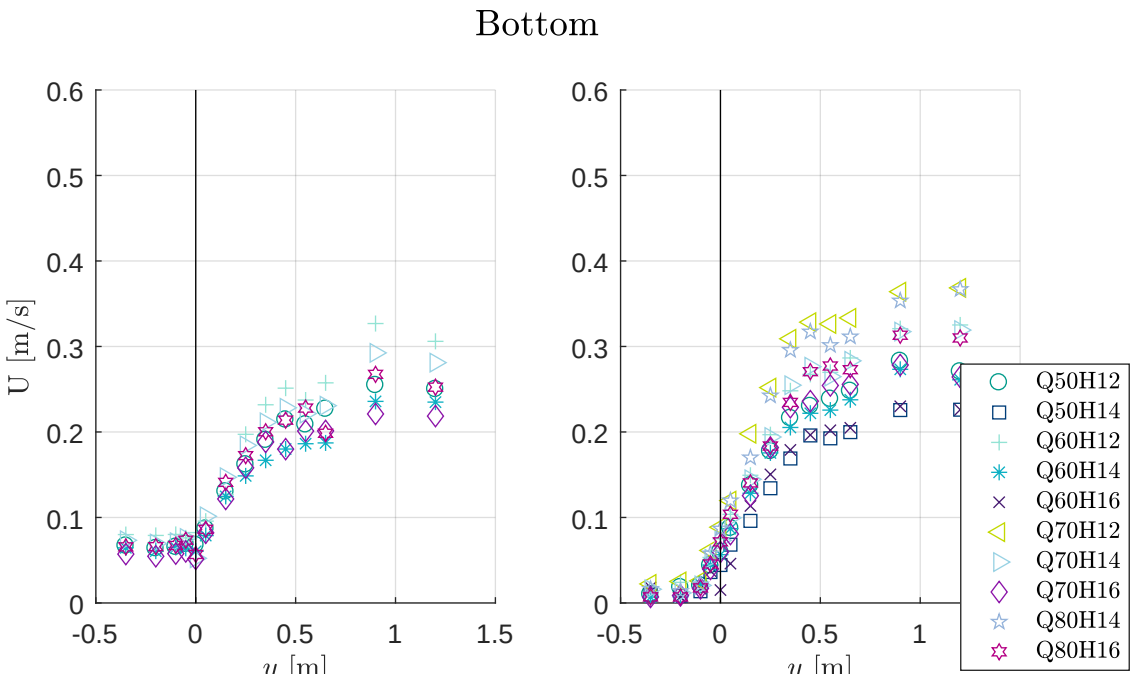


Figure B.2: Mean U profiles at the bottom

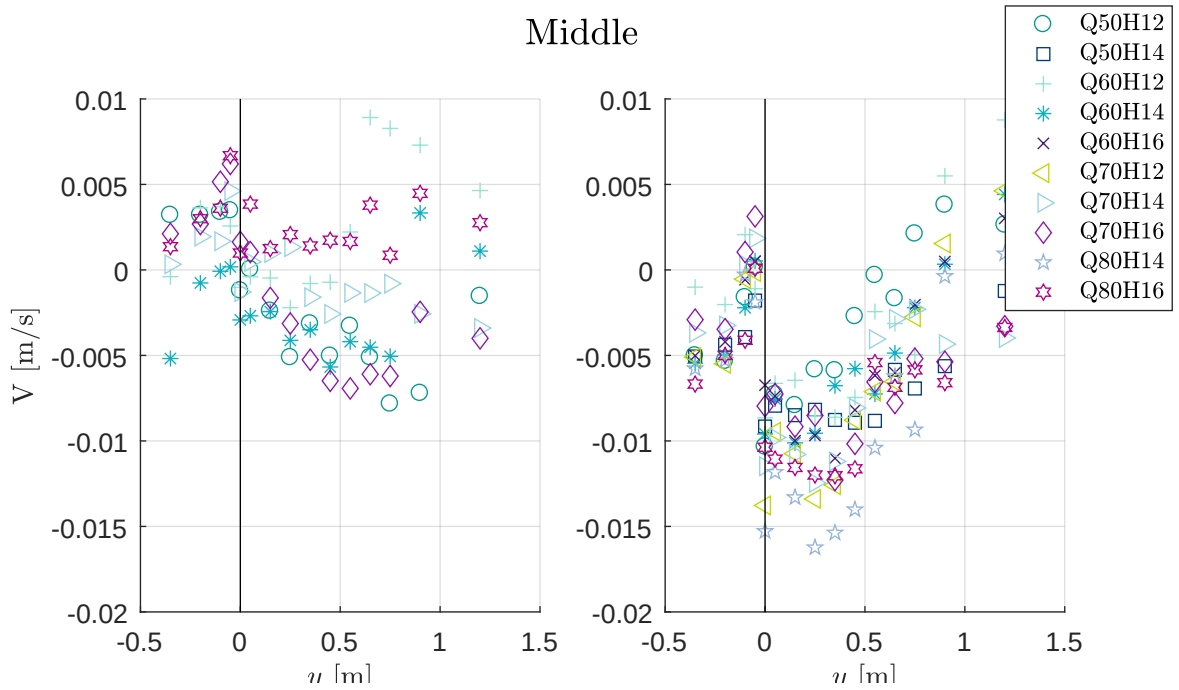


Figure B.3: Mean V profiles at mid-depth

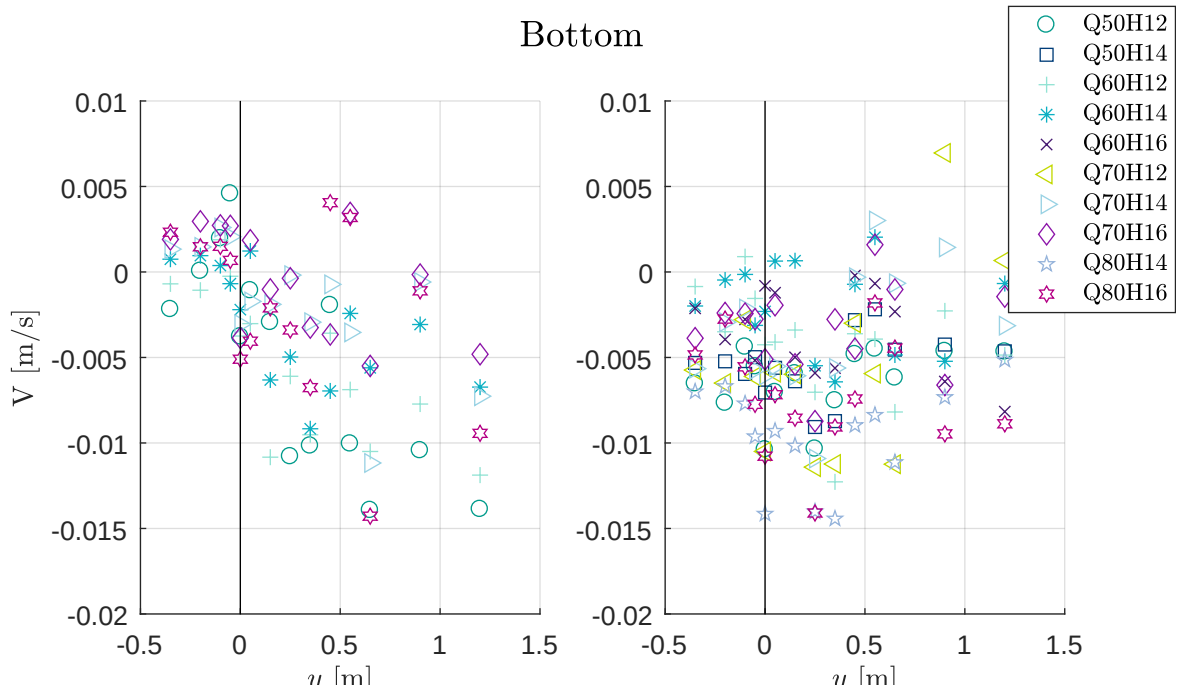


Figure B.4: Mean V profiles at the bottom

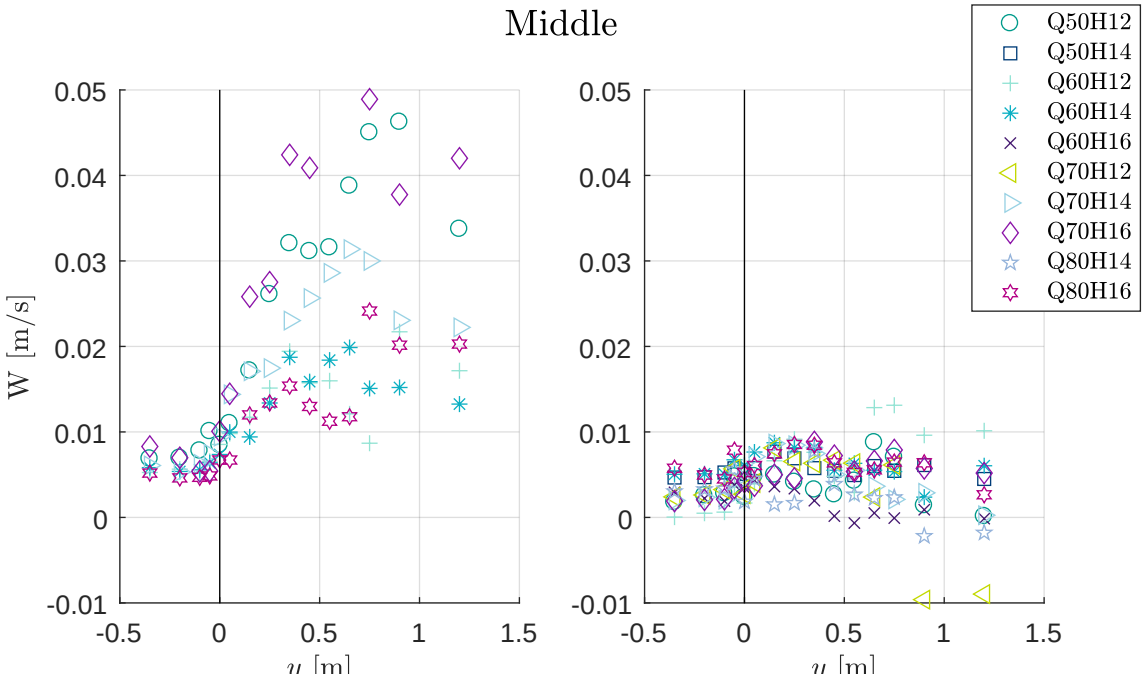


Figure B.5: Mean W profiles at mid-depth

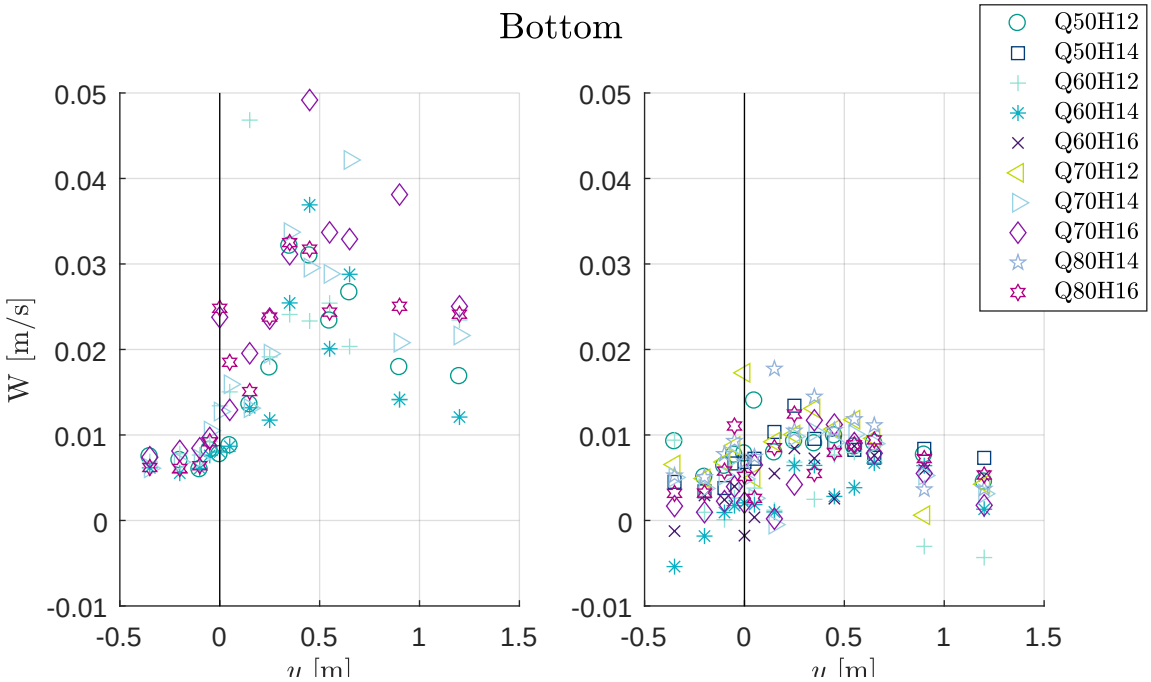


Figure B.6: Mean W profiles at the bottom

C

Velocity time series Q60H14

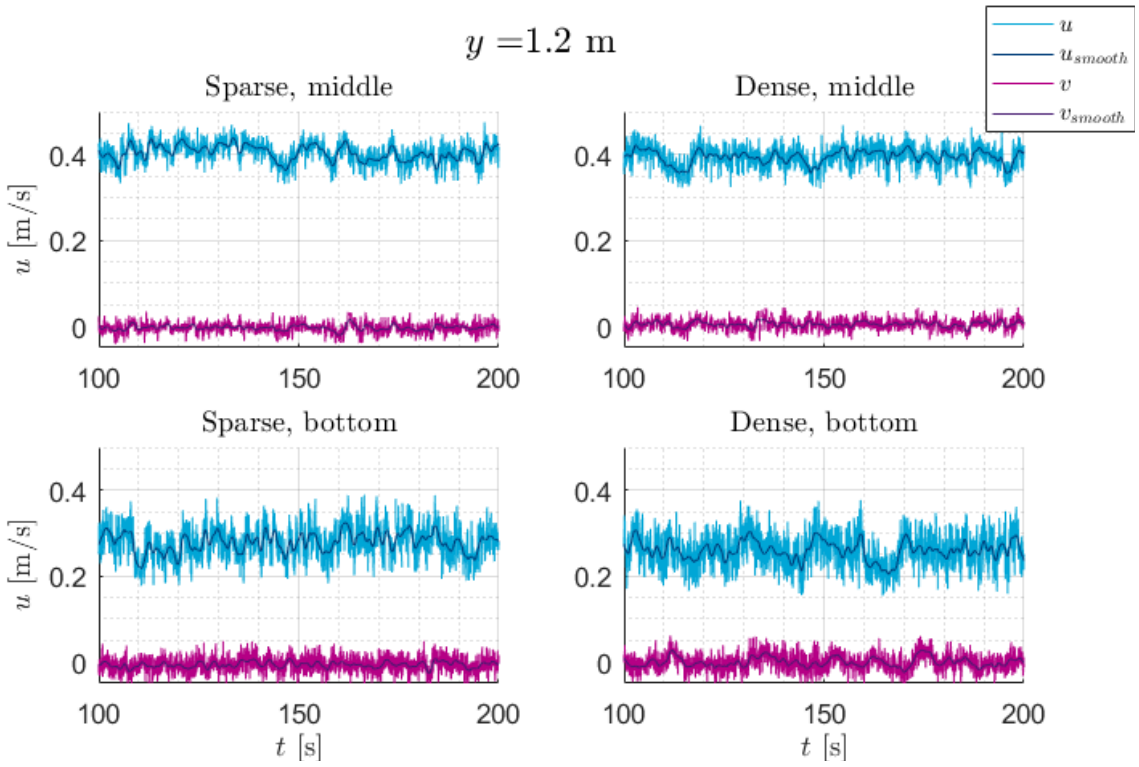


Figure C.1: Q60H14 flow time series, at location y = 1.2 m

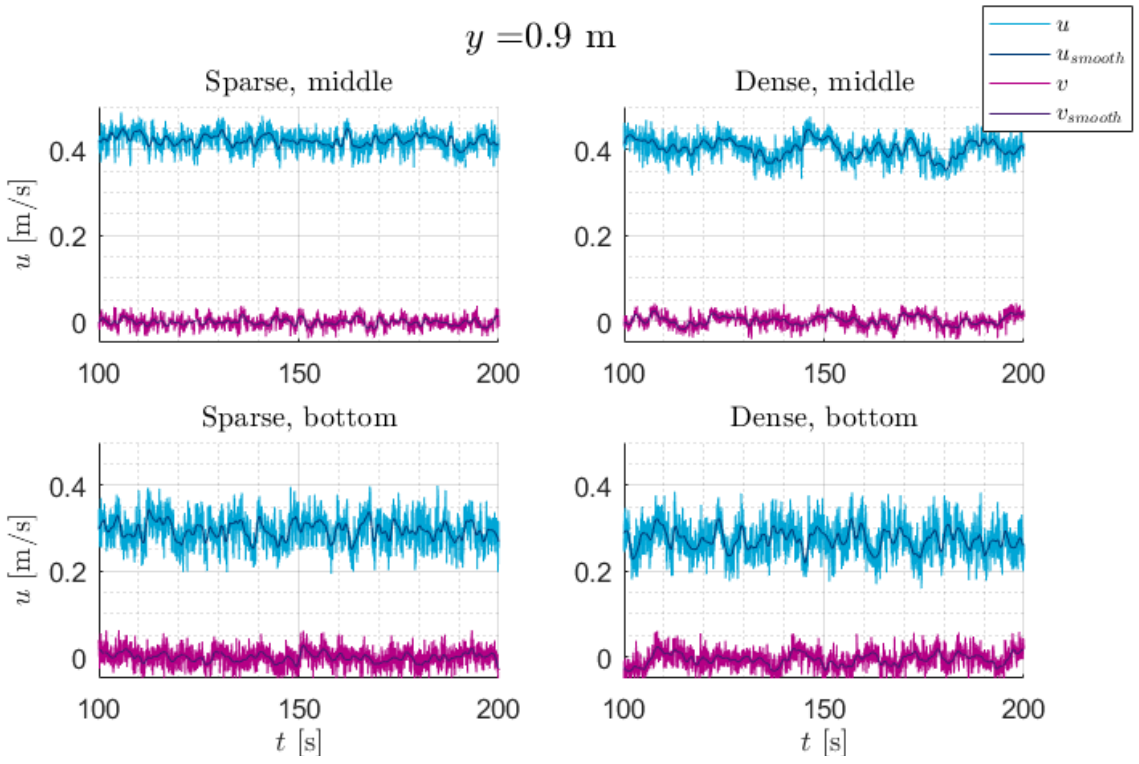


Figure C.2: Q60H14 flow time series, at location y = 0.9 m

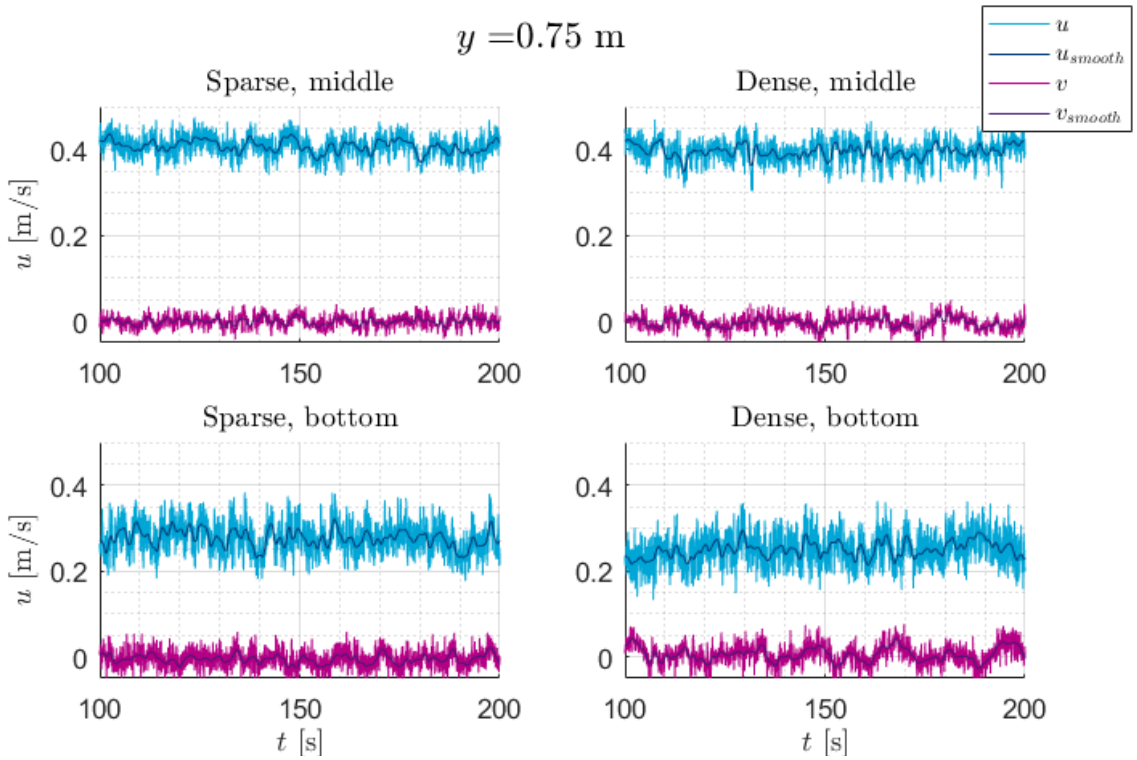


Figure C.3: Q60H14 flow time series, at location y = 0.75 m

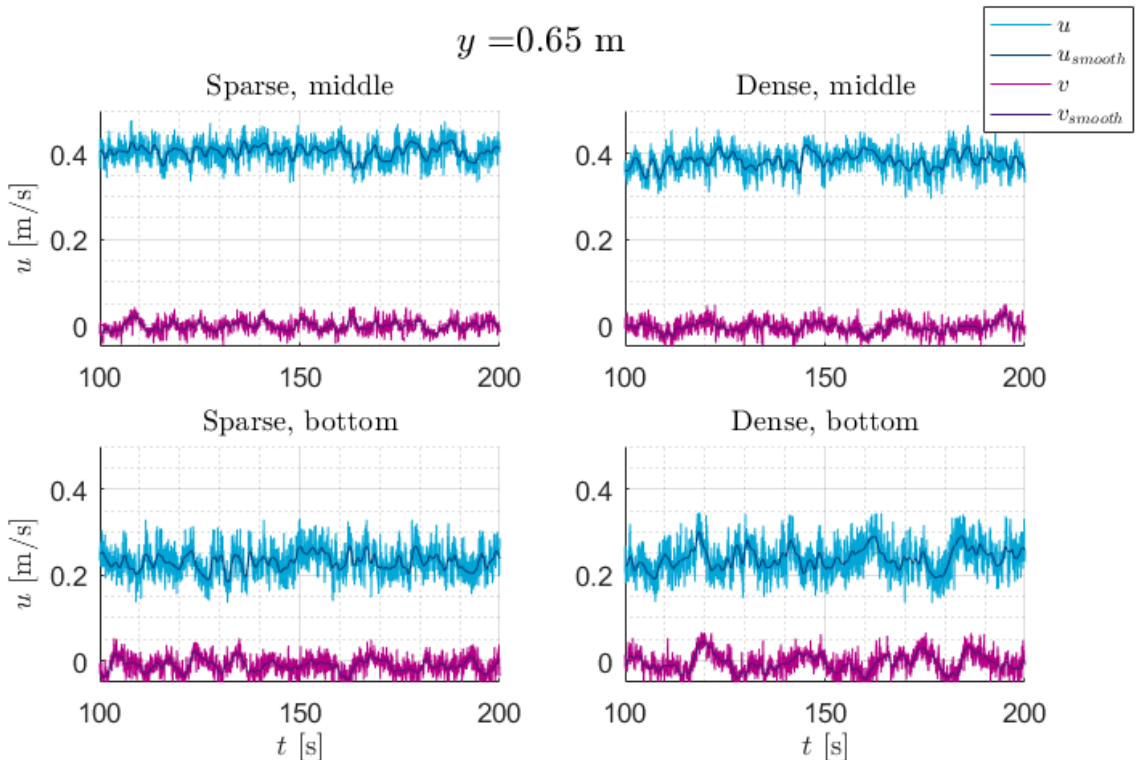


Figure C.4: Q60H14 flow time series, at location y = 0.65 m

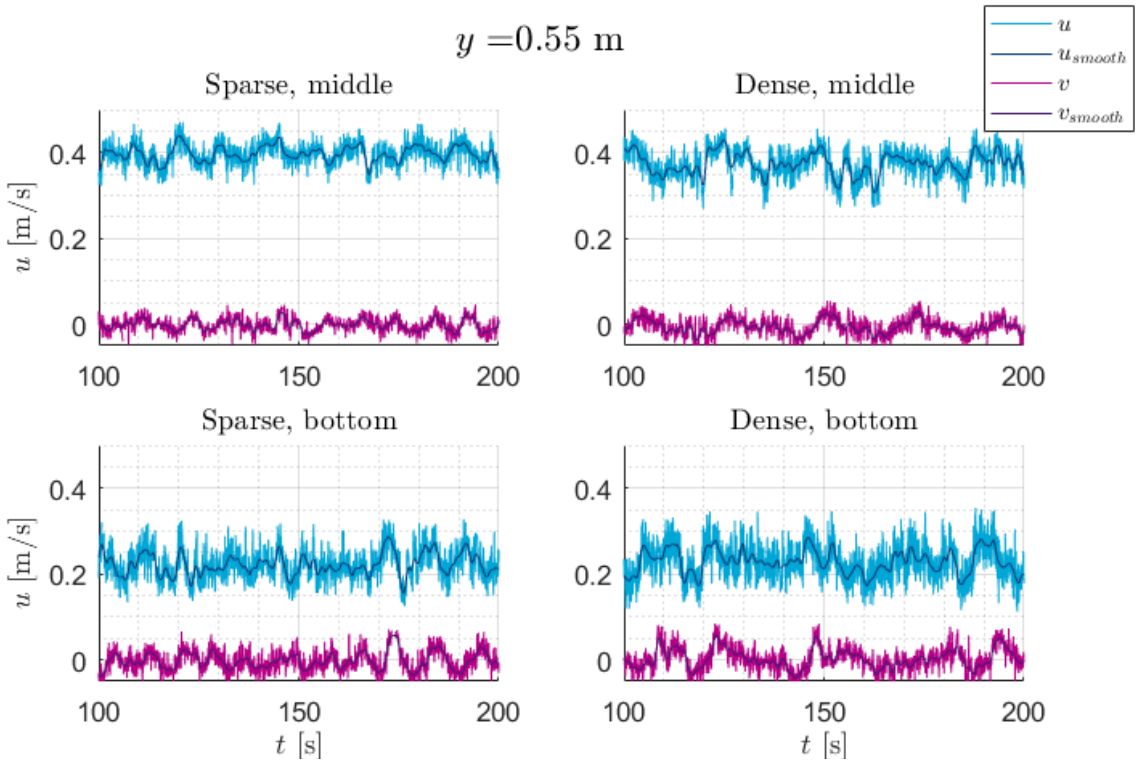


Figure C.5: Q60H14 flow time series, at location y = 0.55 m

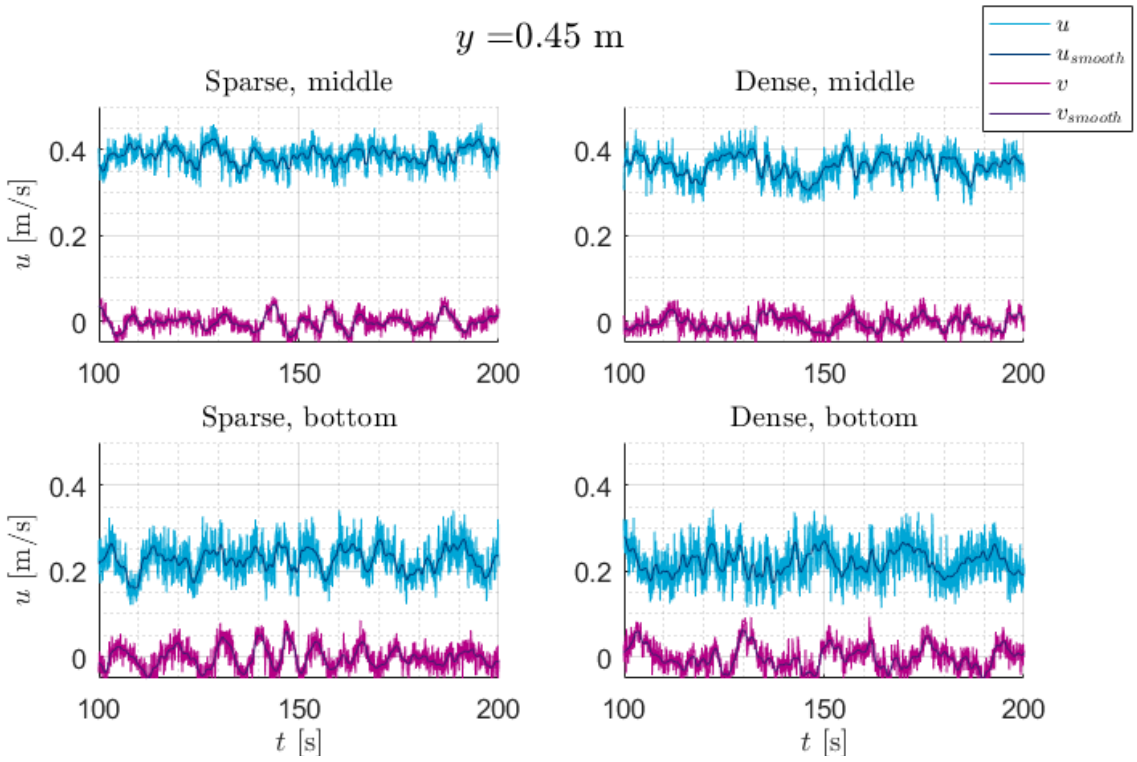


Figure C.6: Q60H14 flow time series, at location y = 0.45 m

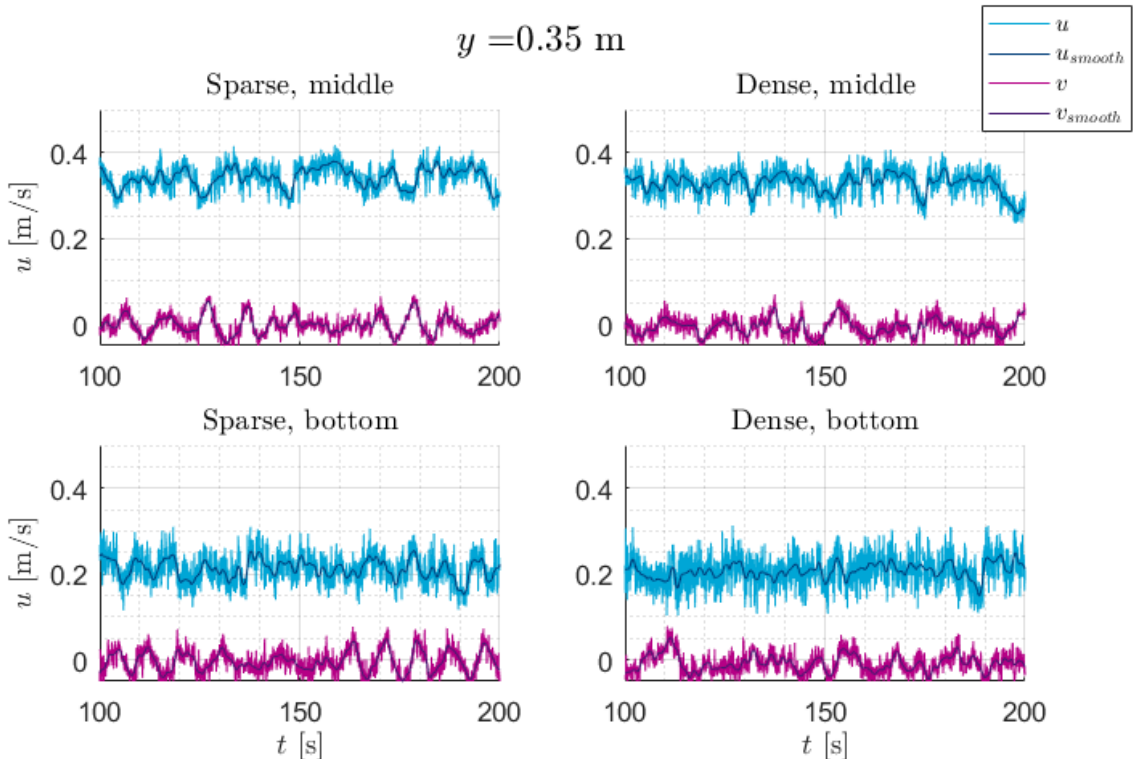


Figure C.7: Q60H14 flow time series, at location y = 0.35 m

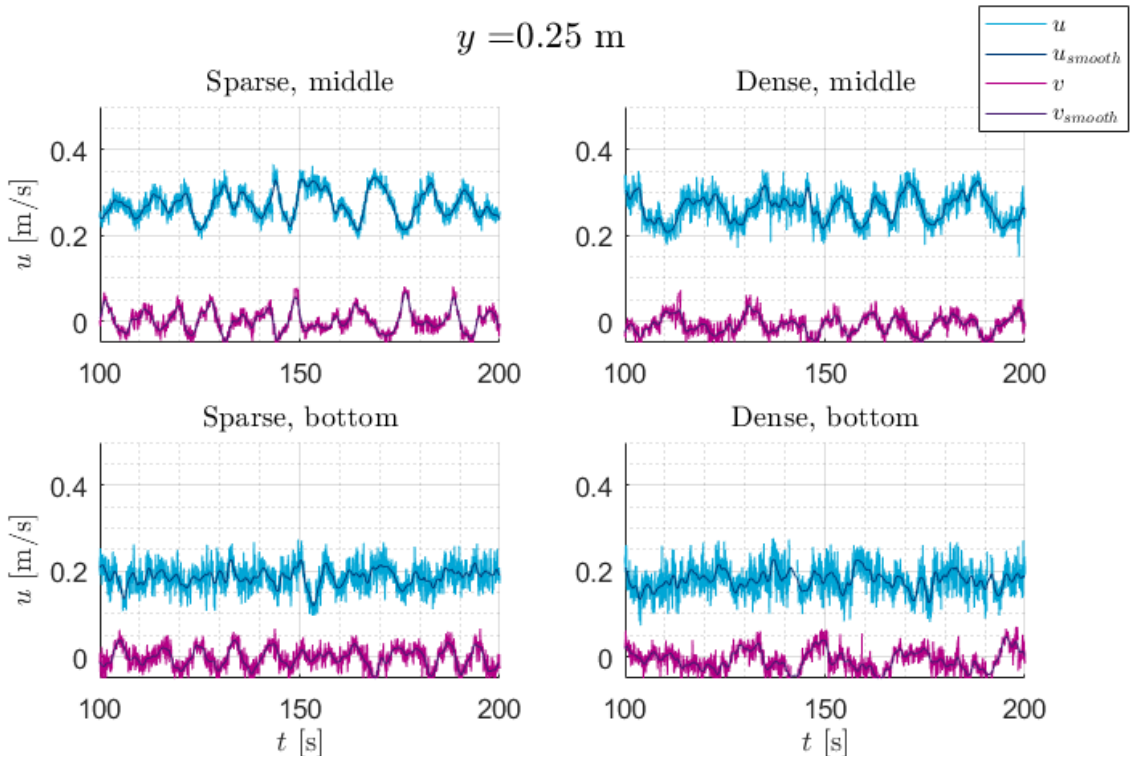


Figure C.8: Q60H14 flow time series, at location y = 0.25 m

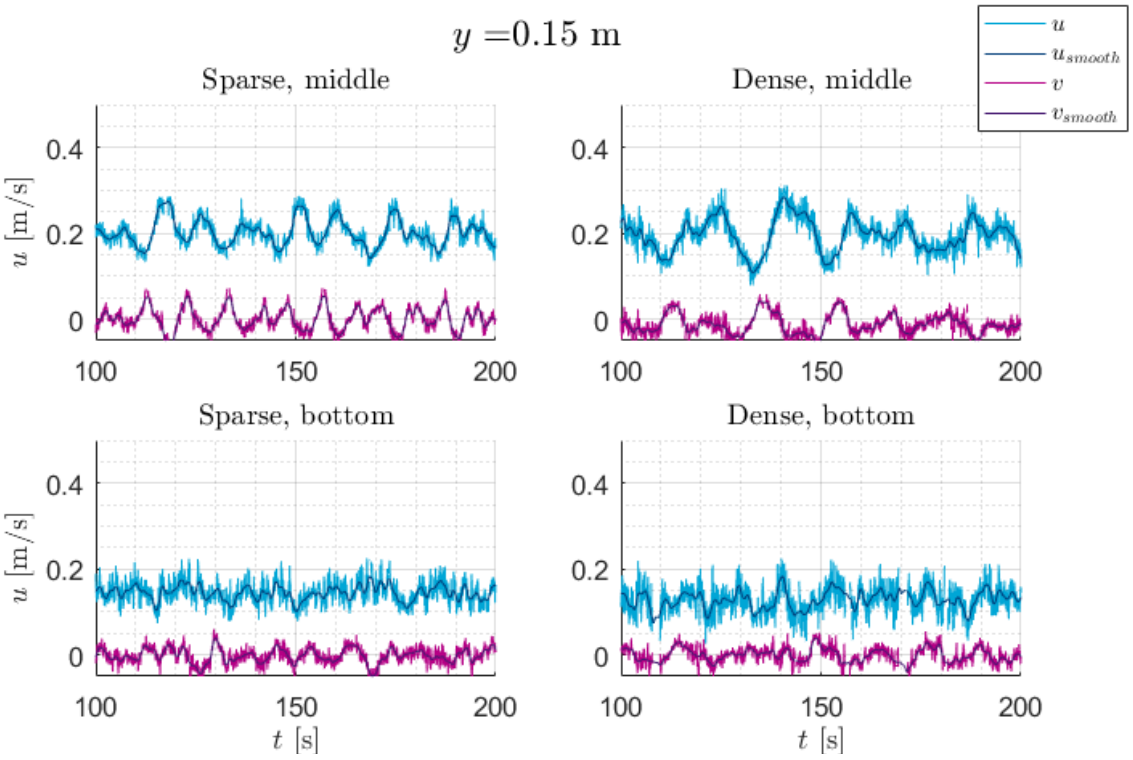


Figure C.9: Q60H14 flow time series, at location y = 0.15 m

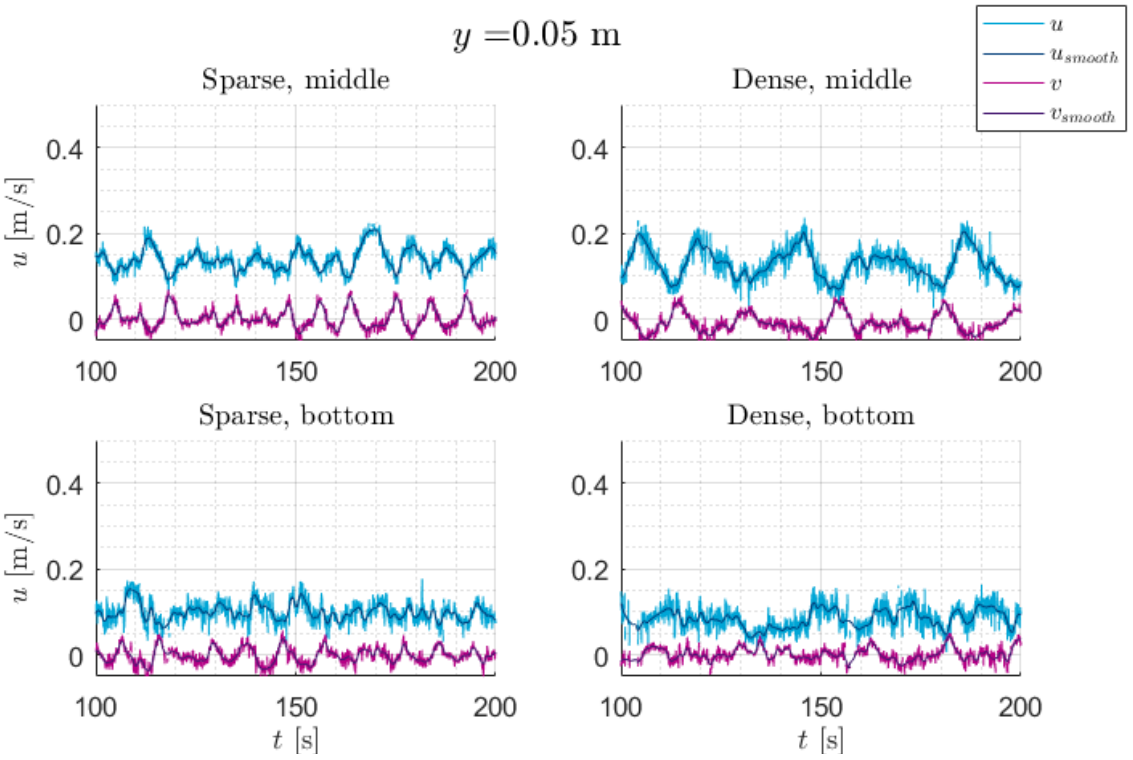


Figure C.10: Q60H14 flow time series, at location y = 0.05 m

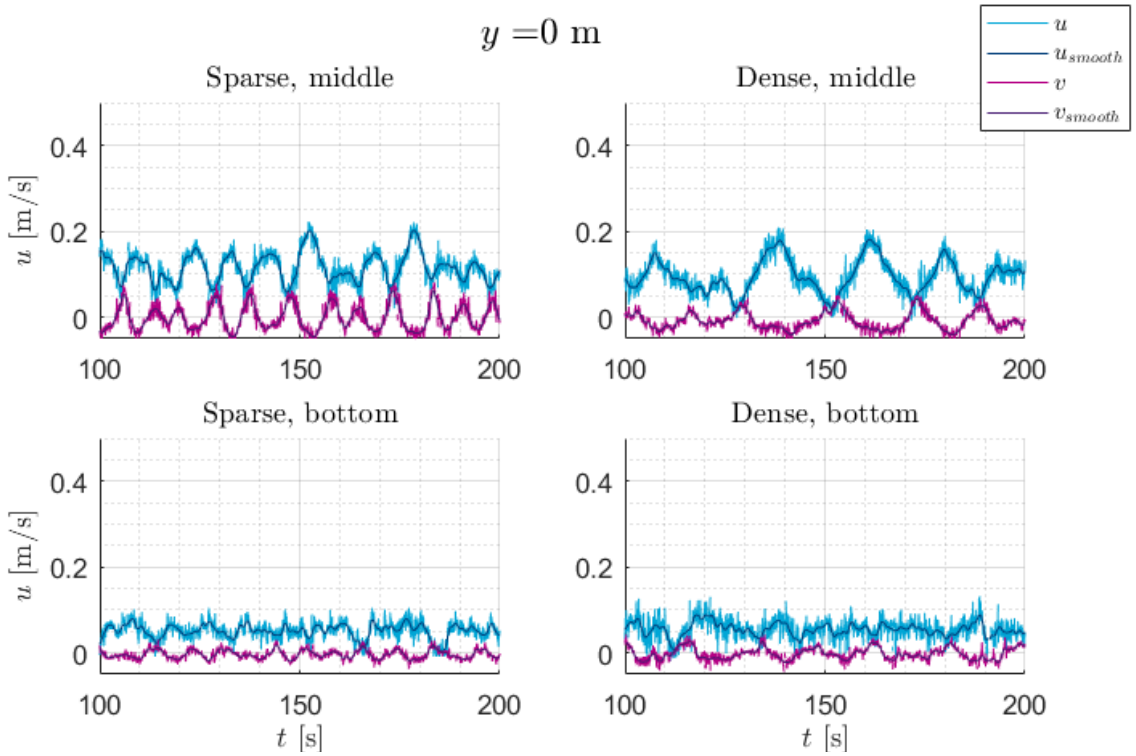


Figure C.11: Q60H14 flow time series, at location y = 0.0 m

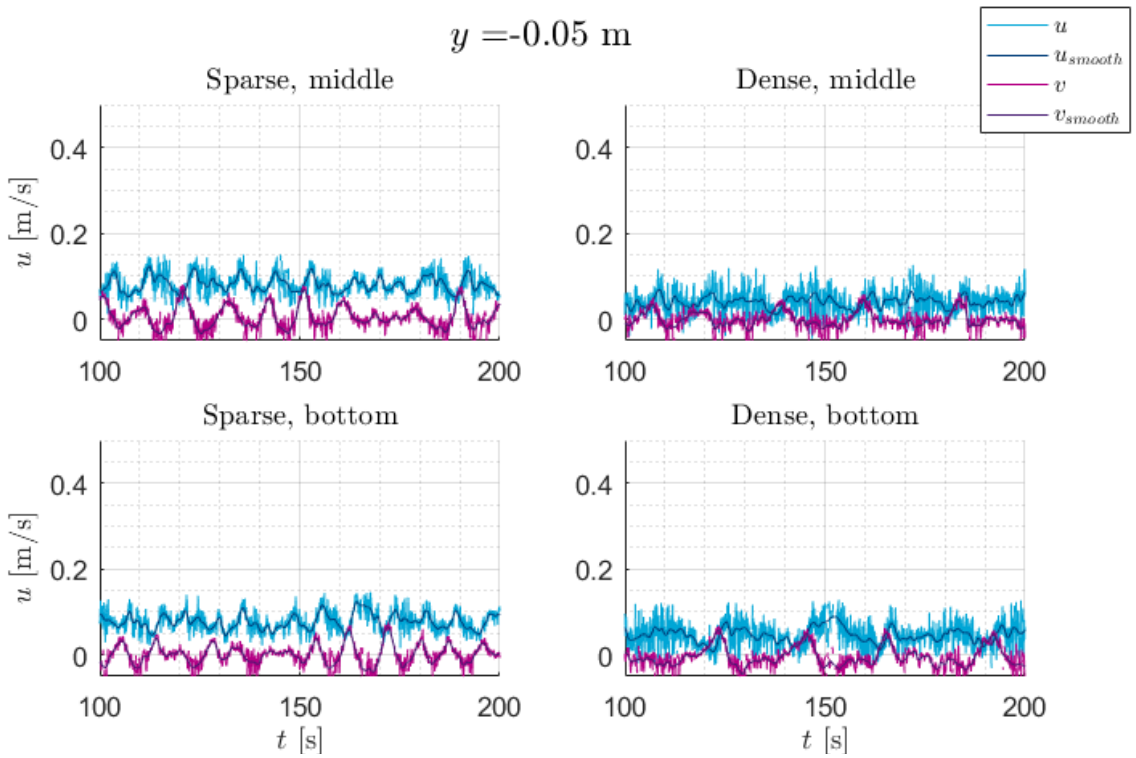


Figure C.12: Q60H14 flow time series, at location y = -0.05 m

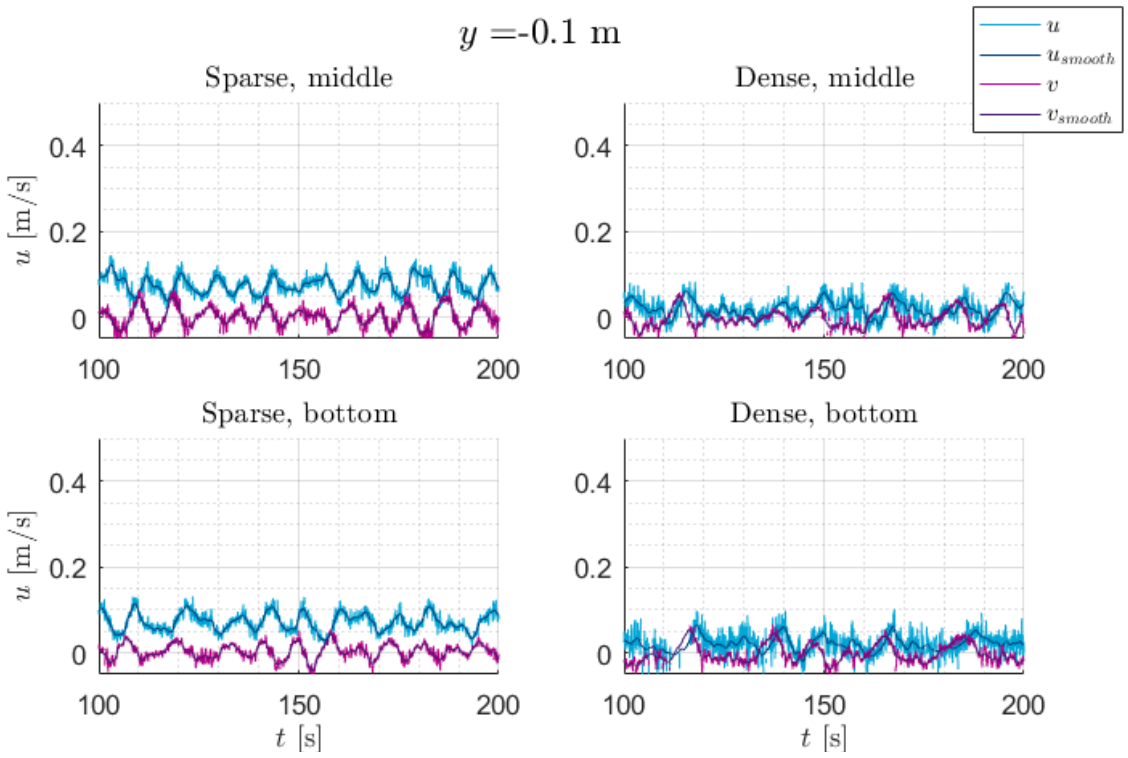


Figure C.13: Q60H14 flow time series, at location y = -0.10 m

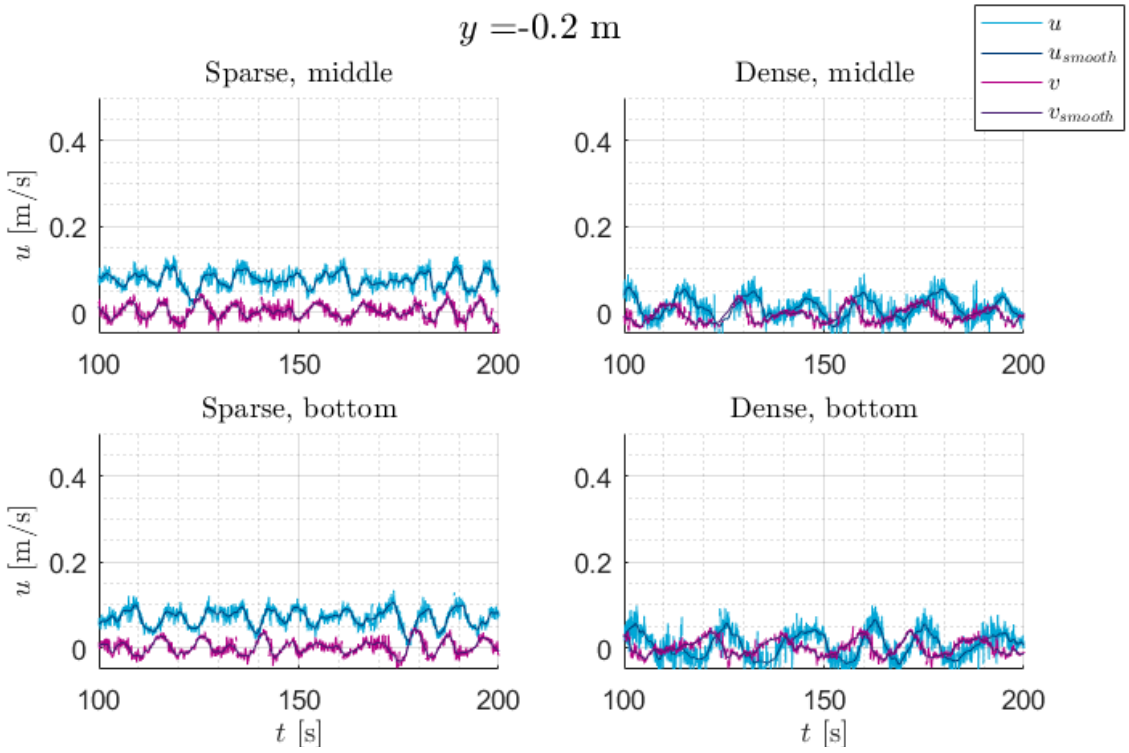


Figure C.14: Q60H14 flow time series, at location y = -0.2 m

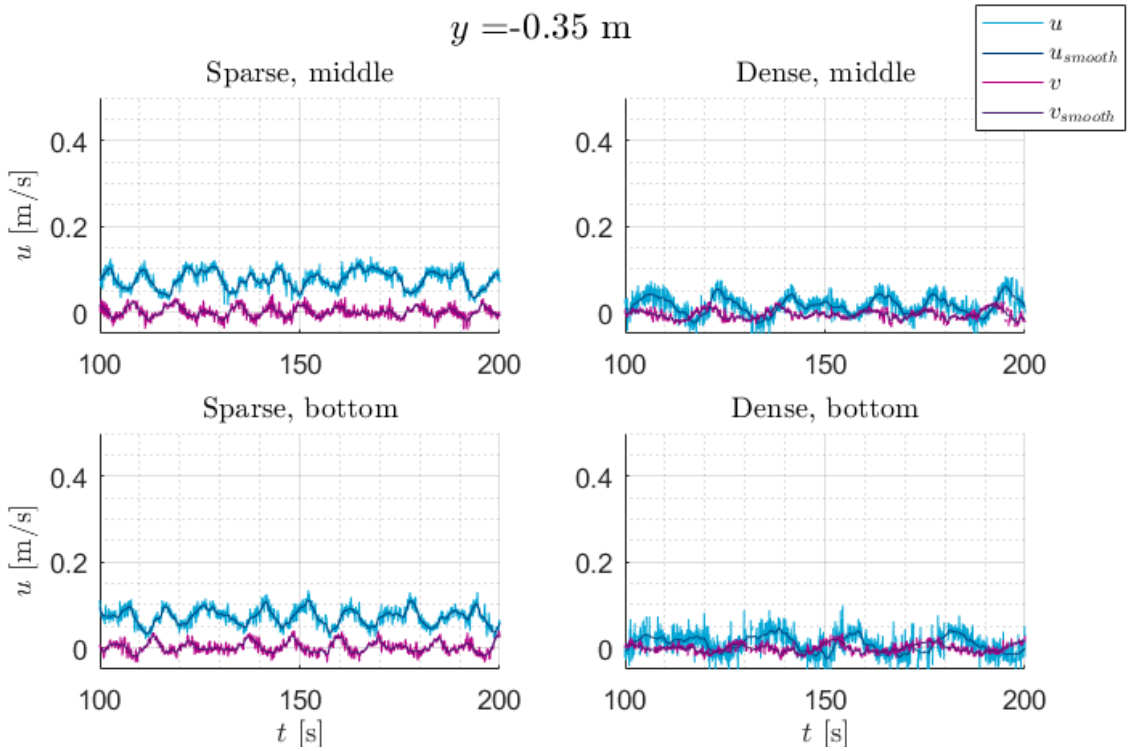


Figure C.15: Q60H14 flow time series, at location y = -0.35 m